The molecular spring model for docosahexaenoic acid (22:6w3) function in biological membranes
by Laura Lee Holte

A thesis submitted in partial fulfillment of the requirements for the degree of Doctor of Philosophy in Chemistry
Montana State University
© Copyright by Laura Lee Holte (1992)

Abstract:
Docosahexaenoic acid (22 : 6ω3), the most polyunsaturated fatty acid found in vertebrates, is abundant in retinal rod disk membranes, synaptic endings and sperm head membranes.

To date, no explanation for the role(s) of highly unsaturated fatty acids in membranes has emerged clearly as widely accepted and fully satisfactory. We have used rhodopsin, the major protein in retinal rod disk membranes, as a tool for studies of the role of 22 : 6ω3, since rhodopsin's functional state can be followed by color changes. Stimulation of retinal rod membranes by light rapidly leads to an equilibrium between an inactive orange form and an active yellow form. The active form excites the photoreceptor cell by activating many copies of a GTP binding protein. There is evidence that 22:6ω3 chains may prefer to exist in a short helical conformation but may stretch to a longer, thinner conformation with modest energy input. The molecular spring model for 22: 6ω3 function entails changing the pitch of the 22:6&omega:3 chain to compensate for and assist conformational changes of stimulated membrane proteins. The active form of rhodopsin is thought to require an expansion of planar area in the membrane to form a functional state. Use of deuterium labeled fatty acids and deuterium nuclear magnetic resonance order parameters provides information on the average conformation of the membrane fatty acid chains and the membrane thickness. Membrane thickness measurements obtained from nuclear magnetic resonance data agree well with other experimental methods. The deuterium nuclear magnetic resonance data obtained with a mixture of forms that exist after light excitation of the protein shows a thickening of the membrane hydrocarbon containing 22 : 6ω3 at the transition of rhodopsin from the inactive to the active form in support of the molecular spring model.

THE MOLECULAR SPRING MODEL FOR DOCOSAHEXAENOIC ACID (22:6ω3) FUNCTION IN BIOLOGICAL MEMBRANES

by

Laura Lee Holte

A thesis submitted in partial fulfillment
of the requirements for the degree

of

Doctor of Philosophy

in

Chemistry

MONTANA STATE UNIVERSITY
Bozeman, Montana

November 1992

D378
H7127

APPROVAL

of a thesis submitted by

Laura Lee Holte

This thesis has been read by each member of the thesis committee and has been found to be satisfactory regarding content, English usage, format, citations, bibliographic style, and consistency, and is ready for submission to the College of Graduate Studies.

11/30/92
Date

Edward A. Dratz
Chair, Graduate Committee

Approved for the Department of Chemistry and Biochemistry

11/30/92
Date

John R Cronin
Head, Department of
Chemistry and Biochemistry

Approved for the College of Graduate Studies

12/4/92
Date

R L Brown
Graduate Dean

STATEMENT OF PERMISSION TO USE

In presenting this thesis in partial fulfillment of the requirements for a doctoral degree at Montana State University, I agree that the Library shall make it available to borrowers under rules of the Library. I further agree that copying of this thesis is allowable only for scholarly purposes, consistent with "fair use" as prescribed in the U.S. Copyright Law. Requests for extensive copying or reproduction of this thesis should be referred to University Microfilms International, 300 North Zeeb Road, Ann Arbor, Michigan 48106, to whom I have granted "the exclusive right to reproduce and distribute copies of the dissertation in and from microfilm and the right to reproduce and distribute by abstract in any format."

Signature Laura L Holte

Date December 1, 1992

TABLE OF CONTENTS

Page

INTRODUCTION 1

PURIFICATION AND CHARACTERIZATION OF POLYUNSATURATED PHOSPHOLIPIDS 12

High Performance Liquid Chromatography 13
Materials and Methods 16
Reagents 16
Instrumentation 16
Second Derivative UV Spectroscopy 17
Results 18
Discussion 24
Phosphorous Assay 28
Gas Chromatography 30
Thin-Layer Chromatography 31
Mass Spectrometry 32

PURIFICATION OF RHODOPSIN AND PREPARATION OF RECONSTITUTED MEMBRANES 39
Protein Purification 39
Rhodopsin Reconstitution with Phospholipids 42

ABSORBANCE SPECTROSCOPY ON NATIVE ROS AND RECONSITUTED MEMBRANES 45
Introduction 45
Experimental 51
Results 52
Membranes Reconstituted with $16:0_{d31}22:6$PC 53
Native ROS 58
Membranes Reconstituted with $16:0_{d31}22:6$PC/PE/PS 3:3:1 60
Discussion 67

DEUTERIUM NMR THEORY AND EXPERIMENT 72
Theory 72
The Deuterium NMR Experiment 79
Spectrometer and Data Processing 82

DEUTERIUM NMR STUDIES OF RECONSTITUTED MEMBRANES 84
Introduction 84
Results 86
The First Moment, M_1 86
Delta Two, Δ_2 87
The Zeroth Moment, M_0 94

Discussion 99
Conclusions 108

LITERATURE CITED 119

LIST OF TABLES

Page

1. Retention Times for 16:022:6 Phospholipids 23

2. Sample Characteristics of Reconstituted Membranes Containing PC/PE/PS 3:3:1 61

LIST OF FIGURES

		Page
1.	Rod Outer Segment	2
2.	Rhodopsin Photointermediates	3
3.	Fatty Acid Composition of Frog ROS	5
4.	Molecular Spring Model	11
5.	Mechanism of Docosahexaenoate Autoxidation	14
6.	Second Derivative Spectrum of Oxidized 16:022:6PC	19
7.	Second Derivative Spectrum of Purified 16:022:6PC	20
8.	HPLC Recordings of 16:22:6PC Purification	21
9.	FAB Mass Spectra of Selected Phospholipids	38
10.	Absorbance Spectrum of 16:0_{d31}22:6PC Rhodopsin Reconstituted Membranes	55
11.	Curve Fitting Analysis of Absorbance Spectrum Taken 5 minutes Post-bleach	56
12.	Curve Fitting Analysis of Absorbance Spectrum Taken 3 hours Post-bleach	57
13.	Absorbance Spectrum of Native ROS	59
14.	Absorbance Spectrum of Preparation A	63
15.	Absorbance Spectrum of Preparation B	64
16.	Absorbance Spectrum of Preparation C	66
17.	Energy Levels for I=1 Spin System	73
18.	Angle Dependent Doublets in ^2H NMR Spectrum	74
19.	^2H NMR Powder Pattern and dePaked Spectrum	76
20.	Quadrupole Echo Pulse Sequence	81

21. First Moment versus Time for Preparation A 88

22. First Moment versus Time for Preparation B 89

23. First Moment versus Time for Preparation C 90

24. Delta Two Plot for Preparation A 91

25. Delta Two Plot for Preparation B 92

26. Delta Two Plot for Preparation C 93

27. Zeroth Moment Plot for Preparation A 95

28. Zeroth Moment Plot for Preparation B 96

29. Zeroth Moment Plot for Preparation C 97

30. First Moment for 16:0_{d31}22:6PC Liposome versus Temperature 100

31. First Moment for 16:0_{d31}22:6PC/PE/PS Liposome versus Temperature 101

32. First Moment for Preparation A versus Temperature 102

33. Change in First Moment for Preparations A, B, and C 104

34. Models for Fatty Acid Chain Conformations 110

35. A Model Membrane Built of 16:022:6 Phospholipids 118

ABSTRACT

Docosahexaenoic acid (22:6ω3), the most polyunsaturated fatty acid found in vertebrates, is abundant in retinal rod disk membranes, synaptic endings and sperm head membranes. To date, no explanation for the role(s) of highly unsaturated fatty acids in membranes has emerged clearly as widely accepted and fully satisfactory. We have used rhodopsin, the major protein in retinal rod disk membranes, as a tool for studies of the role of 22:6ω3, since rhodopsin's functional state can be followed by color changes. Stimulation of retinal rod membranes by light rapidly leads to an equilibrium between an inactive orange form and an active yellow form. The active form excites the photoreceptor cell by activating many copies of a GTP binding protein. There is evidence that 22:6ω3 chains may prefer to exist in a short helical conformation but may stretch to a longer, thinner conformation with modest energy input. The molecular spring model for 22:6ω3 function entails changing the pitch of the 22:6ω3 chain to compensate for and assist conformational changes of stimulated membrane proteins. The active form of rhodopsin is thought to require an expansion of planar area in the membrane to form a functional state. Use of deuterium labeled fatty acids and deuterium nuclear magnetic resonance order parameters provides information on the average conformation of the membrane fatty acid chains and the membrane thickness. Membrane thickness measurements obtained from nuclear magnetic resonance data agree well with other experimental methods. The deuterium nuclear magnetic resonance data obtained with a mixture of forms that exist after light excitation of the protein shows a thickening of the membrane hydrocarbon containing 22:6ω3 at the transition of rhodopsin from the inactive to the active form in support of the molecular spring model.

INTRODUCTION

The process of visual transduction has been the focus of scientific investigation from many perspectives. The molecular mechanisms of many of the steps in the vision process are unsolved. At a macroscopic level, two types of photoreceptors are responsible for vision in the human retina. Cone cells are responsible for perceiving color vision and rod cells are dim light photoreceptors which allow us to discriminate between shades of black and white.

This study is focused on the rod cells, which are abundant in the retina and are relatively easy to isolate in large quantities. Light is absorbed by photoreceptor proteins that are concentrated in the rod outer segment (ROS) in stacks of disks called rod disk membranes (RDM's) shown in Figure 1. Over 80% of the protein in RDM's is the visual protein rhodopsin (Papermaster & Dreyer, 1974). Rhodopsin is thought to be a 7-helical transmembrane protein that is activated by single photons of light to initiate the primary event in visual transduction (Liebman et al.1987; Dratz & Hargrave, 1983). Upon absorption of light, rhodopsin is converted to a series of photointermediates each having a characteristic light absorption maximum (Matthews et al.1963; Ostroy, 1977; Blazynski & Ostroy, 1984), shown in Figure 2. Metarhodopsin II (MII), which forms in milliseconds, is the last photo induced

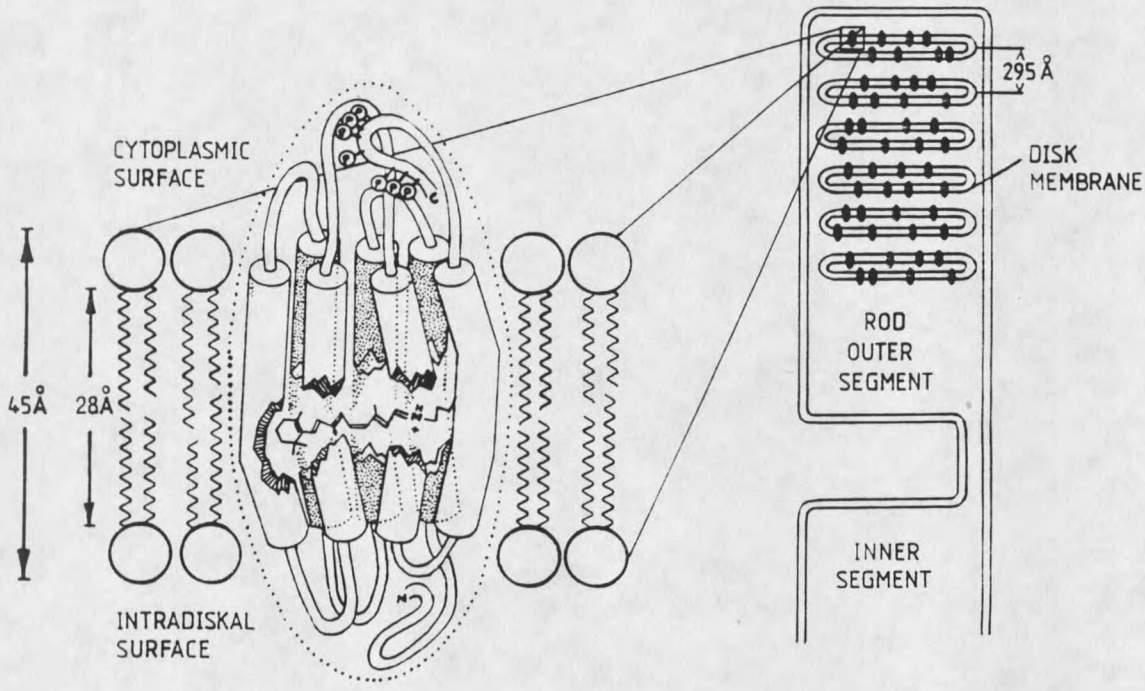


Figure 1. Diagram of a cross-section of the rod outer segment (not to scale). A magnified portion of the rod outer segment is shown on the left, which is a schematic model of the general structure of rhodopsin and its association with the lipid bilayer of the rod outer segment disk membrane. The 11-*cis* retinal binding site, oriented nearly parallel to the membrane plane, is also schematically shown. (from Dratz & Hargrave, 1983)

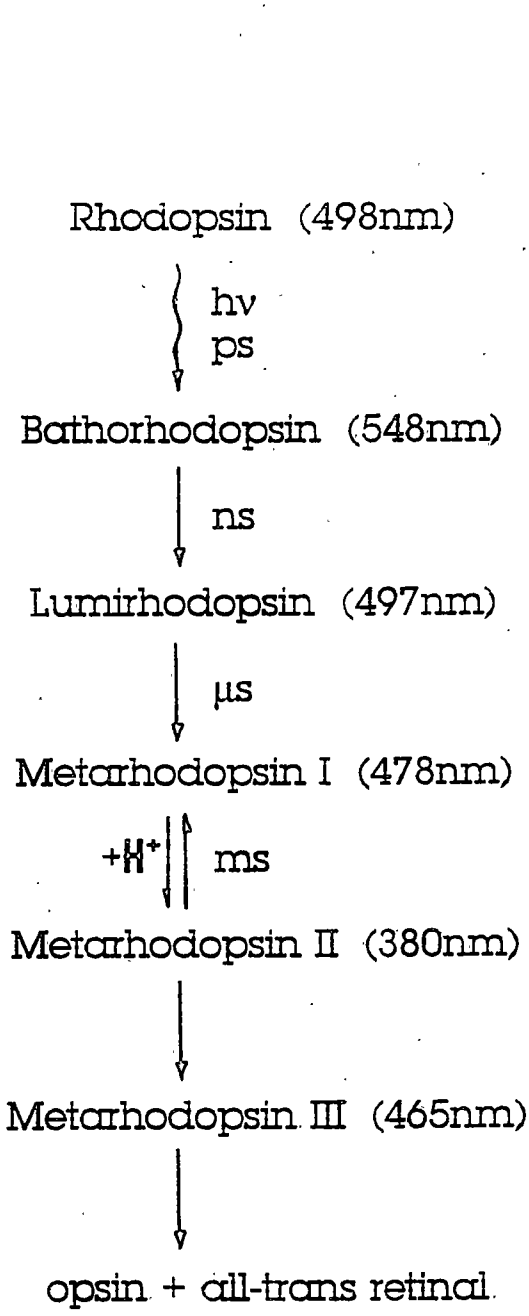


Figure 2. Shown is the series of photointermediates formed by rhodopsin upon absorption of light. The absorption maximum given for each intermediate.

intermediate formed on a timescale fast enough to be implicated in triggering vision. Metarhodopsin II is the photointermediate which activates the cell by coupling with the G-protein transducin, or G_t (Emeis et al.1982). This interaction between MII and G_t initiates an enzyme cascade which results in an electrical signal that modulates neurotransmitter release at the photoreceptor cell synapse.

Rhodopsin is embedded in a phospholipid bilayer in the RDM's. The fatty acid composition of these phospholipids has been characterized for many vertebrate retina (Stone et al.1979). In nearly all cases, the most abundant fatty acid is docosahexaenoic acid, 22:6ω3 or 22:6, which accounts for nearly 50 molar percent of all fatty acids found in the RDM. Figure 3 itemizes the mole % fatty acid content of frog ROS. 22:6ω3 is the most polyunsaturated fatty acid in vertebrate tissue and is found in such great abundance in only two other tissues: brain gray matter and spermatozoa (Salem et al.1986).

The double bonds in 22:6 are methylene-interrupted which make them very susceptible to autoxidation. The polyunsaturated fatty acid oxidation products pose a toxic threat to cells and are thought to be causative agents in cancer, heart disease, and aging (Salem & Karanian, 1992; Davis et al.1976; Armstrong et al.1984). This susceptibility to oxidation of 22:6 and the high content of 22:6 in the retina suggests that this fatty acid is used at

some peril and is indirect evidence that 22:6 plays an important role in the visual membrane. Yet, to date, no generally accepted role for 22:6 or other highly unsaturated fatty acids in biological membranes has been elucidated.

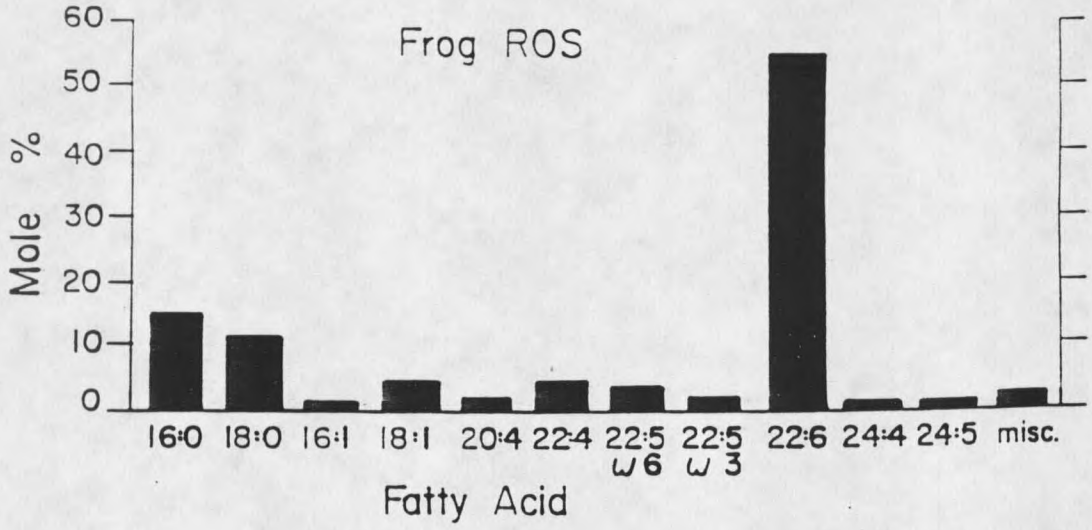


Figure 3. A representative mixture and molar percentage of phospholipid fatty acids found in vertebrate ROS is shown by this data taken from the frog ROS. The numbers below the bars indicate the chain length and number of double bonds found in each fatty acid. The ω's refer to the number of bonds from the methyl end of the chain where the unsaturation begins. Unsaturation is always in the form of methylene interrupted *cis* double bonds. (data from Stone et al.1979)

Nutritional studies indicate an essential role for 22:6. Rhesus monkeys subjected to dietary deprivation of ω3 fatty acid precursors of 22:6 showed decreased signal from electroretinograms suggesting deteriorated visual function (Neuringer et al.1986). In the retina, 22:6ω3 tends to be conserved upon dietary deprivation of ω3 fatty acids. In contrast, in the brain, a diet containing ω6 fatty acids but not ω3 leads to a loss of 22:6ω3 but a concomitant increase in 22:5ω6 (Bayerl & Bloom, 1990; Bush et al.1991). This fatty acid substitution is problematical for membrane biophysicists as most would predict little change in the overall physical state of the membrane in this case. Recent studies have also shown that long chain polyunsaturated fatty acids, such as 22:6ω3, are necessary in the diets of preterm infants for optimum visual development (Birch et al.1992).

An important piece of evidence that provides hints on the role for 22:6 in membranes is derived from the pressure dependence of the MI ↔ MII equilibrium. Rhodopsin undergoes a volume increase during the transition between inactive MI and active MII as evidenced by a pressure induced reversal of the reaction back towards MI (Lamola et al.1974). The pressure sensitivity of the MI ↔ MII equilibrium is observed in native membranes but not in membranes solubilized in mild. The lack of sensitivity of the MI ↔ MII equilibrium to pressure in detergent micelles suggests a coupling

between rhodopsin and lipid bilayer. Additionally, unpublished work by Dratz and coworkers has shown that the pressure reversibility of MI $\leftrightarrow$ MII is observed in rhodopsin reconstituted in 16:022:6PC but is not observed in reconstitutions containing a 16:016:1PC fatty acid complement. (Interestingly, the minimally unsaturated fatty acid, 16:1 has approximately the same melting point as 22:6.) The results discussed above support the suggestion that there is a direct coupling between rhodopsin and 22:6 in the membrane bilayer.

Direct experimental evidence for the conformation of 22:6 in a fluid bilayer and the interaction with rhodopsin is difficult to obtain. Thus, computer simulations have become an important tool for exploring energetically preferred conformations for the 22:6 hydrocarbon chain. MM2 calculations have suggested that 22:6 adopts a helical conformation as its lowest energy form (Dratz, unpub.).

In recent work by Baenziger et al., ^{2}H NMR experiments provided sufficient information to calculate both average orientations and structure of the pair of double bonds in a fluid bilayer containing 18:2ω9 (Baenziger et al.1991; Baenziger et al.1992). The data was interpreted in terms of two possible models whereby in each case the double bonds are oriented at a "tilt" that is nearly perpendicular with respect to the bilayer normal rather than parallel to it as earlier, purely computational methods had suggested

(Applegate & Glomset, 1986). The pair of *-cis* double bonds are thought to have relatively restricted local motion. They propose that polyunsaturated fatty acyl chains can exist in a dynamic state but the presence of polyunsaturation should maintain a high degree of local order leading to compact structures that pack well in lipid bilayers.

The high levels of 22:6 in retinal rod membranes is associated with a thinner membrane hydrocarbon bilayer of about 27-28Å relative to saturated chains (Dratz & Hargrave, 1983; Dratz et al.1985). The importance of this number is that it implies that the 22:6 chain prefers a compact conformation in the membrane. The much shorter 18:0 saturated chains lead to a membrane bilayer thickness of about 29-30Å in melted bilayers(Lewis & Engelman, 1983). Using the helical conformation for 22:6 as its lowest energy form, the conformational energy of the system was calculated as a function of chain extension. The calculations implied that the 22:6 coil could expand and contract over a range of 3-4Å with a rather small input of energy (Dratz, unpublished work). The RDM hydrocarbon is quite thin (27-28Å) as shown by low angle x-ray and neutron diffraction experiments (Dratz & Hargrave, 1983; Dratz et al.1985). These considerations have led to the hypothesis that 22:6 in the membrane exists as short, compact coils that can lengthen to accommodate conformational changes

associated with photobleaching of rhodopsin (Holte et al.1990; Dratz & Holte, 1992).

There is substantial evidence that MII is the stage where light activation is triggered (Liebman et al.1987; Kibelbek et al.1991) and that protein conformational changes occur in rhodopsin upon excitation by light (Liebman et al.1987; Ostroy, 1977). The water soluble reagents hydroxylamine and sodium borohydride are unable to react with rhodopsin's Schiff's base-linked chromophore in native rhodopsin or in intermediates formed before MII (Bownds & Wald, 1965). However, these same water soluble reagents gain facile access to the retinal Schiff's base site deep within MII. Accessibility of aqueous reagents to the chromophore site at MII implies an opening of the protein structure at MII since the chromophore site is known to be deeply buried in the membrane (Thomas & Stryer, 1982). Flash photolysis studies show an entropy of activation for the transition between MI and MII to be very high, well above +50 cal/deg per mole (Parkes & Liebman, 1984; Ostroy, 1977) which indicates considerable increase in disorder of protein side chains, lipids, and solvent. Light excitation causes a decrease in birefringence and diamagnetic anisotropy of the membrane which is qualitatively consistent with a splaying of the seven-helix cluster away from axial orientation during the formation of MII (Parkes & Liebman, 1984). Opening of the helix bundle at MII is also

consistent with an increased interaction between the MII•G protein interface. Surface loops on rhodopsin are thought to form a "binding pocket" for G_t that becomes available as the protein opens up at MII (Hamm et al.1988; Konig et al.1989).

The hypothesis we have developed to explain the role of 22:6ω3 is called the "molecular spring model". The essence of the molecular spring model is sketched schematically in Figure 4. It is believed that formation of MII requires an opening of the helix bundle which increases the membrane surface area of the protein while the lipids decrease their surface area to compensate for the planar area expansion of the protein. The 22:6 chain is thought to prefer to be in a compact conformation favoring a thin bilayer in the presence of rhodopsin and in intermediates preceding MII. The expansion of the protein at MII is proposed to force lipid chains to lengthen and reduce their planar area. Thus, the molecular spring model predicts that the lipid hydrocarbon region thickens with formation of MII. We have designed experiments to measure the lipid hydrocarbon thickness in the presence of rhodopsin and to seek changes in membrane thickness with MII formation to test this mechanistic explanation for the role of 22:6 in the membrane.

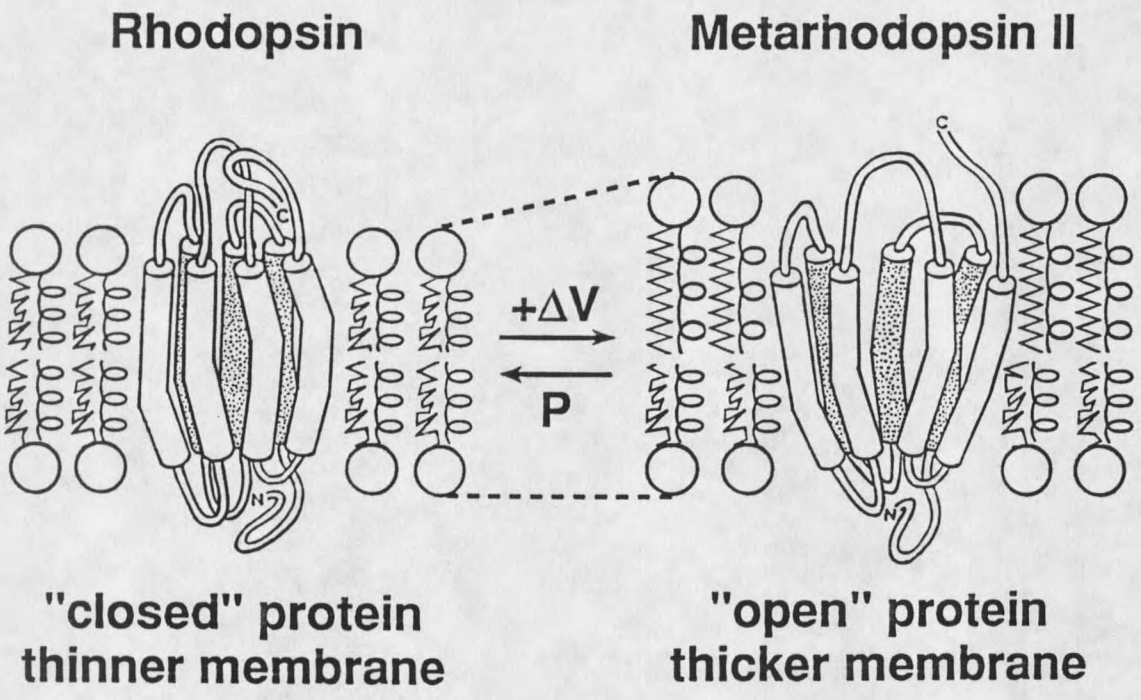


Figure 4. The molecular spring model is shown schematically. In rhodopsin and MI the lipid bilayer is relatively thin. As rhodopsin opens up at the MII intermediate the lipid bilayer is thought to compensate and becomes thicker. The volume increase and pressure reversibility are indicated above and below the arrows denoting the equilibrium.

PURIFICATION AND CHARACTERIZATION OF POLYUNSATURATED PHOSPHOLIPIDS

A model lipid/protein system was prepared in order to introduce probes to test the membrane thickness changes implied by the molecular spring model. The probes used are fully deuterated (perdeuterated) fatty acids in phospholipids which allow changes in fatty acid chain conformation to be monitored by using ^{2}H NMR. The model system was built around rhodopsin that had been stripped of native phospholipids. The purified rhodopsin was recombined with synthetic 22:6-containing phospholipids of interest to generate reconstituted model membranes with a well defined lipid composition.

When preparing model systems containing easily oxidized polyunsaturated phospholipids, it is essential to work with lipid components which are intact and structurally defined. Useful analytical methods must overcome the considerable challenges posed by phospholipids, i.e., they are non-volatile, thermally labile, and contain no chromophores that absorb above 210nm. The methods used in this study to purify, characterize, and quantitate synthetic, polyunsaturated phospholipids are described in the following.

High Performance Liquid Chromatography

A crucial consideration when studying polyunsaturated phospholipids is their extreme sensitivity to oxidative degradation (Frankel, 1980). The most readily oxidized lipids contain polyunsaturated fatty acids, PUFA, which have methylene interrupted double bonds that facilitate free radical oxidation by abstraction of the bisallylic hydrogens. The oxidizability of PUFA is linearly dependent on the number of bisallylic methylenes present in a fatty acid (Cosgrove et al.1987).

We are working with the most highly unsaturated fatty acid in biological systems, docosahexaenoic acid, which contains six double bonds (22:6). Docosahexaenoic acid is typically esterified to the *sn*-2 position of a phospholipid glycerol backbone. The mechanism of initial steps in the free radical (R•) initiated autoxidation is shown in Figure 5. Steps I and II show the abstraction of a hydrogen from a bisallylic hydrogen, the formation of a resonance stabilized free radical intermediate, and subsequent addition of oxygen. A free radical is regenerated in step III which allows propagation of the radical chain reaction. The autoxidative addition of an oxygen molecule to docosahexaenoic acid can yield up to 10 positionally isomeric hydroperoxides containing a conjugated diene (vanRollins & Murphy, 1984). Oxidized fatty acids can lead

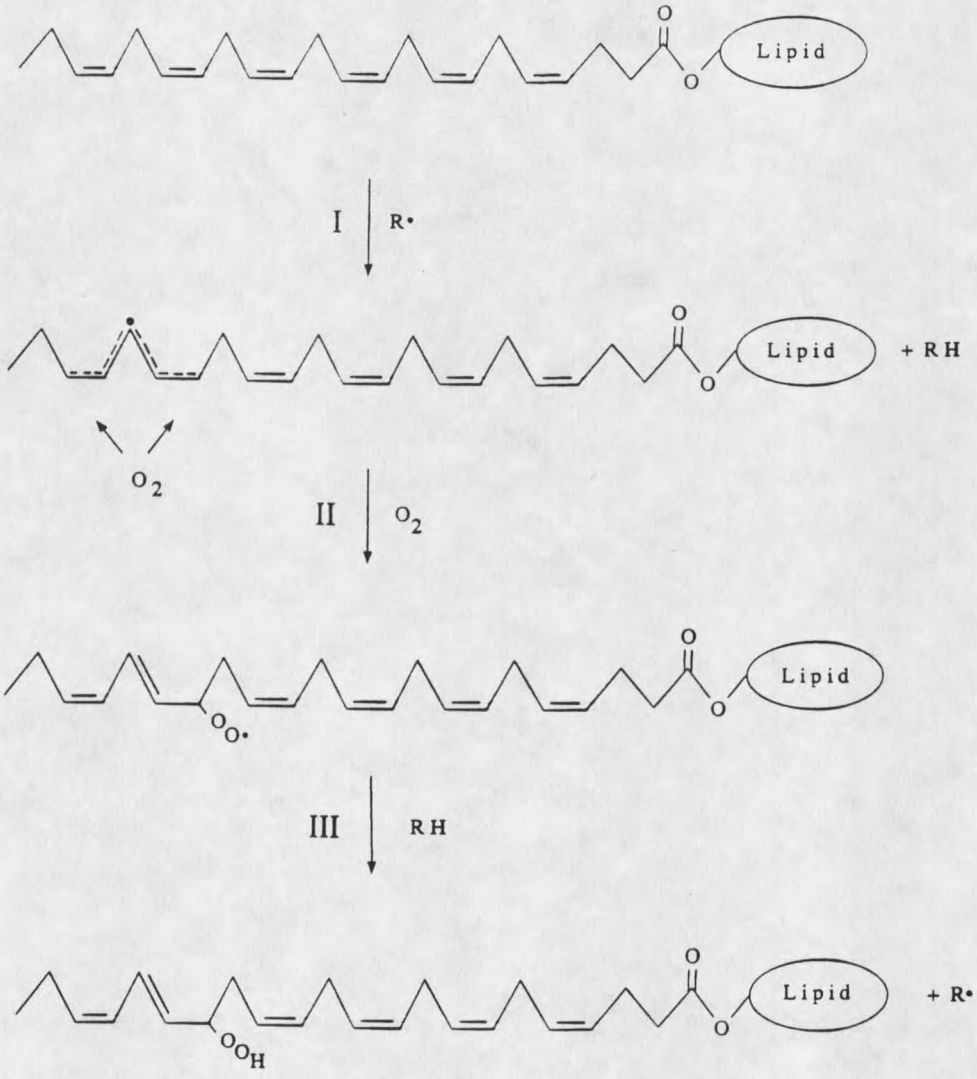


Figure 5. Mechanism of docosahexaenoate autoxidation:
I) An allylic proton is abstracted by a free radical (R•).
II) Attack by an oxygen molecule can occur at one of two positions on the resonance stabilized intermediate. Addition of oxygen results in formation of a peroxy radical (-OO•).
III) The peroxy radical abstracts a hydrogen from another donor, regenerating a free radical (R•) which can propagate the chain process.

to cellular damage (Marx, 1987; Bulkley, 1983) and may adversely affect the properties of membranes (vanKuijk et al.1987; O'Brian, 1987). Oxidized fatty acids can further decompose to highly cytotoxic products (Esterbauer, 1982; Dratz et al.1989). To avoid oxidation product induced artifacts in biophysical studies or to investigate oxidative reactions as potential components of pathology, techniques are required to efficiently purify nonoxidized lipids and to separate and identify oxidation products.

The HPLC method of van Kuijk et al., (vanKuijk et al.1985a) developed for separating intact and oxidized phosphatidylcholine on an analytical scale was extended to purification of phospholipids with other head groups and modified for use on a preparative scale. Intact phospholipids absorb light strongly only in the far UV, near 205nm, so many common liquid chromatography solvents cannot be used with UV absorption monitoring. The methanol and 0.1% ammonium acetate mobile phase used here is sufficiently transparent to permit detection by phospholipid absorbance at 206nm. The isocratic system employed avoids column re-equilibration between runs and allows for relatively rapid separations.

Derivative UV spectroscopy was used to routinely characterize the presence or absence of oxidation products in samples before and after HPLC purification. Derivative techniques applied to UV spectroscopy greatly enhance

resolution and contribute to an increase in the reliability of detection for minor oxidized components compared to standard, zero-order UV spectroscopy (Butler & Hopkins, 1970). Lipid oxidation products have several characteristic features in the second derivative UV spectra and therefore, derivative spectroscopy was useful for rapid monitoring of crude or purified fractions to ascertain phospholipid purity.

Materials and Methods

Reagents. All solvents were HPLC grade from J.T. Baker Chemical Co. (Phillipsburg, NJ) and were used as received. HPLC grade ammonium acetate was from Fisher Scientific (Fair Lawn, NJ). The mobile phase solvent containing 0.1% ammonium acetate was filtered through a 0.5μm Millipore Type FH (Millipore Corp., Bedford, MA) filter prior to use. 1-Palmitoyl-2-docosahexaenoyl phosphatidylcholine 16:022:6PC, 1-palmitoyl-2-docosahexaenoyl phosphatidylethanolamine, 16:022:6PE, and a 1-palmitoyl-2-docosahexaenoyl phosphatidylserine/phosphatidic acid mixture/phosphatidylcholine, 16:022:6 PS/PA/PC, were obtained from Avanti Polar Lipids (Birmingham, AL).

Instrumentation. Chromatography was performed on a system composed of two Altex 110A pumps and a Beckman 210A sample injector. Initial separations were performed on a 4.6 × 250mm Alltech analytical column with a 20μL sample

loop operating at a flow rate of 1.5ml/min. Preparative separations were done on a 22.5 x 250mm Alltech preparative column with a 22.5 x 100mm guard column and a 2000µl sample loop at ambient temperature. All columns were packed with Alltech Adsorbosphere HS C18-7µm reversed-phase material. This is a high surface area packing with 60Å pore size and 20% carbon loading. A 100% methanol mobile phase containing 0.1% (w/w) ammonium acetate was delivered with two pumps, each at 8ml/min for a combined flow rate of 16ml/min. A typical preparative run required 30 minutes or less.

The column effluent was passed through two detectors in series. The first was a Hitachi Model 100-10 variable wavelength UV absorbance detector operating at a wavelength of 234nm. The second detector was an LKB 2238 Uvicord SII UV monitor equipped with a 206nm interference filter. The outputs of both detectors were displayed on a Hewlett Packard 7132A two pen recorder.

Second Derivative UV Spectroscopy

Ultraviolet absorbance and derivative spectroscopy were performed on a Shimadzu UV-3000 recording spectrophotometer. Fractions were collected from the HPLC effluent, aliquots were transferred to a quartz cuvette, and scanned from 190-300nm versus a mobile phase blank. Zero-order absorbance scans were typically recorded at 2.0-2.5 absorbance units full-scale while a range of 0.1 absorbance units was used for the second derivative spectroscopy. This expanded scale

provided a more sensitive enhancement of features of interest in the region 230-290nm even though the derivative of the peak at 206nm was off scale.

Results

Intact polyunsaturated phospholipids are colorless, but are observed to turn yellow if they oxidize and deteriorate. The yellow color results from conjugated double bond oxidation products (see Figure 5) whose UV absorption peaks tail into the visible region and absorb blue light. Figure 6A shows a UV absorption spectrum of rather heavily oxidized, yellowed 16:022:6PC with absorption maxima at 206, 234, and 275nm. Figure 7A shows an absorption spectrum of a colorless, freshly purified 16:022:6PC which retains the 206nm peak but is essentially devoid of absorption in the region of 230 to 290nm.

The oxidized products of the polyunsaturated phospholipids (such as those shown in Figure 5) are more polar than the native, intact lipids. The oxidized lipids can therefore be separated from the intact lipids by reversed-phase HPLC. Figure 8 shows a reversed-phase HPLC separation of 16:022:6PC from its oxidized products. The oxidation products were monitored at 234nm in Figure 8B and comprise a complex mixture of isomeric species that elute between 4 and 18 minutes. The intact, native phospholipids are monitored at 206nm in Figure 8A and elute at 23 minutes.

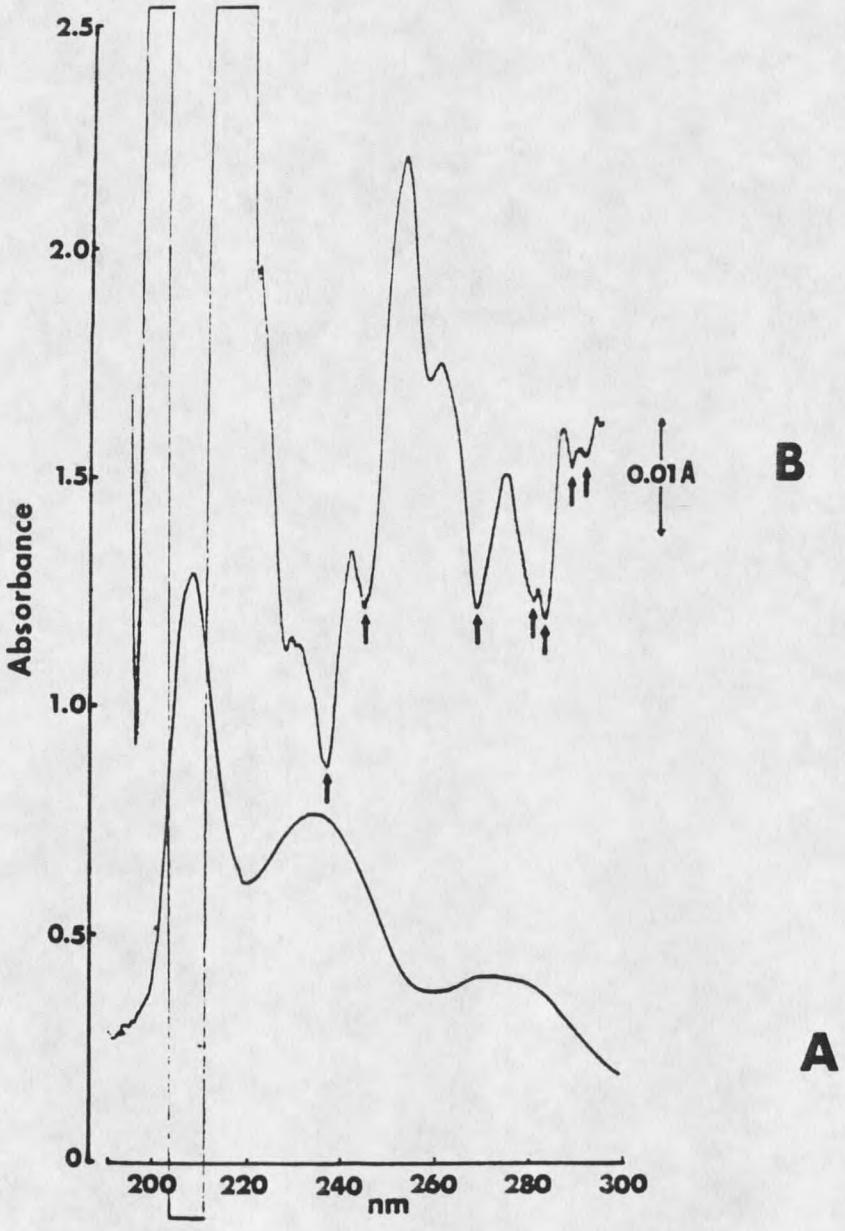


Figure 6. (A) Zero-order UV spectra and (B) second derivative UV spectra of partially autoxidized 16:022:6PC. A range of 2.5 AUFS was used for Trace A and a range of 0.1 AUFS for Trace B.

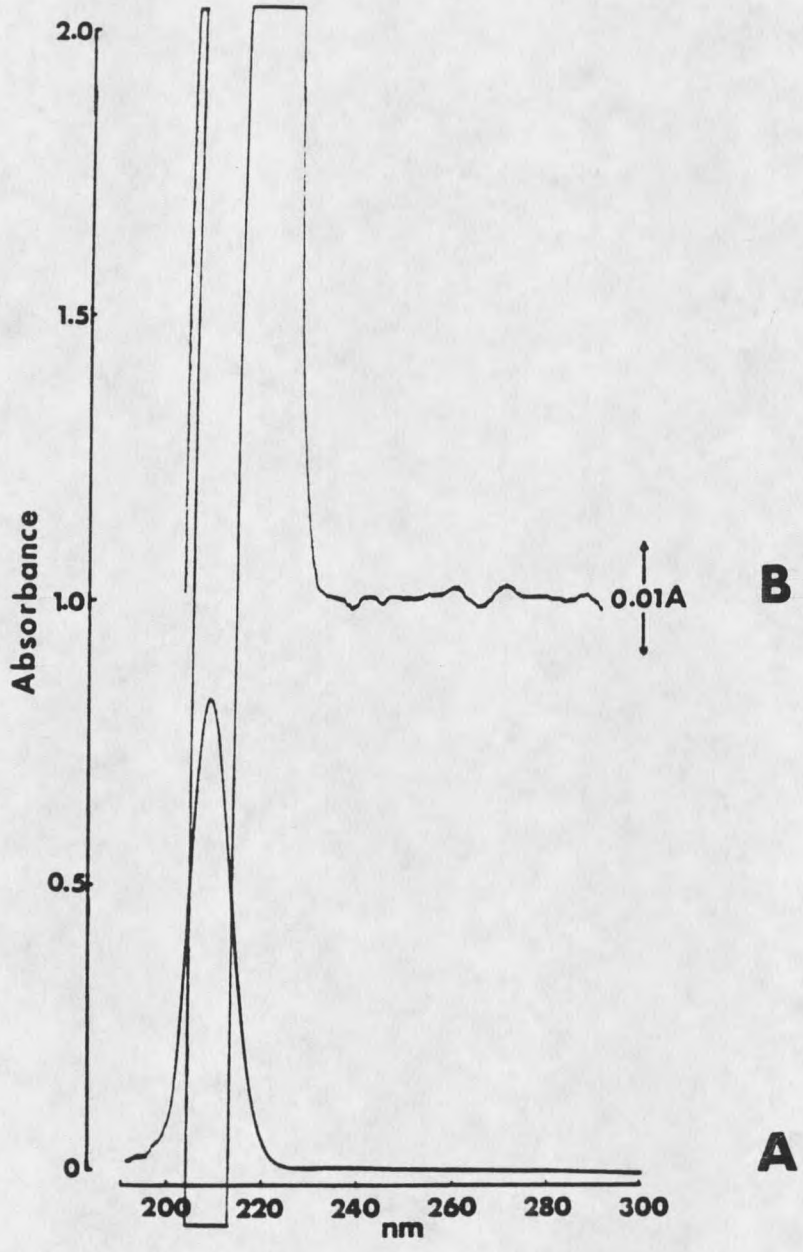


Figure 7. (A) Zero-order UV spectra and (B) second derivative UV spectra of a HPLC purified sample of 16:022:6PC. A range of 2.0 AUFS was used for Trace A and a range of 0.1 AUFS for Trace B.

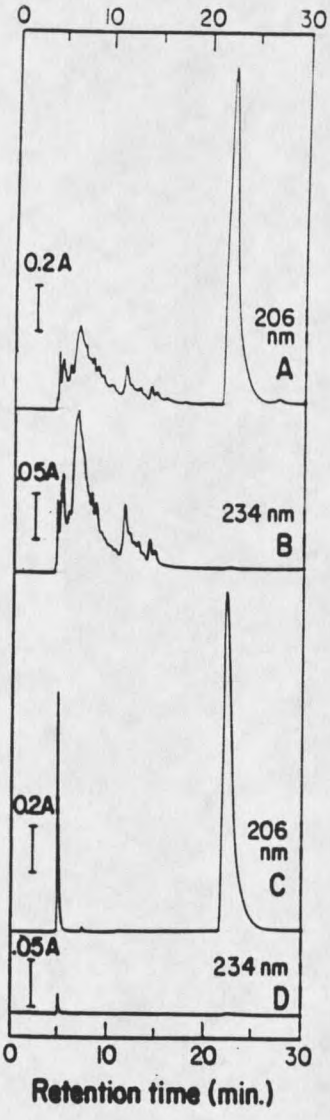


Figure 8. Preparative HPLC separation of 16:022:6PC from its oxidation products. Traces A and B were obtained by injecting 0.2mL of methanol containing 10 mg of partially oxidized phospholipid. The UV absorbance at 206nm was monitored in Trace A showing the diene oxidation products and the non-oxidized precursor phospholipid. Trace B shows only the oxidation products which absorb at 234nm. Traces C and D show chromatograms obtained by injecting 7 mg of freshly purified 16:022:6PC and monitoring at 206nm and 234nm, respectively. The first two peaks correspond to the solvent front and the added BHT in both traces.

A freshly purified 16:022:6PC fraction was collected from the HPLC and the methanol was evaporated to a small volume with argon. A small amount of the antioxidant, butylated hydroxylated toluene (BHT), was added (4μg) to obtain a lipid to BHT ratio of 500:1. The sample was rechromatographed as shown in Figure 8C and 8D. The single sharp peak at the solvent front is due to ammonium acetate which was concentrated from the eluant obtained during initial purification. The small peak at 7 minutes is due to BHT. Few peaks remain in the 234nm trace (Fig. 8D) due to the removal of the oxidized components by HPLC. The nonoxidized lipids monitored at 234nm also produced a small peak at 23 minutes due to a slight end absorption from the strong 206nm peak. HPLC purification of 16:022:6PE is very similar to that shown above for PC (data not shown). Both PC and PE could be purified on a preparative scale with typical sample loadings of 10mg or more per run.

The retention times of PS and PA differ by only 1.3 minutes. Thus, in the preparative purification of PS from the commercially supplied PS/PA/PC mixture, best separation was achieved with total sample loading of 5-6mg. The solubility of the PS/PS/PC mixture was poor in pure methanol. Adequate solubility of the mixture was obtained in methanol/ethanol, 2:1. A summary of retention times for phospholipids containing the head groups mentioned are shown in Table 1 for preparative and analytical columns.

Table 1. Retention Times for 1-Palmitoyl 2-docosahexaenoyl Phospholipids[a]

	Retention time (min)			
	Analytical column		Preparative column	
lipid head group	oxidized[b]	nonoxidized	oxidized[b]	nonoxidized
choline	1-7	11.5	4-18	23.6
ethanolamine	1-5	9.1	4-18	23.0
serine	1-5	7.0	4-10	16.4
phosphatidic acid	1-5	6.0	4-10	15.1

[a]Conditions as described in Materials and Methods

[b]The oxidation products include many isomers which elute over a range of retention times.

Traces of oxidation products could be recognized by characteristic "fingerprint" spectral features in the second derivative UV spectra. The second derivative spectra of heavily oxidized polyunsaturated PC is shown in Figure 6B. The position of the centroid minima in a second derivative spectrum corresponds to the peak maximum in conventional zero-order spectra. Peaks of interest are marked by arrows in Figure 6B. The absorption peak centered at 234nm has a shoulder at 242nm, both of which emerge as minima in the second derivative spectrum. The peak centered at 275nm has

spectral features and second derivative minima at 269, 281, 284, 289, and 292nm. These spectra are taken in the absence of the antioxidant BHT but if BHT were present it would produce minima at 220, 275, and 282nm in the second derivative spectra (data not shown).

Figure 7B shows a second derivative UV spectrum of freshly purified 16:022:6PC. The second derivative spectrum shows small features but they also occur in the instrument baseline and do not occur at wavelengths characteristic of oxidized, polyunsaturated phospholipids.

Discussion

The HPLC procedure described rapidly and completely separates polyunsaturated phospholipids from their oxidation products. An important advantage was gained by using HPLC columns with a high surface area/high carbon load C18 packing. This packing maximizes exposure of hydrophobic bonded phase and more strongly retained the nonoxidized fatty acid chains and increased their retention times whereas the more polar oxidation products experienced rather little retention on the hydrophobic stationary phase. The high carbon loading on the stationary phase extends the separation distance between the oxidized and nonoxidized lipids. Extended separation is an important feature when employing preparative HPLC where resolution obtained on an analytical scale often deteriorates on scale-up. Van Kuijk et al (vanKuijk et al.1985a) previously reported that the

addition of 0.1% (w/w) ammonium acetate to the methanol mobile phase greatly sharpens phosphatidylcholine peaks relative to a pure methanol mobile phase. This sharpening effect was confirmed in preparative HPLC on phosphatidylcholine and phosphatidylethanolamine. The HPLC procedure described here was also found to be useful for a slightly smaller scale separation of a mixture of polyunsaturated phosphatidylserine, phosphatidic acid, phosphatidylcholine and their oxidation products.

The reverse phase retention of phospholipid species is primarily due to interactions of their fatty acid side chains with the alkyl ligand of the stationary phase. Retention times increase as the total number of carbon atoms in the fatty acid chains increases. A decrease in retention times is observed as the number of double bonds in the fatty acid chains increases (Smith & Jungalwala, 1981). Thus, the method is also useful for the separation of phospholipids containing different fatty acids that may have been produced during the synthesis of the desired compound.

The addition of BHT is useful for inhibiting oxidation of the purified lipids after HPLC purification and a lipid to BHT molar ratio of 500:1 is recommended. However, UV spectroscopy on lipids is best performed prior to addition of BHT as it absorbs in the UV region of interest. The BHT is added as soon as possible after pure lipid fractions are collected from the HPLC effluent. Purified phospholipids

should be stored under argon at as low a temperature as possible. A freezer temperature of -120°C or -75°C is preferred.

Once polyunsaturated phospholipids are purified, it is desirable to have a routine procedure that can easily and accurately verify sample integrity without the need for chemical derivatization (vanKuijk et al.1985a; vanKuijk et al.1985b) or other extensive manipulation of these delicate compounds. Derivative UV absorption spectroscopy was found to be very useful for quickly indicating the presence or absence of oxidized polyunsaturated fatty acids directly on fractions collected from the HPLC effluent.

Standard zero-order UV spectra has relatively low sensitivity for detection of small amounts of oxidized lipids. In derivative spectroscopy small spectral features are accentuated, especially for second and higher derivatives (Fell, 1983). While this serves to reveal more spectroscopic information, higher derivatives also tend to amplify noise which may obscure the desired information. It was found that the second derivative was the best compromise between resolution enhancement and increased noise for the compounds of interest.

The derivative resolution is a selectable parameter with lower resolution leading to noise averaging. The spectrophotometer used in this study calculates the derivative by fitting a polynomial to seven data points. We

found that a derivative resolution of 3.5nm (0.5nm per point) reproduced all the features of the spectrum and the highest sensitivity for traces of oxidation products was obtained with 6.3nm resolution. Freshly purified lipid samples were found to be devoid of detectable oxidation products, judged by the absence of characteristic fingerprint peaks in the second derivative UV spectra (see Figure 7B).

Weenen reported UV absorbance values for autoxidized linoleic acid of 232.5nm for the purified *t,t* isomer and 236nm for the purified *c,t* isomers (Weenen, 1982; Porter et al.1979). Work by Corongiu et al. employed second derivative UV spectroscopy to distinguish between mixtures of *t,t* and *c,t* stereoisomers of conjugated diene fatty acid hydroperoxides in rat liver microsomes by their respective second derivative minima at 233nm and 242nm (Corongiu et al.1989). In the present study the *t,t* and *c,t* -diene stereoisomers of autoxidized 16:022:6PC were attributed to second derivative minima at 237 and 246nm, respectively (left two arrows in Figure 6). Presumably, the 4nm wavelength shift we observe compared to Corongiu et al. (Corongiu et al.1989) is due to additional unsaturation in the 22:6ω3 fatty acid used in our work.

Discrimination of oxidation product stereoisomers spectra also appears to occur among the conjugated trienes, where the broad peak centered around 275nm consists of up to

five detectable components as revealed by minima in the second derivative spectra. Using the rule that a *cis* conformation leads to longer wavelength absorption than the *trans* conformation (Williams & Fleming, 1980), the following assignments were proposed: the peak at 269nm is attributed to the *t,t,t* triene; *t,c,t* and *t,t,c* isomers are proposed to absorb at 281nm and 284nm; while the 289nm and 292nm peaks are thought to correspond to *c,t,c* and *c,c,t* triene isomers. The *cis* isomers tend to have lower extinction coefficients than the *trans* isomers, so the relative peak heights are not expected to directly reflect the relative amount of each product. Further work would be needed to firmly identify the stereoisomers responsible for the different second derivative minima.

The HPLC purification and UV spectroscopy characterization procedures described are rapid and straightforward and utilize equipment common to many chemical and biological laboratories. Purification and frequent monitoring are important to avoid oxidation product induced artifacts in studies requiring polyunsaturated phospholipids.

Phosphorous Assay

Quantitation of phospholipids was carried out with a slight modification of the method of Chen et al. (Chen et al.1956) to enhance sensitivity of detection of phosphorous

for small samples. This method is based on the color formed by the reduction of a phosphomolybdate complex. A typical sample generally contained 1-3µg phosphorous.

Samples containing phospholipid were pipetted into a graduated conical glass tube and taken to dryness under a stream of nitrogen for removal of organic solvents or by baking in a 100°C oven in the case of an aqueous sample. One drop of concentrated sulfuric acid was added to the dry sample and the tube was heated over a flame until white fumes of sulfur trioxide appeared. When the sample had cooled, 1 drop of 72% perchloric acid was added and the sample heated again until it was clear and colorless. After cooling, the volume was adjusted to 2mL with distilled water.

A mixture called Reagent C was prepared fresh for each analysis. It contained 1 volume 6M sulfuric acid, 2 volumes distilled water, 1 volume of 2.5% (w/v) ammonium molybdate, and 1 volume 10% (w/v) ascorbic acid. The ascorbic acid solution is stable for about 7 weeks at 4°C and was prepared accordingly. All other stock solutions are stable indefinitely at room temperature.

To each sample tube was added 2mL Reagent C. Tubes were mixed, capped with parafilm, and incubated in a 37°C oven for 2 hours. After cooling, absorbance was read in a Shimadzu UV-3000 spectrophotometer at 820nm versus a reagent blank. Total phosphorous was determined by comparison to a

standard phosphorous curve. Periodically, standards were run simultaneously with samples to ensure accuracy of the standard curve.

Gas Chromatography

It is desirable to frequently monitor the integrity of the 22:6 fatty acid due to its extreme sensitivity to oxidation. A convenient and informative way to quantitate the amount of 22:6 is by transesterification of the fatty acid portions of the phospholipid into fatty acid methyl esters (FAME's). These volatile products can be analyzed and quantitated by gas chromatography. Integrity of the 22:6 fatty acid can be estimated by comparison of peak areas for $16{:}0_{d31}$ and 22:6. The molar ratio of $16{:}0_{d31}$ to 22:6 is 1:1 so each fatty acid should produce an equal detector response when corrected for number of carbons. Comparing the peak areas for $16{:}0_{d31}$ and 22:6 reveals the gross percentage, if any, of 22:6 that oxidized over the course of an experiment. This is not a very sensitive method of detecting oxidative loss of 22:6 but it did serve to monitor the gross integrity of the sample, particularly when it was part of a complex mixture such as in native or reconstituted membranes.

Fatty acid methyl esters were prepared by treatment of phospholipid extracts (vanKuijk et al.1985a) with 14% boron tri-fluoride in methanol (Morrison & Smith, 1964). They

were analyzed on a Perkin-Elmer 3220 gas chromatograph equipped with 4 foot packed columns containing either Supelco SP2330 or SP2100. Peak separation was optimized with a temperature gradient of 160°C to 220°C at 4°C/min using helium as the carrier gas. To quantitate total lipid in the extract, an internal standard of 17:017:0PC was added to the extract and subjected to the transesterification procedure. The 17:0 fatty acid is not naturally occurring so there is no danger of the internal standard co-eluting with a native fatty acid. The 17:0 FAME elutes between $16:0_{d31}$ and 22:6 and is well separated from both.

Thin-Layer Chromatography

As discussed in the earlier section on HPLC, it was necessary to purify the phosphatidylserine from a crude reaction mixture containing phosphatidic acid, phosphatidylserine, and phosphatidylcholine.

In order to identify the location of PS in the reverse phase elution profile, thin-layer chromatography (TLC) was used with ninhydrin detection. Approximately 5 μg of the crude reaction mixture was applied to a TLC plate coated with C18-bonded silica. A mobile phase of 0.1% NH_4OAc in methanol, identical to that used for the HPLC described previously, was used to elute the lipids. The dried plate was developed by spraying with 0.25% ninhydrin in a 9:1 mixture of acetone and pyridine. Detection with ninhydrin

is specific for free amino groups which appear as a purple spot on a TLC plate. In the crude mixture, only the phosphatidylserine would be detected with ninhydrin. Thus, two plates were loaded identically and run simultaneously. One plate was developed with ninhydrin and the other developed with iodine vapor. Iodine is a nonspecific reagent that reveals the location of all three species in the mixture. Using this combination, it was determined that phosphatidylserine elutes as the second peak after the solvent front and BHT in both the reverse-phase TLC and HPLC elution profile. Phosphatidylserine elutes after phosphatidic acid and before phosphatidylcholine.

Mass Spectrometry

Even with the variety of chromatographic techniques available, characterization of complex lipids is still a challenging task. Mass spectrometry represents a powerful technique for the study of both intact phospholipids and fragments of these compounds. Very significant advances have taken place in recent years in mass spectrometry for biochemical applications in the area of ionization techniques.

Early work used electron ionization (EI) for analysis of the fatty acid portion of complex lipids after esterification to form fatty acid methyl esters (Jensen & Gross, 1988). However, molecular ions are formed in low

abundance and information is gained regarding only the acyl portion of the molecule. The low volatility of phospholipids and their susceptibility to thermal degradation makes EI unsuitable for direct analysis of phospholipids.

A lack of molecular ions also afflicts the chemical ionization (CI) spectra of intact phospholipids, especially those of higher molecular weight (Games, 1978). Heat must be applied to vaporize the sample and thermal degradation often occurs.

Field desorption (FD) has been a useful technique for producing abundant phospholipid molecular ions (Jensen & Gross, 1988). The ionization process results in a much smaller quantity of internal energy being applied to the molecule than EI, reducing fragmentation. It also differs from EI and CI in that the sample is ionized without prior vaporization, making it a much softer method of ionization. However, the sensitivity of FD is very difficult to predict since markedly different sensitivities are obtained with different compounds. Field desorption can be quantitative but is limited by difficulty with reproducibility of conditions. Problems arise in FD when samples are contaminated with alkali metals, particularly sodium (Games, 1978; Jensen & Gross, 1988). Intermolecular methyl group transfer can also create ambiguities for assigning molecular weight.

Since its development in the early 1980's, fast atom bombardment (FAB) has proven to be a very useful desorption technique for many labile biomolecules. FAB gives a more stable spectrum over a considerably longer time scale with reasonably constant sensitivity and has a mass spectrum that is more reproducible and less sensitive to instrumental characteristics than other desorption techniques. Positive and negative ion FAB spectra of phospholipids have been produced by choice of an appropriate matrix (Jensen et al.1986; Munster et al.1986; Dasgupta et al.1987). The matrix serves to solubilize the compound and provide a source of ions. In many cases, FAB spectra are characterized by an abundance of $(M+H)^+$ or $(M-H)^-$ ions and a limited amount of fragmentation. It is for this reason that FAB is often used for molecular weight determination. With use of isotopically-labeled internal standards, which are often not available, FAB can be used quantitatively.

Although FAB analysis of phospholipids has many attractive features, one must be aware of the potential problems of matrix effects. A number of interferences and artifacts can affect the formation and/or detection of ions from the liquid sample and markedly complicate the spectra (Caprioli, 1988). These include high chemical background (from the matrix), addition of salts to molecular ions, suppression of ion currents by other compounds, and ion cluster formation, all of which may complicate

interpretation of data. In practice, these problems make conventional probe FAB unreliable for monitoring sample purity.

Some of these undesirable effects in FAB have been significantly reduced by use of a technique called continuous flow FAB (CF-FAB). This technique makes use of liquid samples having 80-95% solvent and much reduced matrix, 5-20%. The basic principle of operation involves the balance of the flow of liquid to, and evaporation from, the sample stage of the insertion probe in the source of a FAB mass spectrometer. A narrow bore (e.g. 75μm) fused silica capillary is used to deliver the liquid to the probe tip. Many mass spectrometer source vacuum pumps can handle a solvent flow of up to 10μL/min. Extensive sample handling can be eliminated since injections can be accomplished directly or by coupling the CF-FAB probe to an HPLC system (Games et al.1988; Ito et al.1985; Ashcroft et al.1987).

Several performance benefits have been noted when the CF-FAB probe is used for sample introduction as compared to the standard FAB probe. Mass spectra show a significantly lower background, primarily as a result of the higher solvent (and thus lower matrix) content of the solutions being analyzed (Caprioli, 1988). Thus, more detail can be seen in the FAB mass spectrum and a much lower detection limit may be achieved. A second benefit of the CF-FAB probe is a greatly decreased ion "suppression" effect, i.e., the

suppression of the signal of one compound in a mixture by another that preferentially occupies the surface of the sample droplet, even though the two may be present in equimolar concentrations (Caprioli, 1988). An ion chromatogram is generated and with an internal standard, peak areas can be used as a measure of sample concentration.

Progress was made in this laboratory using CF-FAB to ascertain phospholipid composition and purity. A mobile phase of 9:1 v/v methanol and triethanolamine was used for negative ion FAB and 9:1 v/v methanol and 3-nitrobenzyl alcohol for positive ion FAB. The mass spectra were characterized by abundant molecular ions and low background noise. A few representative spectra are shown in Figure 9.

It was initially hoped that the FAB mass spectral data could be used to ascertain the purity of phospholipids in terms of the oxidation products that may have been present. In some rather heavily oxidized samples, we were able to observe mass peaks corresponding to oxidized lipids, but it was difficult to determine if the method was really sensitive enough for detecting trace amounts of unstable oxidation products. However, molecular ions of the intact species did provide important information regarding the perdeuteration of the sn-1 fatty acid, which was incorporated during synthesis of the phospholipids, as well as the identity of the sn-2 fatty acid. In summary, the relatively high sensitivity, unambiguous spectra, and low

amount of sample handling required of CF-FAB make it a desirable method for verifying structural composition and intactness of phospholipids.

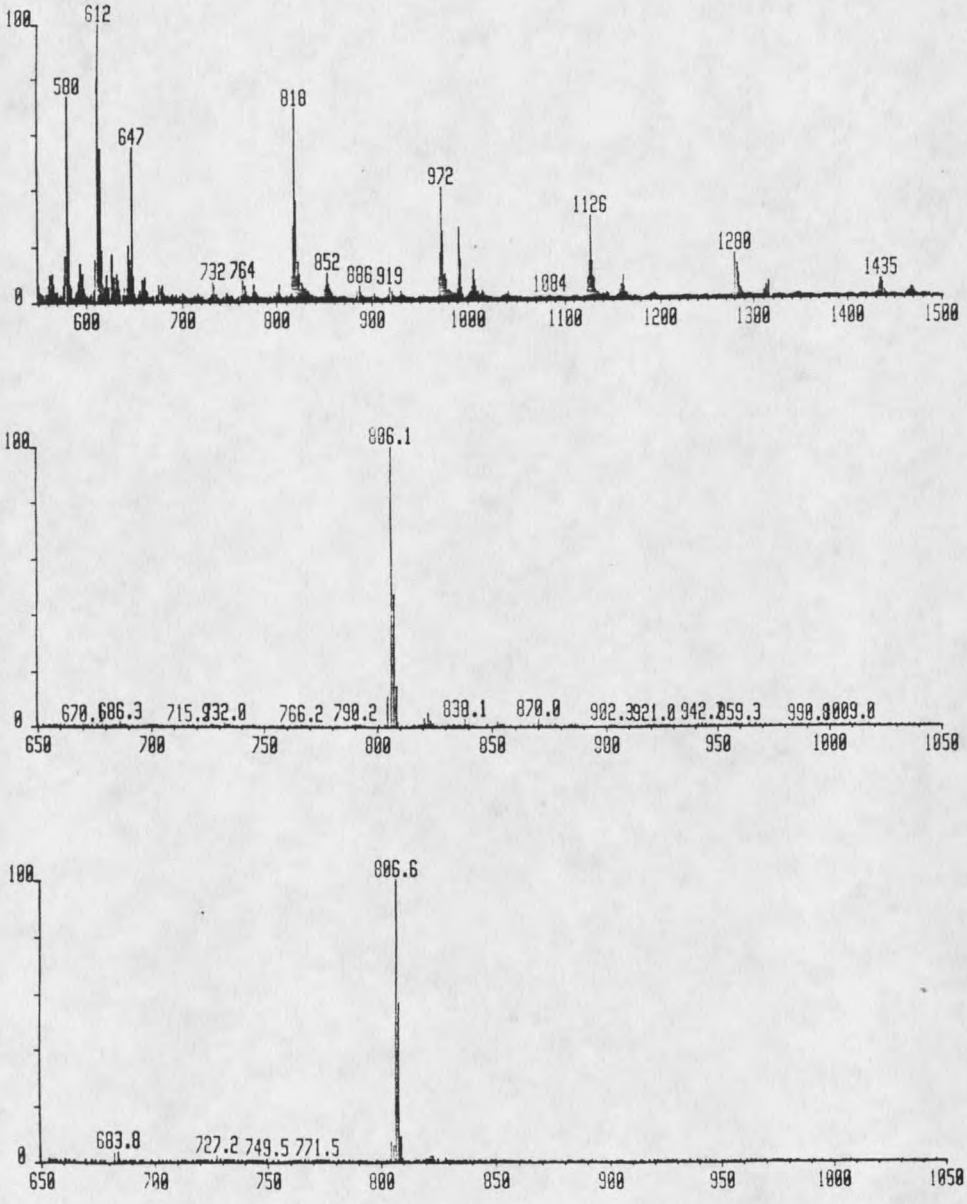


Figure 9. A comparison of FAB+ and CF-FAB+ mass spectra of phospholipids. The top trace corresponds to a FAB mass spectrum of 16:022:6_{d12}PC (MW=817) obtained using a dithiothreitol/dithioerythritol (1:1) matrix. The peaks at masses 972, 1126, 1280, and 1435 result from matrix ion additions to the molecular ion. The middle and bottom traces are CF-FAB spectra of 16:022:6PC (MW=805) using a methanol/3-nitrobenzyl alcohol (9:1) mobile phase. The sample in the middle trace was contaminated with lipid oxidation products and the sample in the bottom trace was freshly purified.

PURIFICATION OF RHODOPSIN AND PREPARATION OF RECONSTITUTED MEMBRANES

Protein Purification

Frozen, dark-adapted, bovine retinas were purchased from J.A. Lawson, Lincoln, NE. Unless otherwise stated, all preparations involving rhodopsin were carried out at 4°C under dim, red light. For the initial crude isolation of ROS membranes from the retinas we utilized the "shakate" preparation (Stone et al.1979). 50 or 100 retinas were thawed in the collection solution of 43% buffered sucrose (see HEPES buffer composition given below). Stirring with a glass rod broke up the lumps of retinas. Retinas were transferred to a 250mL plastic centrifuge cone with a screw top cap and shaken hard for several minutes. The percent sucrose was checked with a refractometer and adjusted to 34.5±0.5% sucrose. After a 5 minute centrifugation at 5000 rpm in a Sorvall SS34 rotor, the supernatant was collected and diluted with 4 volumes of 10mM HEPES containing 0.1mM CaEDTA and 0.15M NaCl, pH 7.4. The supernatant was spun at 15000 rpm for 20 minutes to pellet the crude membranes.

A further purification of the ROS membranes was accomplished with step-float sucrose gradients (Raubach et al.1974). The pelleted membranes from the shakate preparation were resuspended in 100mL of 34% buffered sucrose. The suspension was diluted to 31% sucrose with

HEPES buffer. The final volume was adjusted to 216mL with additional 31% sucrose and divided evenly into six 38mL centrifuge tubes. The ROS membrane suspension in each tube was overlaid with 2mL HEPES buffer and centrifuged for 2 hours at 4°C at 25K rpm in a Beckman L3-50 Ultracentrifuge using an SW-28 swinging bucket rotor. After centrifugation, the membranes at the sucrose-buffer interface were collected with a teflon needle and pooled. Membranes were washed twice with water and finally with 20mM PIPES buffer, pH=6.5, containing 1mM $MgCl_2$, 1mM $CaCl_2$, 1mM $MnCl_2$, and 150mM NaCl. For experiments requiring native ROS membranes, purification was complete at this step.

For experiments requiring reconstituted membranes, a final purification of rhodopsin was required to remove native phospholipids and other trace membrane proteins. We chose to do this via affinity chromatography on immobilized concanavalin A generally following the method of DeGrip, et al. 1980. The pelleted, washed, membranes from the step-float gradients were solubilized in ice-cold 100mM β-nonyl-glucose detergent (approx. 55nmol rhodopsin/mL detergent) by stirring for 3 hours. Any remaining turbidity was cleared by sonication. This solution was diluted to 50mM detergent with PIPES buffer. Approximately 50mg rhodopsin was applied to a column containing 12mL settled Con-A gel (Sigma Chemical Co., St. Louis, MO) containing 14mg lecithin per mL settled gel. Protein was applied to the column at a flow

rate of approximately 8mL/hr. Nonbound materials (non-glycoproteins and lipids) were eluted first with 10 column volumes of 20mM detergent/20mM PIPES buffer at 9ml/hr. Bound rhodopsin was eluted next with approximately 1 column volume 200mM α-methylglucose. The flow was stopped and the column allowed to equilibrate for 2 hours before flow was resumed. Interrupted flow allowed the exchange of rhodopsin for α-methylglucose on active column sites and a more thorough elution of rhodopsin. The column eluate was passed through a UV detector with a 280nm filter and fractions collected with a Gilson fraction collector. Fractions containing rhodopsin were pooled and absorbance spectra taken on an aliquot. The rhodopsin content was quantitated by the absorbance at 500nm using an extinction coefficient of $40,500 M^{-1}cm^{-1}$ and a molecular weight of 36,000g/mol for rhodopsin. Finally, the column was washed with PIPES buffer containing 1M NaCl to remove residual aspecifically bound material. The column was stored in PIPES buffer containing 1M NaCl at 4°C until its next use.

Pooled fractions containing rhodopsin were concentrated to a volume of approximately 20mL by pressure filtration using Amicon YM10 ultrafiltration membranes. If rhodopsin was not to be used immediately, it was stored, under argon, at -100°C.

Rhodopsin Reconstitution with Phospholipids

This step of the preparation brings together delipidated rhodopsin with purified, synthetic phospholipids. We chose to do this by combining the two under detergent solubilizing conditions and subsequently removing the detergent by dialysis. Phospholipids in methanol were taken to dryness by rotary evaporation in a round bottom flask. On ice and under argon, 40mM detergent was added to the phospholipid film until the suspension cleared indicating that all phospholipids had solubilized (approx. 1mL detergent per 5mg lipid). The mixture was stirred on ice for 1-2 hours. An appropriate amount of detergent solubilized rhodopsin was added to the lipids and stirring continued on ice for another 1-2 hours.

This mixture was poured into Spectra/Por dialysis tubing having a molecular weight cutoff of 6-8000. Before use, dialysis tubing was treated by boiling it in a solution of 10mM EDTA and 50mM Na_2CO_3 to remove any metals. Dialysis was carried out in a 4 liter container that was wrapped with black tape to keep it dark. It was fitted with an air stone and a black gas escape tube to allow continuous bubbling with argon to maintain an inert atmosphere. The bubbling also stirred the contents. The rhodopsin mixture was dialyzed against 5mM PIPES buffer, pH 6.5. The buffer was changed 2-3 times daily and dialysis was continued for 1

week in a 4°C cold room. Residual detergent remaining in a reconstituted membrane could lead to artifacts in NMR experiments. Since there is no simple way to monitor residual detergent after dialysis, our approach was to exhaustively dialyze.

After dialysis was complete, the dialysis contents were harvested by centrifugation at 40,000rpm for 30 minutes in a TI60 Beckman rotor. The reconstituted membranes were collected as a pellet in the bottom of the centrifuge tube. To adjust the pH, 1-5mL of an appropriate buffer was added to the centrifuge tube and clumps of membrane were broken up with a glass stirring rod or by vortex mixing. The mixture was allowed to equilibrate overnight to ensure a uniform pH environment. For samples requiring a pH between 5.5 and 6.5, a 20mM succinate buffer containing 100mM KCl, 2mM $MgCl_2$, 1mM EDTA, and 100μM DTT (dithiothreitol) was used. For samples requiring a pH between 7.0 and 8.0, an otherwise identical buffer containing 20mM HEPES was used.

The final step in the sample preparation was to load the membranes into the NMR sample tube. For best NMR signal to noise, it was desirable to load as much sample as possible into a 5mm diameter tube. For this reason we used ultracentrifugation to load sample aliquots into 5x41mm, 800μL, polyallomer centrifuge tubes. Membranes were centrifuged at 40,000rpm in an SW-55 rotor with adapters for the 800μL tubes. After a spin, the supernatant was drawn

off and another aliquot loaded. In this way, we could easily load 20-30mg of membranes into a small volume of approximately 250-300μL. The tube length was cut to fit the transverse NMR coil, capped with a natural rubber cap, and stored under argon at 4°C until use.

ABSORBANCE SPECTROSCOPY ON NATIVE ROS AND RECONSTITUTED MEMBRANES

Introduction

Rhodopsin belongs to a super family of receptors that couple external stimuli to internal cellular responses via a G-protein amplifier or link. The external stimulus in this case is a photon of light which is absorbed by rhodopsin. Absorption of light converts rhodopsin to an activated conformational state, rho*, which is capable of activating the G-protein, transducin or G_t. The α-subunit of G_t activates the cGMP phosphodiesterase (PDE). This cascade of events is amplified because one rho* can catalyze the activation of several hundred G-proteins and each activated PDE can hydrolyse over 1000 cGMP per second. As cGMP is depleted the cGMP dependent ion channel closes to produce membrane hyperpolarization - the cell signal that ultimately may be transmitted to the brain (Applebury, 1987).

The absorption of light by rhodopsin causes very rapid isomerization of the 11-*cis* configuration of retinal to the all-*trans* form. Light initiates the well known bleaching cascade, a series of spectrally identifiable rhodopsin intermediates (see Figure 2). The spectral intermediates represent retinal-protein interactions as well as reflecting rhodopsin conformation changes (Ostroy, 1977). The first

photoproduct, bathorhodopsin, forms in picoseconds and thermally decays to lumirhodopsin in nanoseconds. Metarhodopsin I is in a pH and temperature dependent equilibrium with MII above -15°C (Matthews et al.1963; Ostroy, 1977). MII is the intermediate believed to be the active conformation of rhodopsin that interacts with G_t (Kibelbek et al.1991). MII decays slowly to MIII (minutes at 37°C) and/or directly to opsin and all-*trans* retinal (Ostroy, 1977). There is evidence that MII is in equilibrium with MIII (Kibelbek et al.1991; Chabre & Breton, 1979) and that MIII may be an energy storage side pathway that is favored under very high rates of bleaching (Chabre & Breton, 1979). Intermediates beyond MI may decay to NRO, N-Retinylidine-Opsin, the protonated (λ_{max}=440nm) or deprotonated (λ_{max}=365nm) forms of the Schiff's base link, a pathway which becomes more favorable under acid (pH<4) or base conditions (pH>7.7) (Ostroy, 1977; Blazynski & Ostroy, 1981). The NRO species maintain a characteristic Schiff's base absorbance spectrum which represents the chromophore-lysine amino group linkage with no evidence of secondary interactions due to the protein. Finally, all-*trans* retinal dissociates from the protein, and the retinal-free protein is called opsin.

As stated earlier, the retinal binding site appears to be well protected in native rhodopsin. The binding site does not react with the water soluble Schiff's base reducing

agent, sodium borohydride, in rhodopsin. Also, the rhodopsin visible absorption spectrum shows no changes over the pH range from 4 to 8 (Radding & Wald, 1956). In the native state, the retinal binding site is well established to be a protonated Schiff's base bond (Lewis et al.1973; Bownds & Wald, 1965; Fager et al.1972).

Significant conformational changes appear to occur during the thermal decay of MI to MII (Rothschild et al.1987). MII is the first stage that sodium borohydride or water soluble amines will react with the binding site (Bownds & Wald, 1965) which is buried deep inside the protein. MI and MII are in a pH-dependent equilibrium with acid, high temperature, and glycerol favoring MII (Matthews et al.1963; Blazynski & Ostroy, 1984; Parkes & Liebman, 1984). The pressure reversibility of the MI to MII transition is consistent with a protein conformational change resulting in an increased volume for the MII•lipid complex (Lamola et al.1974). Reaction parameters for the MI to MII transition are also indicative of substantial conformation and charge disordering processes. The enthalpy of activation ($\Delta H^{\ddagger}$) is 36-41kcal/mol and the entropy of activation ($\Delta S^{\ddagger}$) is +75-90cal/degree per mol (Ostroy, 1977) for the MI $\rightarrow$ MII transition.

Further conformational changes are evident during the thermal decay of MII. During the thermal decay of MII to MIII, two additional sulfhydryl groups of the protein become

exposed to reagents simultaneously indicating a conformational change (Kimble & Ostroy, 1973). Linear dichroism shows a rotation of the retinal chromophore during the MII ↔ MIII transition (Chabre & Breton, 1979) which is also consistent with a protein conformational change.

There is substantial evidence that MII is the functional equivalent of the activated form of rhodopsin, rho* (Kibelbek et al.1991; Emeis et al.1982; Bennett et al.1982). For example, binding of G_t to MII shifts the MI ↔ MII equilibrium towards MII presumably by forming a tight MII·G_t complex which is stable almost indefinitely in the absence of GTP or a GTP analog (Emeis et al.1982). Recent work by Kibelbek, et al. (Kibelbek et al.1991) has shown that G_t can also stabilize MII formed from the MIII pool and will induce a shift in the MII ↔ MIII equilibrium back towards MII. This result supports the existence of a dynamic equilibrium between MI, MII, and MIII previously suggested by others (Chabre & Breton, 1979; Ostroy, 1977; Bennett, 1980; Baumann & Zeppenfeld, 1981)

In this study we are interested in changes in the lipid bilayer associated with protein conformational changes, thus it is desirable to produce and maintain the protein in the intermediates that are associated with the largest protein conformational changes. To accomplish this, we adjusted the conditions of the system, i.e., temperature and pH, to optimize production and stability of the desired

intermediates and monitored them by UV/VIS absorbance spectroscopy.

In native membranes, MI and MII coexist in a pH dependent equilibrium (pK_a = 6.5 at 4°C (Matthews et al.1963)) containing significant fractions of each species. In the transition from MI to MII rhodopsin takes up a proton from the surroundings. Adjustment of the pH to less than 6.5 has been shown to shift the equilibrium direction towards MII (Parkes & Liebman, 1984; Matthews et al.1963). The MI $\leftrightarrow$ MII equilibrium is also temperature dependent and has a pK_a of ~7.2 at 37°C (Leibman, P., personal communication).

An additional consideration in the production of rhodopsin intermediates is preventing or slowing their decay to the dissociation of the chromophore from the protein to form retinal + opsin. Our NMR experiments required a relatively extended time period (hours) to collect data so high stability of MII equilibrium products was essential. After several NMR experiments at 4°C that showed little change in bilayer thickness after bleaching, we began to more closely investigate the stability of the MII species for extended periods of time in PC vesicles.

We turned to the literature to explore lowering the temperature such that MII would still be formed but its decay may be slowed down. It was important that this temperature be above the phase transition of the

phospholipids used in the preparation, approximately -13°C for the pure lipids (Barry et al.1991), so that they would remain in the fluid phase. It is known that the addition of protein to a pure lipid bilayer will broaden the phase transition of the lipids compared to pure lipid bilayers (Deese et al.1981), an experiment which we repeated and will be reported in a subsequent chapter on ^{2}H NMR results.

Work by Blazinski and Ostroy (Blazynski & Ostroy, 1984) showed that when a rhodopsin solution in 50% glycerol was bleached at -13.5°C, its absorption spectrum showed a MI $\leftrightarrow$ MII equilibrium mixture that was approximately 65% MII at pH 6. The MI $\leftrightarrow$ MII equilibrium was stable indefinitely and would not proceed to retinal + opsin when the temperature was maintained at -13.5°C; however, MII did decay at higher temperatures. We wished to extend this method of stabilizing MII to our absorption (and ultimately NMR) experiments but wanted to eliminate glycerol from the sample preparation. The drawback to added glycerol in the preparation is that glycerol is known to alter the ratio of MI and MII could introduce artifacts to the experiment (Matthews et al.1963). An alternative to adding glycerol to a liquid sample is to use a short path length optical cell designed to allow scanning through a thin layer of relatively solid material. This approach to monitoring rhodopsin bleaching intermediates at low temperatures is desirable because it allows the sample to exist in the

identical conditions, i.e., temperature, concentration, and composition as is later used in the solid state NMR experiments.

Absorption spectra were utilized to provide information on the identity of the intermediates that were present at a given time. The purpose of the absorption spectroscopy experiments to be described was to characterize the spectral intermediates of reconstituted membranes and to allow selection of conditions optimized to enhance and stabilize MII and other intermediates near it by manipulation of the temperature and pH. Characterization of the absorption profile of the reconstituted membranes under NMR compatible conditions and time scale were crucial to meaningful interpretation of later NMR data.

Experimental

Absorption measurements done at 4°C utilized a black-sided quartz cuvette with a 1cm path length. Buffered membrane solutions were approximately 0.001-0.01mM in rhodopsin concentration. Temperatures of -13.5°C required the measurements to be carried out on a thin sample of membrane pellet using an appropriate cell. The thin layer absorption cell consisted of a pair of quartz plates that were held together by a spring loaded clamp (Starna Cells, Inc., Atascadero, CA). The assembly fits into a standard cuvette holder. One plate contained a chamber that was

0.1mm thick and held up to 30μL sample. 20-30μL of sample pellet were loaded into the cell with a positive displacement pipet. Rhodopsin concentrations were typically on the order of 1mM.

Solution or solid samples were inserted into a pre-cooled sample holder of the spectrophotometer and allowed to equilibrate for 15 minutes or up to 1 hour if the temperature was to be maintained at -13±1°C. Quartz absorbance cuvettes were cooled to the desired temperature in a thermally jacketed cuvette holder of the spectrophotometer. The sample was bleached in place in the spectrophotometer sample chamber with a light pipe connected to a halogen lamp illuminator having a long wavelength pass yellow filter with a 525nm cutoff. Absorbance measurements were made on a Shimadzu UV-3000 recording spectrophotometer interfaced with a personal computer. Data was processed using Spectracalc software (Galactic Industries, Salem, NH). This software contained routines to process absorbance data such as: smoothing, subtraction of a scattering baseline, difference spectra, curve-fitting, and plotting on an HP7550 plotter or graphics printing on a Postscript laser printer.

Results

Absorbance measurements were taken on aliquots of rhodopsin membranes to determine production and stability of MII species over time scales compatible with our NMR

experiments. Native membranes were used to gain experience with the thin layer absorption cell and to explore conditions under which to bleach reconstituted membranes. Subsequent experiments on reconstituted systems were carried out using conditions similar to those used on native ROS. Representative data and results are reported in the following section.

Membranes Reconstituted with $16:_{d31}22:6$PC

Visible absorption spectra taken on reconstituted membranes containing $16:0_{d31}22:6$PC and rhodopsin will be summarized by description of a representative set of data. An aliquot of $16:0_{d31}22:6$PC/rho (50:1) was added to a succinate buffer, pH 5.5, to yield a solution concentration of approximately 0.005mM. After taking several absorption measurements it was bleached for a total of 2 minutes at 5°C. The irradiation was performed in 30 second intervals which showed that bleaching was complete after 30 seconds. Absorption spectra were taken periodically for 3 hours after bleaching. The series of spectra are shown in Figure 10. Generally, there appears to be a decay in the MI species absorbing at 480nm, an increase of the species absorbing at 380nm, with possible contribution from MIII absorbing at 465nm.

A better indication of individual species present is obtained by deconvolution of the equilibrium mixture of

peaks into the individual contributors with a mathematical fitting program. Subtraction of a pure rhodopsin spectrum from a particular post-bleach absorbance scan results in what is called the difference spectrum which has residual scattering contributions essentially eliminated. Rhodopsin absorption can also be subtracted leaving only absorption signals attributable to the rhodopsin intermediates present. Using a routine in SpectraCalc called curvefit, we were able to deconvolute the difference spectra generated from absorption peaks shown in Figure 10 reasonably well. We found that the best fit peaks contributing to the overall absorption profile had absorption maxima centered at 480nm, 465nm, 440nm, 387nm, and 380nm corresponding to MI, MIII, NRO, retinal, and MII, respectively. These are the generally accepted maximums for the respective intermediates (Blazynski & Ostroy, 1984; Ostroy, 1977) and they were included as a "fixed" parameter in the curve fitting. The peak widths were also fixed at 100nm for MI and 80nm for the remaining intermediates (Kibelbek et al.1991). The distributions observed within 5 minutes after bleaching and 3 hours post-bleach are shown in Figures 11 and 12 respectively.

The large peak centered at 387nm, peak 6, in both fitted spectra (figures 11 & 12) suggested that bleached rhodopsin in 16:0_{d31}22:6PC membranes rather quickly decays to retinal + opsin at 4°C. Other contributors to absorbance

intensity correspond to smaller amounts of MI, MII, MIII, and NRO_{440}.

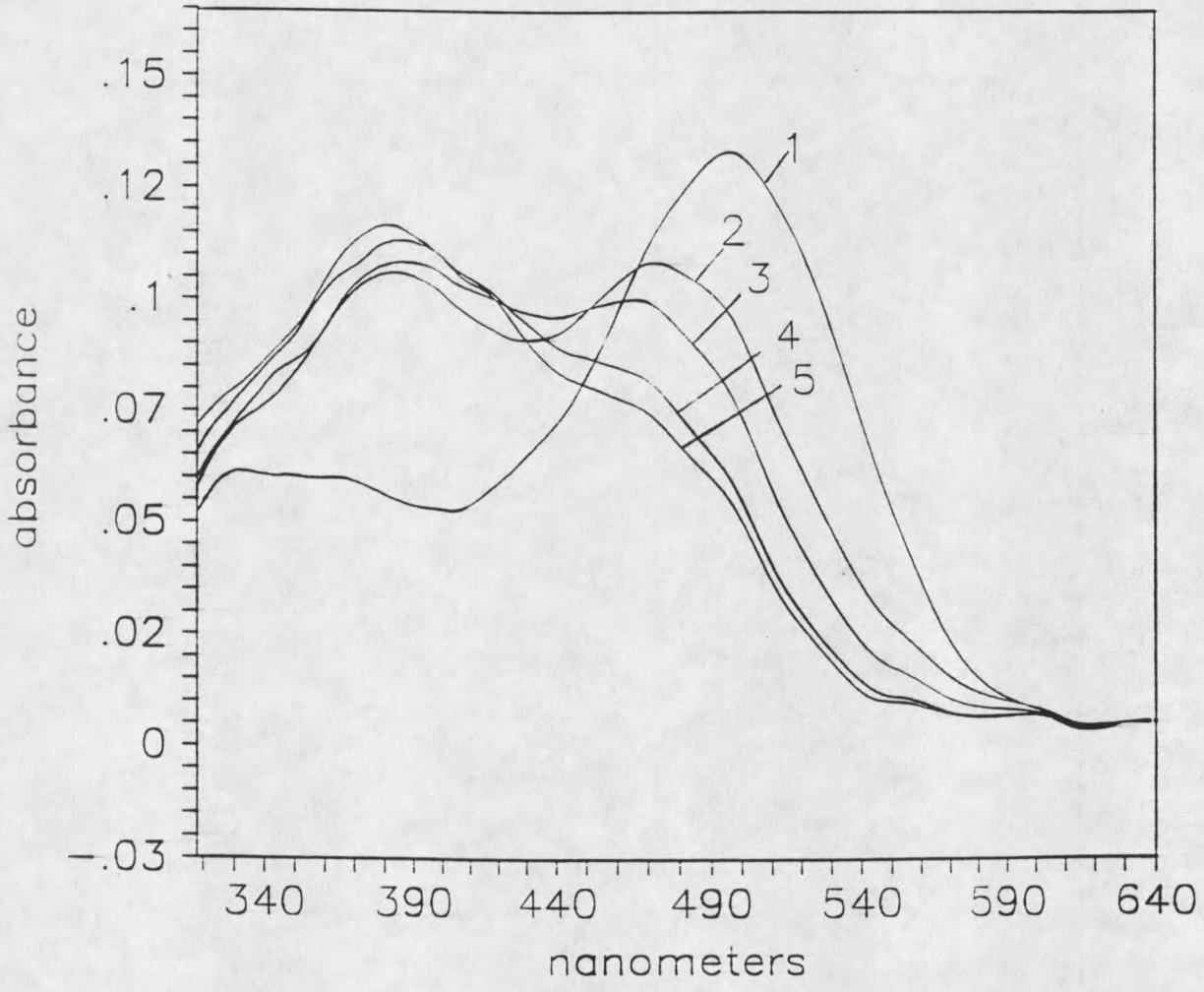


Figure 10. The absorption spectrum for the reconstituted membrane containing $16:0_{d31}22:6$PC/rhodopsin (lipid:protein, 50:1) was monitored for 3 hours after bleaching. Curve 1 was taken before illumination, and curves 2-5 were taken 5 minutes, 45 minutes, 2 hours, and 3 hours, respectively, after illumination.

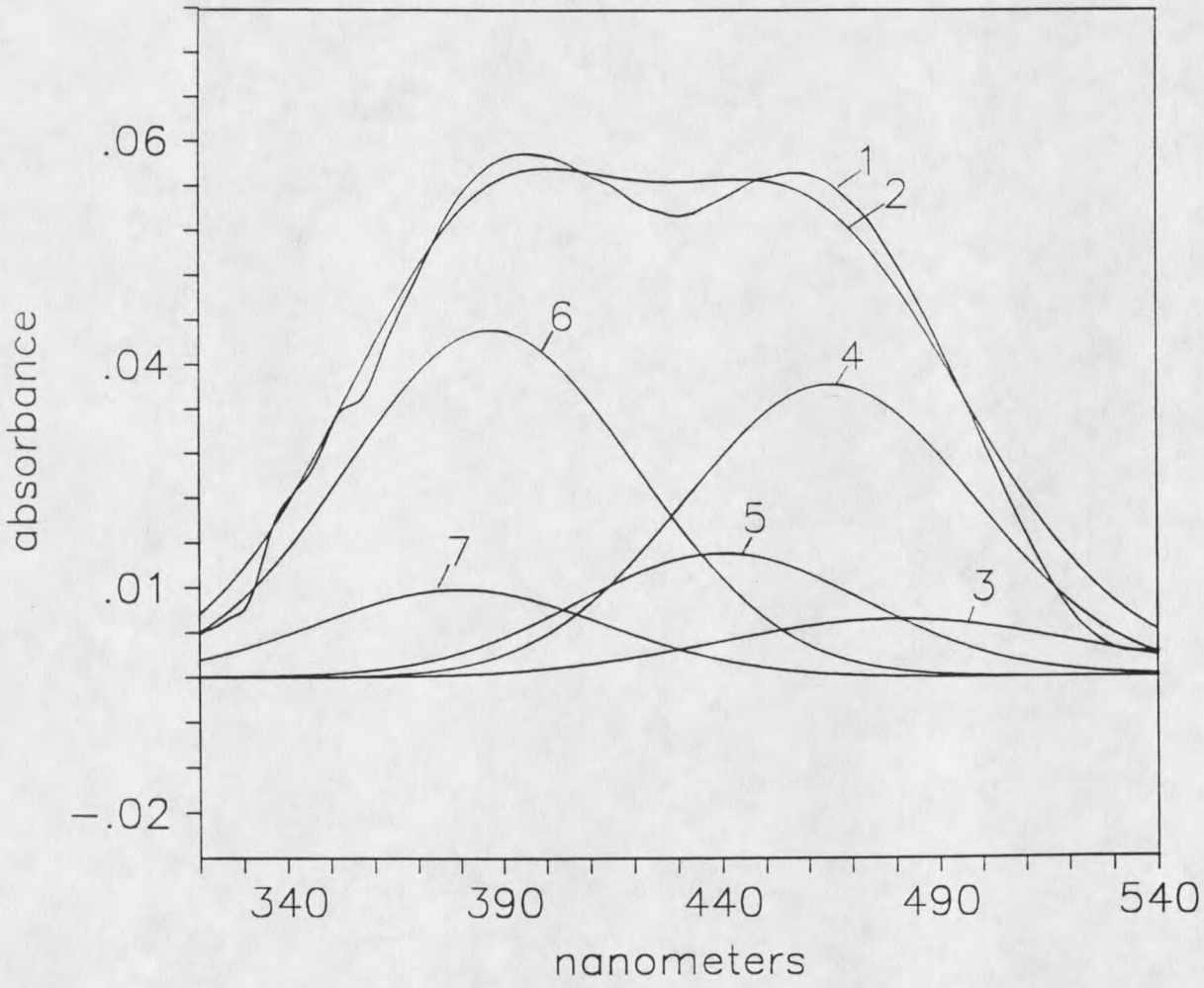


Figure 11. Curve 2 of Figure 10 was deconvoluted to a mixture of rhodopsin intermediates. Curve 1 is the original data, Curve 2 is the sum of peaks 3-7, Curve 3 is MI, Curve 4 is MIII, Curve 5 NRO_{440}, Curve 6 is retinal, and Curve 7 is MII.

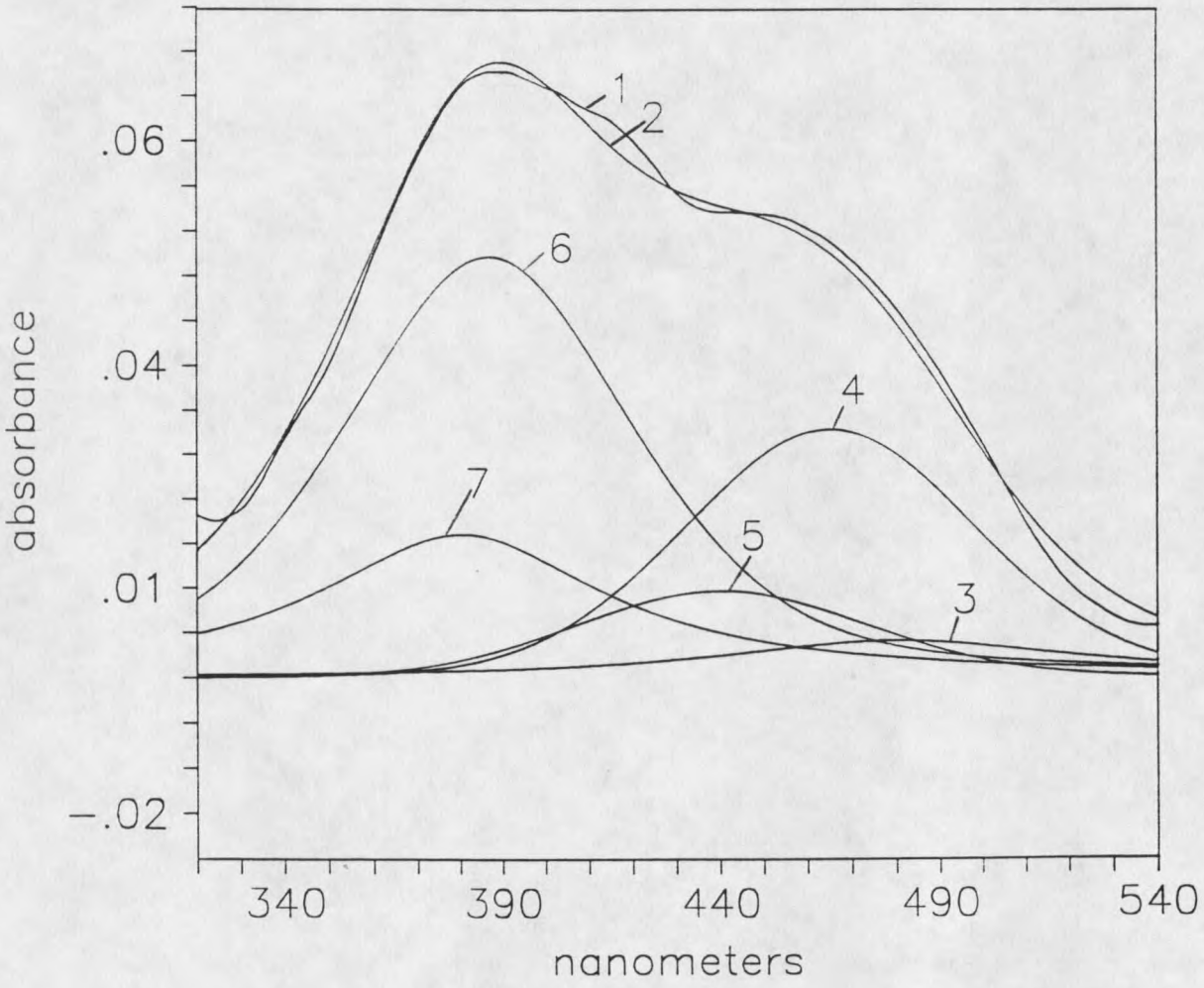


Figure 12. Curve 5 of Figure 10 was deconvoluted to a mixture of rhodopsin intermediates. Curve 1 is the original data, Curve 2 is the sum of Curves 3-7, Curve 3 is MI, Curve 4 is MIII, Curve 5 is NRO_{440}, Curve 6 is retinal, and Curve 7 is MII.

Native ROS

Retinal ROS were isolated as described earlier and allowed to equilibrate overnight in 20mM succinic acid buffer, pH=5.5. After centrifugation, 30μL were pipetted to the 0.1mm path length cell and equilibrated at -13±1°C for 1 hour in the spectrophotometer chamber. After measuring a rhodopsin scan, the sample was bleached in the cuvette holder for 2-5 minutes. Subsequent scans were taken every 1 to 2 hours for a period of 12 hours.

Figure 13 presents a representative spectrum of the experiments done on native ROS at pH 5.5. After bleaching the sample immediately formed a mixture of MI and MII that was predominantly MII. Successive scans showed a decay in the MII absorption accompanied by an increase in absorption over the range of 440 to 465nm. The intermediates MIII and $NR0_{440}$ have absorbance maxima in this region and are likely candidates for equilibrium or decay products of MII at pH 5.5 (Blazynski & Ostroy, 1984). Even after 12 hours a substantial amount of what appears to be MII remains with no identifiable formation of $retinal_{387}$, appearing to make these likely conditions for NMR experiments.

In contrast to the Blazinski and Ostroy experiments at -13.5°C, we were not able to limit the formation of intermediates to MI and MII. We believe there are two primary reasons for this. Their experiments were done in

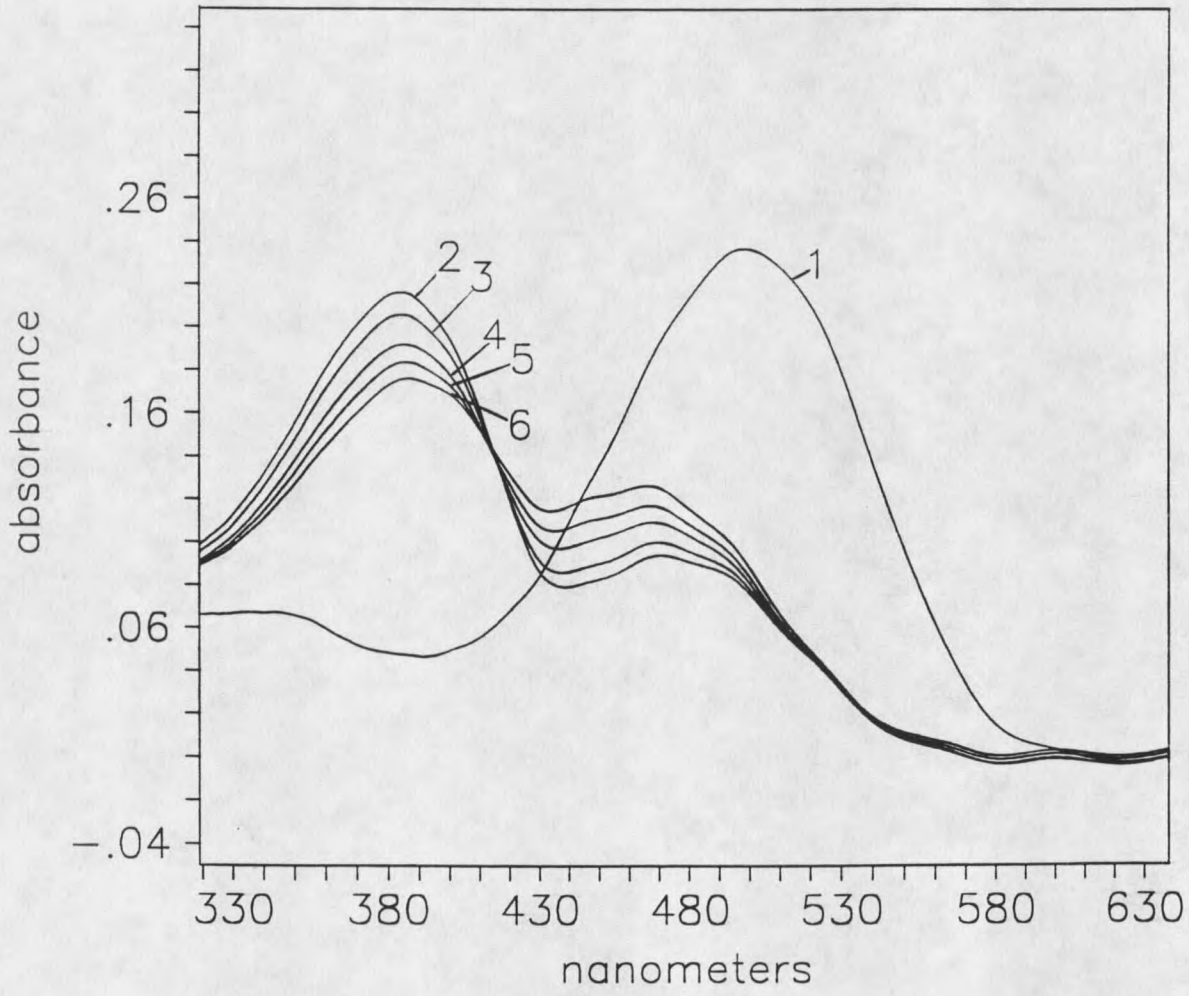


Figure 13. Native ROS at pH 5.5 were bleached at -13.5°C and the spectrum was periodically recorded for a period of 12 hours. Curve 1 is rhodopsin, recorded before illumination; Curves 2-6 were recorded 5 minutes, 2.5 hours, 6 hours, 9 hours, and 12 hours, respectively, after illumination.

50% glycerol which has been shown to favor formation of MII (Matthews et al.1963). This may account for the large stable populations of MII they observed without further decay at -13.5°C that we do not observe. Our experiments were done at pH 5.5 in contrast to their pH of 6.0. We found that we could produce slightly more MII at pH 5.5 in native membranes than we could at pH 6.0. The formation of MIII and NRO_{440} are known to be acid catalyzed and thus may be favored in our more acidic conditions (Blazynski & Ostroy, 1984; Blazynski & Ostroy, 1981). Since our principal experiments were on reconstituted membranes containing deuterated lipids we did not explore the pH dependence of MII stability in native membranes further.

Membranes Reconstituted with $16:0_{d31}$PC/PE/PS 3:3:1

A two-fold approach to enhancing the stability of reconstituted membranes after bleaching was taken. First, rhodopsin was reconstituted into membranes containing the native ratio of lipid headgroups, PC:PE;PS, 3:3:1. It is not known exactly how individual headgroups participate in the formation of rhodopsin intermediates, but it has been proposed that optimum production of MII is achieved only when the native ratio of headgroups and the 22:6 fatty acid are present (Wiedmann et al.1988). Therefore, inclusion of PE and PS headgroups was expected to impart additional stability to MII equilibrium products formed in

reconstituted membranes compared to membranes containing the PC headgroup only. Second, the sample temperature was lowered to -13.5°C to slow the decay of intermediates to retinal + opsin as was found in the native membranes.

Three preparations of reconstituted membranes containing $16:0_{d31}22:6$PC/PE/PS, 3:3:1 were used for absorbance and NMR experiments. Table 2 lists the sample composition of each prep.

Table 2. Sample composition of reconstituted membranes containing PC/PE/PS, 3:3:1.

preparation	lipid:protein	pH
A	65:1	5.5
B	80:1	5.5
C	70:1	8.0

Sample prep A was bleached as described previously for native membranes at -13.5°C. The sample was scanned periodically over a 23 hour period and the resulting spectra are shown in Figure 14. At pH 5.5, the primary product formed after bleaching appeared to be a species absorbing at 465nm indicating MIII. Continual monitoring of the spectrum over a 23 hour period showed little shift in the peak maxima and only a slight drop in overall intensity. The apparent stability of MIII has been observed by other research groups and has a reported half-life of 12 days at 3°C in digitonin extracts (Blazynski & Ostroy, 1981). Similar results were

obtained at pH 6.0 and 6.5; that is, virtually immediate formation and persistence of MIII.

Spectra selected from those shown in Figure 14 were deconvoluted with the curve fitting program into the equilibrium mixtures of peaks. The spectra deconvoluted were scans 2 and 6 shown in Figure 14. The primary products in scan 2 are a mixture of MI, MIII and NRO_{440}, a small amount of MII and negligible contribution from retinal. Over a 23 hour time period, represented by scan 6, a decay of MI and an increase in NRO_{440} are observed . A small increase in MII absorbance is observed over the same time. However, MII absorbance remains small. The retinal absorbance remains very small indicating that intermediates have not decayed to retinal + opsin as would be expected at -13.5°C.

When sample prep B was bleached it formed a species with an absorption centered at 470nm shown in Figure 15. Curve fitting analysis was used to deconvolute peak 2 in Figure 15 into its component parts and revealed that it was a mixture of MI, MIII, NRO_{440}, and a small amount of MII. The final scan shown in Figure 15 (scan 6), taken 21 hours after the sample was bleached, was also deconvoluted by the curve fitting procedure. It showed that the population of MIII decreased and NRO_{440} increased. The absorbance of MII had also increased slightly.

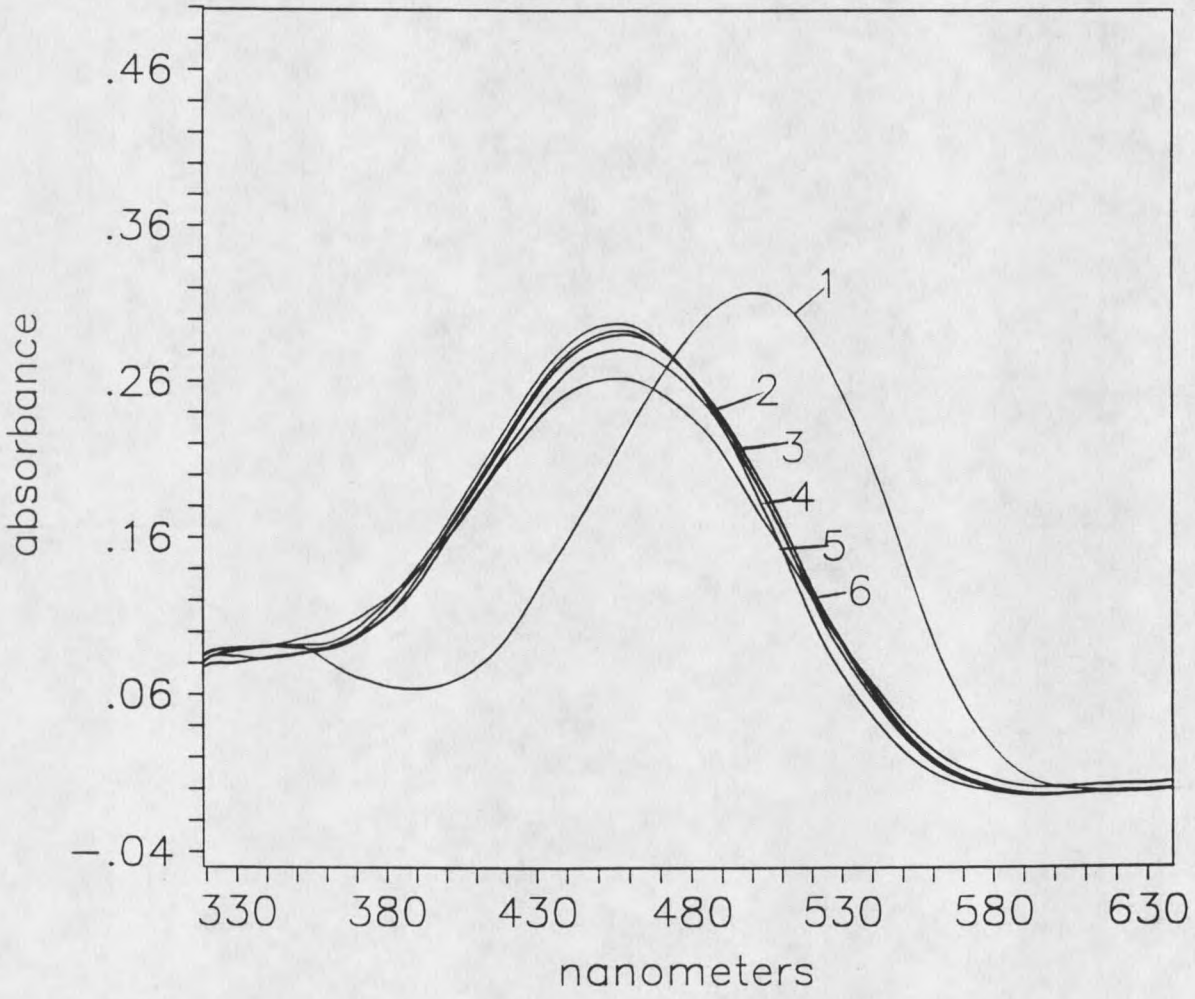


Figure 14. Preparation A at pH 5.5 was bleached at -13.5°C and the spectrum was recorded periodically for 23 hours. Curve 1 is rhodopsin and was recorded before illumination; Curves 2-6 were recorded 5 minutes, 30 minutes, 2.5 hours, 4.5 hours and 23 hours, respectively, after illumination.

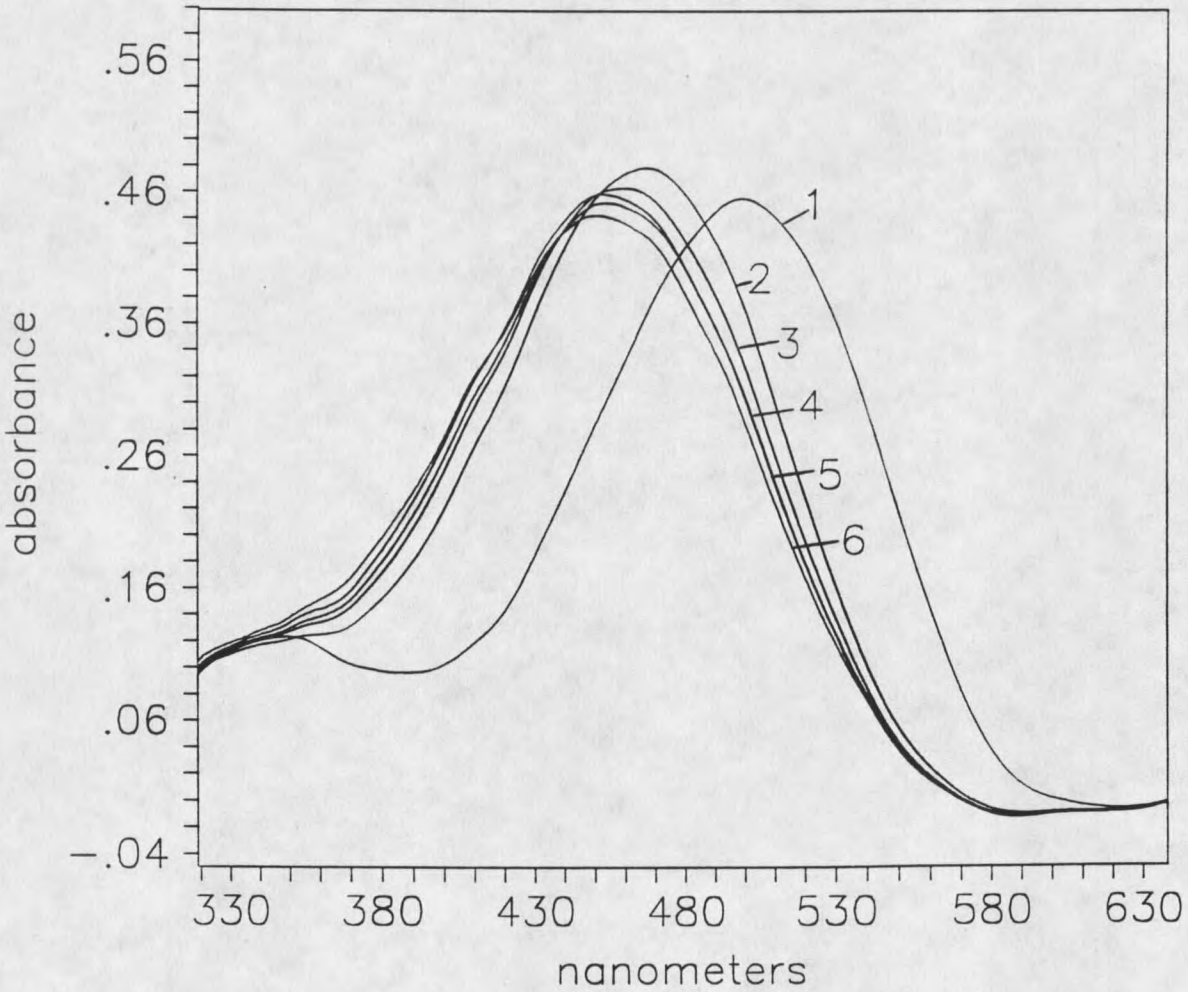


Figure 15. Preparation B at pH 5.5 was bleached at -13.5°C and the spectrum recorded periodically for 21 hours. Curve 1 is rhodopsin recorded before illumination. Curves 2-6 were recorded 5 minutes, 1 hour, 4.5 hours, 8.5 hours, and 21 hours, respectively, after illumination.

It appeared that reconstituted membranes containing PC/PE/PS 3:3:1 strongly favored the formation of acid catalyzed intermediates, MIII and NRO_{440}, when they were bleached at pH 5.5 to pH 6.5. When the pH was raised to 8.0 the spectrum of bleached rhodopsin resembled more "native-like" behavior as is shown in Figure 16. The first scan taken after bleaching consisted of mostly MI and a small amount of MII, similar to what has been found in native membranes at pH 8.0 (Blazynski & Ostroy, 1984). After remaining at -13.5±1°C for 24 hours, the curve fit spectra taken from scan 6 in Figure 16 showed a mixture of intermediates corresponding to MI, MII, MIII, and NRO_{365} (the deprotonated form of NRO). 20 hours after the sample was bleached, curve fitting analysis implied that approximately one third of the sample remained in MI. The remaining two thirds of the sample was approximately evenly distributed between MII, MIII, and NRO_{440}.

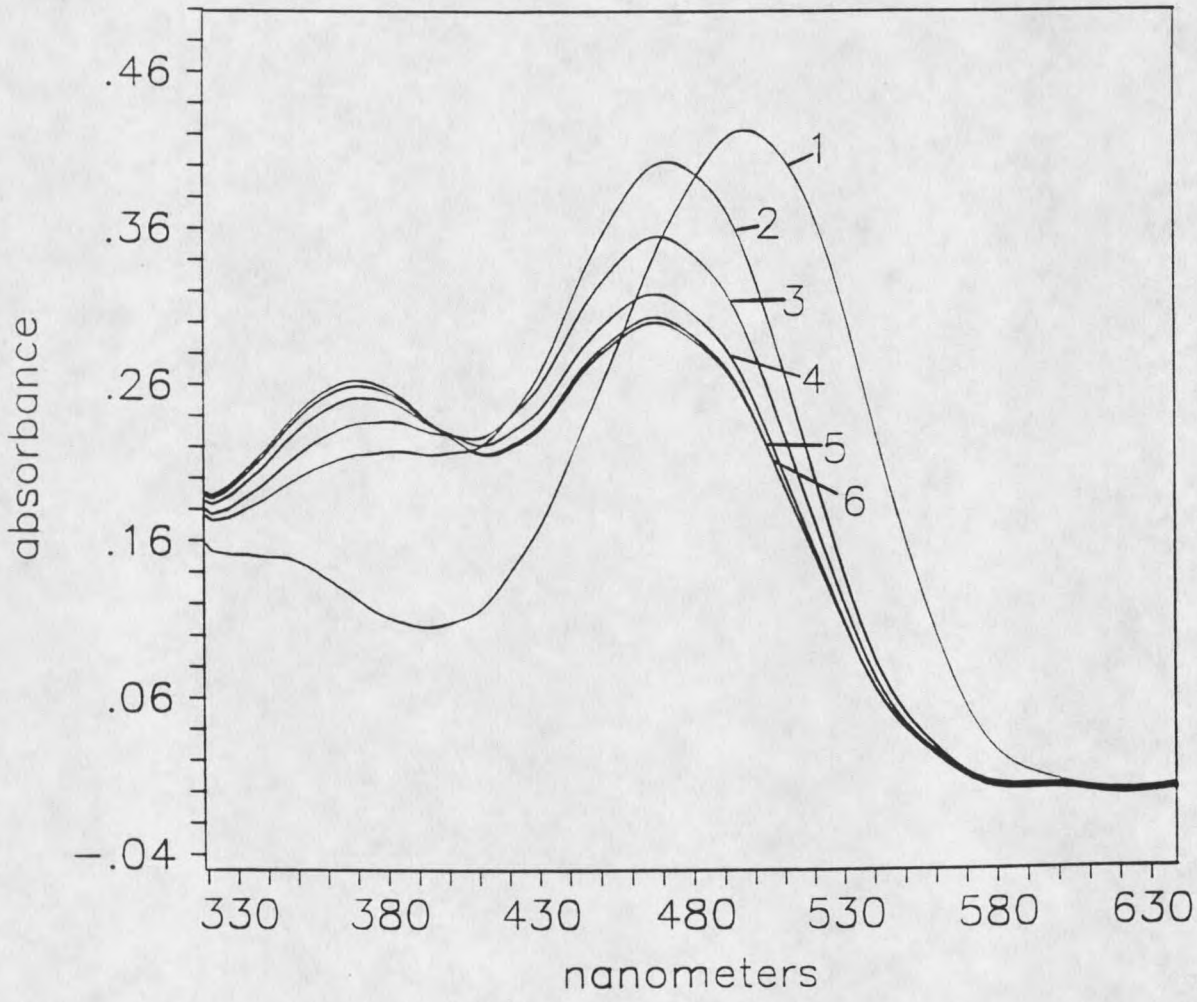


Figure 16. Preparation C at pH 8.0 was bleached at -13.5°C and the spectrum recorded periodically for 24 hours. Curve 1 is rhodopsin and was recorded before illumination. Curves 2-6 were recorded 5 minutes, 2.5 hours, 18 hours, 21.5 hours, and 24 hours, respectively, after illumination.

Discussion

Our goal for monitoring rhodopsin intermediates formed from minutes to hours after bleaching was to characterize (in a semi-quantitative way) which intermediates were most abundant and to ensure that rhodopsin had not decayed to all-*trans* retinal + opsin. The mixture of intermediates present at long times after bleaching appears to be complex and intermediate pathways are controversial even in native membranes. We were not able to confirm the formation of large concentrations of MII under any of the conditions we tried in the reconstituted membranes. Therefore, we examined our data from another perspective. Since we were not interested in rhodopsin intermediates, per se, but rather on the effect protein conformational changes might have on the lipid bilayer, we simplified our consideration of the many possible combinations of rhodopsin intermediates that can form in long times after bleaching into two categories: those formed after MI and before retinal + opsin, that are thought to have an "open" conformation; and those intermediates present before MII, including rhodopsin, which are thought to have a "closed" conformation. With this in mind, we analyzed the bleaching of rhodopsin in reconstituted membranes as classes of intermediates formed after MI and considered the time frame where we were able to prevent their decay to retinal + opsin in the hours needed

to complete NMR experiments.

The behavior of rhodopsin after exposure to light differs considerably in the reconstituted membranes used in this study from that observed in native membranes. Further study of the formation of intermediates observed under various conditions in reconstituted membranes would be necessary to fully elucidate which individual properties of the native membranes are responsible for specific behaviors that differ from those found in the simplified, reconstituted membranes. However, from the collection of available knowledge about rhodopsin intermediates we will offer what we believe to be the most likely explanation for these differences.

Reconstituting rhodopsin into pure PC bilayers was chosen initially for simplicity. When it became apparent that bleached rhodopsin was rather unstable in PC bilayers we began to include the other native headgroups in the reconstitution. At least one other research group has observed that pure PC does not support rhodopsin's photolytic integrity as well as PE or PS (vanBreugel et al.1978). With the hope of optimizing stability of bleached rhodopsin over longer periods of time, we chose to incorporate the native ratio of phospholipid headgroups into the reconstituted membranes.

In native ROS, rhodopsin is oriented with the carboxy-terminal facing the cytoplasmic (external) surface of the

membranes. At neutral pH, charged residues on surface loops of rhodopsin result in a strong bipolarity, leading to a positively charged cytoplasmic surface and a negatively charged intradiscal surface (Tsui et al.1990). Rhodopsin orientation in reconstituted vesicles appears to be essentially symmetrical (Tsui et al.1990).

In addition to the unidirectional orientation of rhodopsin, it has been shown by Miljanich, et al., (Miljanich et al.1981) that phospholipids head groups are asymmetrically distributed between the inner and outer leaflets of ROS membranes and that 77-88% of the PS is in the outer leaflet. The orientation of phospholipid head groups in the membrane has been controversial. However, the surface potential measurement of Tsui et al. (1990) strongly suggests the lipid asymmetry reported by Miljanich et al. (1981). One implication of this result is that the negatively charged PS headgroups have a preference for the positively charged surface of the protein.

Surface potential measurements for the inner and outer surface of ROS disc membranes show that the native distribution of phospholipids, particularly PS, results in a negative potential for both surfaces but is more negative for the inner surface. The surface potential is strongly dependent on the salt concentration of the buffer and decreases rapidly as the concentrations approach 20mM or less. A negative surface potential would be more effective

in attracting H^+ ions which may result in a locally low (acidic) pH and may explain the tendency for PS containing membranes to form acid catalyzed intermediates. However, when samples were equilibrated with a pH 6.0 succinate buffer containing either 30mM or 120mM total salt, no detectable difference in the absorbance spectrum was observed. Surface potential measurements predict a substantial difference between 30mM and 120 mMsalt (Tsui et al.1990) and so the difference in surface potential between the native and reconstituted membranes does not appear to be responsible for the differences in MII stability observed.

It was initially thought that perhaps the molar ratio of PS was higher than it should have been which may have led to an anomalously low surface pH. This could have provided an explanation for the strong preference for formation of MIII and NRO_{440} which are acid catalyzed. The phospholipids were extracted from the reconstituted membrane samples used for the absorbance and NMR measurements, and the headgroup ratio was rechecked by HPLC separation of phospholipids with UV detection. Comparison of peak areas for each lipid species indicated that the PC:PE:PS ratio was approximately 3:3:1 as initially prepared.

The conclusion we can draw at this point is that we are able to convert rhodopsin in reconstituted membranes to a reasonably stable, albeit heterogeneous, mixture of photoproducts that has not decayed to retinal + opsin at

-13.5°C. The atypical absorbance behavior of reconstituted membranes compared to native membranes underscores the importance of phospholipid/protein interactions in membranes and the need to better understand their role in effecting the functional states of proteins.

DEUTERIUM NMR THEORY AND EXPERIMENT

Theory

Deuterium NMR was long thought to be of little use to chemists and biologists due to unfavorable magnetic properties of deuterium. This idea changed in the 1970's when high sensitivity instrumentation capable of observing the ^2H nucleus became available. Deuterium has a much lower magnetic moment than the more frequently used ^1H isotope and therefore resonates at a much lower frequency. The lower resonance frequency leads to smaller energy splittings and a much lower detection sensitivity for ^2H than for ^1H. A natural abundance of 0.015% necessitates synthetic enrichment. Deuterium has a spin of 1 which implies a nuclear quadrupole moment. The mechanism of relaxation is dominated by the interaction of the deuteron quadrupole moment with the local electric field gradient.

Efficient, rapid quadrupolar relaxation, coupled with a spin of 1, gives rise to a wide-line spectrum of doublets under slow motion conditions. The three spin energy levels in a I=1 system have two allowed transitions and thus two resonances (or peaks) in the NMR spectra (Figure 17). The separation of the peaks, the deuterium quadrupole splitting, $\Delta\nu_Q$, is dependent on the angle θ between the external magnetic field and the principle axis of the quadrupole coupling tensor (see Figure 18). In the case of liposomes

or lipid-protein vesicles, the principle axis is the bilayer normal.

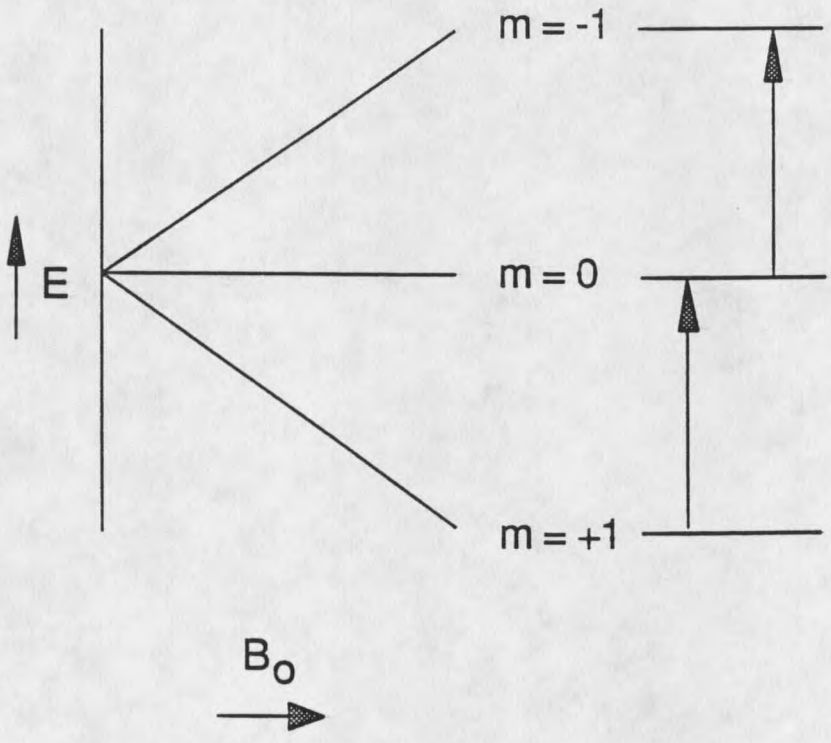


Figure 17. The nuclear energy levels of an I=1 nucleus. The two allowed single-quantum transitions are shown.

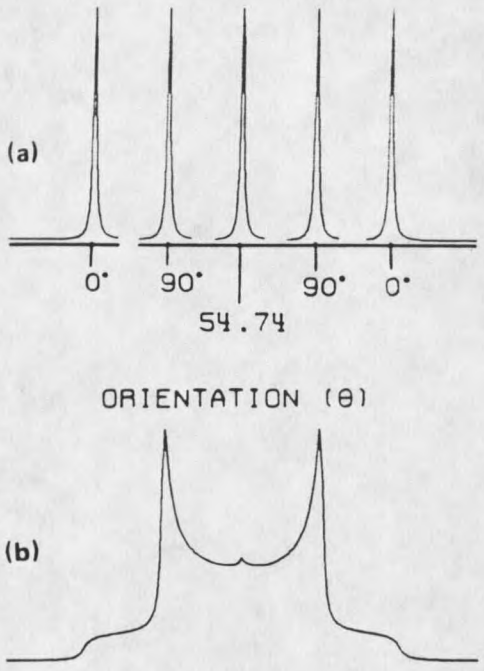


Figure 18. (a). ^{2}H NMR doublets due to different angles between the symmetry axis and the magnetic field. (b). Powder spectrum due to the sum of all possible quadrupole doublets. Note that the peaks in (b) correspond to the 90° doublet in (a), and the shoulders to the 0° shoulders (from Smith, 1983).

Should there be a mixture of orientations of the symmetry axis with respect to the magnetic field, such as in a liposome or a lipid protein vesicle, various spectra will be obtained simultaneously. In the case of a perfectly random distribution of orientations, all possible spectra will be superimposed to yield what is called a powder pattern like that shown in Figure 19. Well defined turning points exist at frequencies corresponding to angles of 0° and 90° between the symmetry axis and the applied magnetic field.

Figure 19 shows the so called "Pake doublet" splitting for a deuterium powder pattern. Also shown in dotted lines is a mathematically deconvoluted powder pattern called the dePaked spectrum. Overlap is reduced by calculating the spectra that corresponds to the θ=0° orientation of the bilayer normal with respect to the magnetic field (Bloom et al.1992; Sternin et al.1983). This process has been called "dePaking" the spectra. The relatively simple spectrum shown in Figure 19 was derived from a phosphatidylcholine, DPPC-d_2, deuterated in the α-position of the polar headgroup. Overlap in the powder pattern can be great when more positions are labeled. The perdeuterated $16{:}0_{d31}$ sn-1 chains of phospholipids used in the present study lead to the superposition of spectra for 15 labeled positions.

In the case of hydrocarbon chains that are frozen in an all-*trans* configuration with slow or no axial diffusion, the spectral width of the powder pattern reaches the so called rigid limit of ±125 kHz. As axial diffusion becomes fast, 10^{-7} s^{-1}, the spectral width narrows to ±60kHz. The spectral width further narrows with segmental motion such as *gauche-trans* isomerizations. As these motions approach values equal to the difference in quadrupole splitting, the motion becomes increasingly effective at averaging the differences in quadrupole splitting due to the rapid visitation of different angles. In the limit of rapid motion that explores all orientations, a single resonance is obtained

whose width decreases with increasing rotational rate.

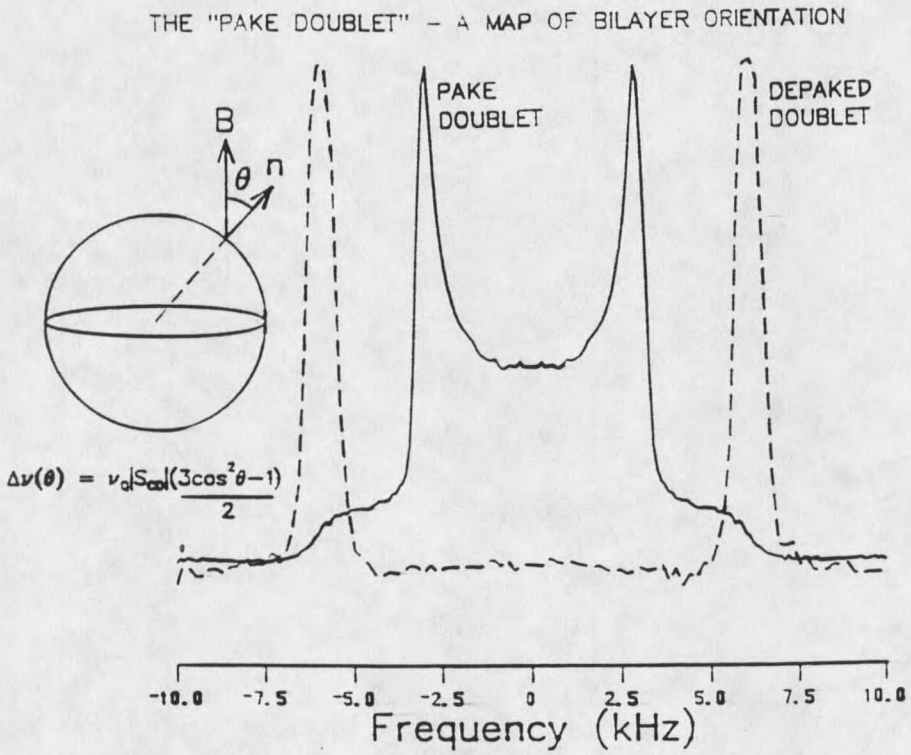


Figure 19. ^2H NMR powder pattern spectrum for DPPC-d_2 deuterated in the α-position of the polar headgroup. Also shown in dotted lines is the depaked spectrum characteristic of the external magnetic field applied along the bilayer normal (θ=0°). (taken from (Bloom & Evans, 1991).)

The study of molecular ordering and mobility in model and biological membranes has been revolutionized by the use of ^2H NMR. One of the most useful parameters readily available from the ^2H NMR spectra of model membranes is the carbon-deuterium bond order parameter, S_{CD}. It gives an indication of the average orientation of the labeled region of the molecule and can be calculated from the deuterium quadrupole peak splitting, $\Delta\nu_Q$, according to (Davis, 1983; Seelig & Seelig, 1980; Bloom & Evans, 1991):

$$\Delta\nu_Q = \frac{1}{2}\,\omega_Q\,(3\cos^2\theta - 1)\,S_{CD} = \frac{3}{4}\,\frac{e^2qQ}{h}\,S_{CD}, \quad for\,\theta = \frac{\pi}{2} \qquad (1)$$

The term e^2qQ/h is the quadrupole coupling constant and is 170kHz for aliphatic C-^2H bonds. The deuterium order parameter, S_{CD}, can be used as a measure of conformational freedom of methylene carbons on a saturated chain. The term containing β describes the orientation of the C-D bond vector with respect to the director of motion (the bilayer normal). Brackets indicate a time average. The term involving the angle α describes the amplitude of motion about the average orientation. Thus, S_{CD} is sensitive to both order and orientation as follows (Baenziger et al.1991):

$$S_{CD} = \frac{1}{2} \langle (3\cos^2\beta - 1) \rangle \frac{1}{2}(3\cos^2\alpha - 1) \qquad (2)$$

S_{CD} approaches 0 if a small bilayer fragment tumbles rapidly on the NMR time scale (100kHz or 10^{-5}s) and a finite value if a higher degree of order is present.

To investigate order when direct measurement of individual quadrupolar splittings is not possible, moments of the spectral lineshapes are used to estimate the average C-^{2}H bond order parameter, $\langle | S_{CD} | \rangle$. For a line symmetric about its center, as in deuterium powder patterns, the *n*th moment of half of a spectral line is expressed as

$$M_n = \frac{\int_0^\infty (\nu - \nu_0)^n g(\nu)\, d\nu}{\int_0^\infty g(\nu)\, d\nu} \qquad (3)$$

where $g(\nu)$ is the distribution function for the line and $(\nu - \nu_o)$ is the symmetric distribution about the resonance frequency, ν_o (Davis, 1983). The first moment, M_1, is directly proportional to the average order parameter, $\langle | S_{CD} | \rangle$ according to (Davis, 1979):

$$M_1 = A_1 \frac{3}{4} \frac{e^2 qQ}{\bar{h}} \langle |S_{CD}| \rangle \qquad (4)$$

A close relationship exists between the average orientational order parameter for saturated hydrocarbon chains and membrane thickness (Hofmann, 1986; Schoenlein et al.1991; Ipsen et al.1990; Seelig, 1977) which makes it possible to calculate membrane thickness using ^2H NMR measurements. Such estimates are good whenever the symmetry axis is normal to the bilayer surface as in the fluid phase of liposomes or lipid protein vesicles. The bilayer thickness, d, is defined as the separation between the first carbon atoms in the acyl chains of the two leaflets, each acyl chain having n C-C bonds. Using $< | S_{CD} | >$ the bilayer thickness is calculated as follows (Bloom & Mouritsen, 1988):

$$d = d_{max} \ (0.5 + < | S_{CD} | >) \qquad (5)$$

$$d_{max} = 2.5n\text{Å} \qquad (6)$$

Because it is anticipated that for $d < d_{max}$, in the fluid phase, all $< | S_{CD} | >$ will have values in the range $0 \leq < | S_{CD} | > \leq 0.5$ (Seelig & Seelig, 1980).

The Deuterium NMR Experiment

The spectroscopic measurement problem associated with solid state ^2H NMR arises because the spectra are very wide, up to 250kHz or more. To overcome this problem, instrumentation must include high power pulsed rf (radio

frequency) power to provide short 90° pulses, a fast transient recorder, and the rapid phase shifting capability to carry out the quadrupole echo pulse experiment (Davis et al.1976) to avoid receiver overload and probe ring-down following rf pulses.

The quadrupole echo pulse sequence is shown in Figure 20. It consists of a pair of 90° pulses (an X and a Y pulse) separated by a time, τ. The first pulse produces a free induction decay and the second pulse refocuses the magnetization via reversal of the phase accumulated by the spins between the two pulses such that an echo occurs at a time 2τ. The data is acquired, beginning at the peak of the echo, and Fourier transformed to yield the spectrum. The data collection occurs in τ μs from the last rf pulse so probe and amplifier ring down are avoided. If τ is kept sufficiently short, then T_{2e} relaxation does not substantially decrease the intensity of the signal.

If deuterium spectra are taken exactly on resonance with quadrature phase detection, then the real channel should contain all the signal, and the imaginary channel should contain none. In practice this is not often the case due to pulse shape distortions and transmitter phase errors. This problem can be overcome by applying a zero-order phase correction to the FID and maximizing the signal in the real channel.

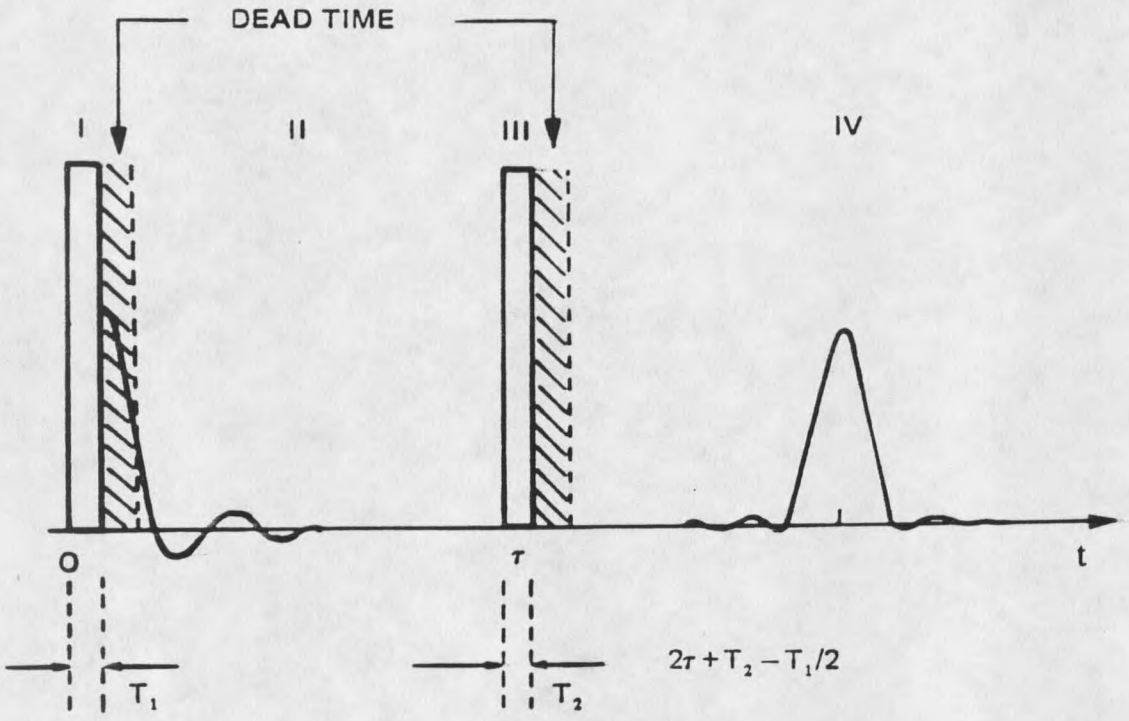


Figure 20. A typical quadrupole echo pulse sequence consists of a pair of 90° rf pulses whose phases differ by 90° (an X and a Y pulse) separated by a time τ. Cross-hatched regions correspond to the dead time of the amplifier following a large amplitude pulse. (from Devaux, 1983)

In order to obtain the correct spectrum, the Fourier transform must be done beginning exactly at the peak of the echo. If there is signal present in the imaginary channel, then the apparent echo peak in the real channel is not the

true echo maximum, and beginning the transform at this point will yield a distorted spectrum. Computer programs for processing NMR data can overcome this limitation by artificially zeroing residual signal remaining in the imaginary channel and locating the exact echo maximum by interpolation between actual FID data points.

A final consideration of the quadrupole echo experiment is width of the 90° pulse. A short, powerful rf pulse is needed to ensure that nuclei are excited uniformly across a spectral width of up to 250kHz. If this condition is not met, powder spectra will be distorted, especially in the higher frequency "wings". In general, a pulse width of 2-5μs will suffice to avoid most of the distortion.

Spectrometer and Data Processing

^{2}H NMR data were recorded at 30.6 MHz on a Chemagnetics CMC 200 spectrometer. Spectra were acquired by using the quadrupolar echo pulse sequence. The 90° pulses were 3.8μs in length and the echo pulse spacing was 35μs. Recycle times were ≥ 600ms and the spectra were generally acquired with a sweep width of 500kHz.

The gas temperature flowing over the sample was monitored and maintained to within ±0.1°C of the desired value with a variable temperature gas heating unit connected in series with a circulating bath maintained at -15°C. To deliver temperatures of <4°C at the probe, a copper coil

immersed in a dewar containing dry ice/ethanol or liquid nitrogen was connected in series with the circulating bath.

The ^{2}H NMR spectra were analyzed on a Microvax workstation using FTNMR software (Hare Research, Inc., Woodinville, WA). A program provided by Jim Davis allowed interpolation between data points to left-shift the FID to the "true" top of the echo before Fourier transformation (Prosser et al.1991). It also included routines for automatic zero-order phasing and calculation of moments. Transformed spectra were depaked by the method of Sternin et al. 1983 to give the 0° oriented-sample spectra.

^{2}H NMR STUDIES OF RECONSTITUTED MEMBRANES

Introduction

In the ^{2}H NMR experiment we wished to examine the interaction between rhodopsin and the lipid bilayer by monitoring changes that occur in the lipid bilayer coupled with the bleaching of rhodopsin. Specifically, our goal was to attempt to test the "molecular spring" model for 22:6ω3 function. Deuterium NMR measurements were made on samples before and after bleaching of rhodopsin. The mixture of intermediates produced was previously discussed in the section on rhodopsin spectrophotometry.

Reconstituted membranes containing $16:0_{d31}22:6$PC/PE/PS in the native headgroup ratio of 3:3:1 (PC:PE:PS) (or pure $16:0_{d31}22:6$PC) were prepared as described previously. The rhodopsin concentration of the preparation was quantitated by measuring absorption at 500nm on a small aliquot. Total phospholipid was quantitated by phosphorous analysis. Relative ratios for individual phospholipid headgroup species from extracts were determined by HPLC separation and measurement of peak area ratios.

The data to be presented was derived from three reconstituted membrane preparations containing $16:0_{d31}22:6$PC/PE/PS and will be referred to as prep A, B, and C as in Chapter 4. The important characteristics of each

preparation are listed in Table 2. All preparations consisted of rhodopsin and a 3:3:1 mixture of $16:0_{d31}22:6$PC/PE/PS at the lipid to protein ratios given. All measurement temperatures were at -13.5°C.

An initial series of ^2H NMR measurements at -13.5°C were made on the sample before it was bleached. These measurements were made over the course of 1-2 days to assess the stability of the spectra before performing the experiment that included bleaching the sample. Many measurements were averaged to obtain a well defined initial value for M_1 on the pre-bleach rhodopsin sample and to obtain a standard deviation for the data points that were averaged.

The next part of the experiment included performing ^2H NMR measurements on the light exposed rhodopsin system converted to the MI $\leftrightarrow$ MII $\leftrightarrow$ MIII mixture that had been studied by earlier absorption experiments. Maximizing a stable population of the MII $\leftrightarrow$ MIII mixture of intermediates for several hours required for the NMR measurements was crucial to this experiment. To enhance stability of MII equilibrium intermediates, a temperature of -13.5°C was used. The sample was irradiated for 5 minutes with a fiber optic illuminator as described earlier. Sample temperature was maintained at -13.5°C or colder during the bleaching that was carried out either in the sample chamber of the spectrophotometer or in a removable cell holder that was

partially immersed in ethanol/dry ice.

During transport to the NMR probe, the sample was kept in a black taped vial partially submerged in ethanol/dry ice. The sample was allowed to equilibrate at -13.5°C in the NMR probe for at least 1/2 hour before subsequent post-bleach NMR measurements were begun. The probe cooling gas temperature was stable to ±0.1°C.

Results

A series of NMR measurements were taken on the post-bleach sample for up to 24 hours. The before and after bleach data was analyzed by comparing calculations including M_1, Δ_2, and M_0. A summary and discussion of the moment analysis follows.

The First Moment, M_1

The first moment measure of average order parameters was plotted as a function of post-bleach time and is reported in Figures 21, 22, and 23 for preps A, B, and C, respectively. A second Y-axis shows the corresponding <S> values. The point at time zero is the average value of M_1 calculated for measurements taken before bleaching. The error bars indicate the standard deviation of the data points averaged.

Reconstituted membranes containing PC/PE/PS show an increase in M_1 (3-6%) after bleaching as shown in Figures 21-23. Post-bleach NMR runs showed that M_1 increased

gradually and then leveled off after 8 hours for prep A and after approximately 14 hours for preps B and C. The M_1's observed correspond to an increase in average bilayer thickness of approximately 1Å after sample bleaching calculated from equations 5 and 6.

Delta Two, Δ_2

The Δ_2 parameter represents the width of the distribution of order parameters (Davis, 1979) and is given by the second moment of the spectrum divided by the square of the first moment (equation 7).

$$\Delta_2 = \frac{M_2}{1.35\ M_1^2} - 1 \qquad (7)$$

Qualitatively, it portrays the heterogeneity of the motional environments. For example, a Δ_2 value of 0 would indicate a homogeneous environment. For a homogeneous lineshape there is a simple relationship between M_1 and M_2, that is, $M_1^2 = M_2/1.35$.

In Figures 24-26 the Δ_2 parameter is plotted for NMR spectra taken before and after bleaching for each preparation. The series of spectra taken after bleaching begin with the point indicated by an arrow on the plots. The data generally shows a rather abrupt decrease in Δ_2

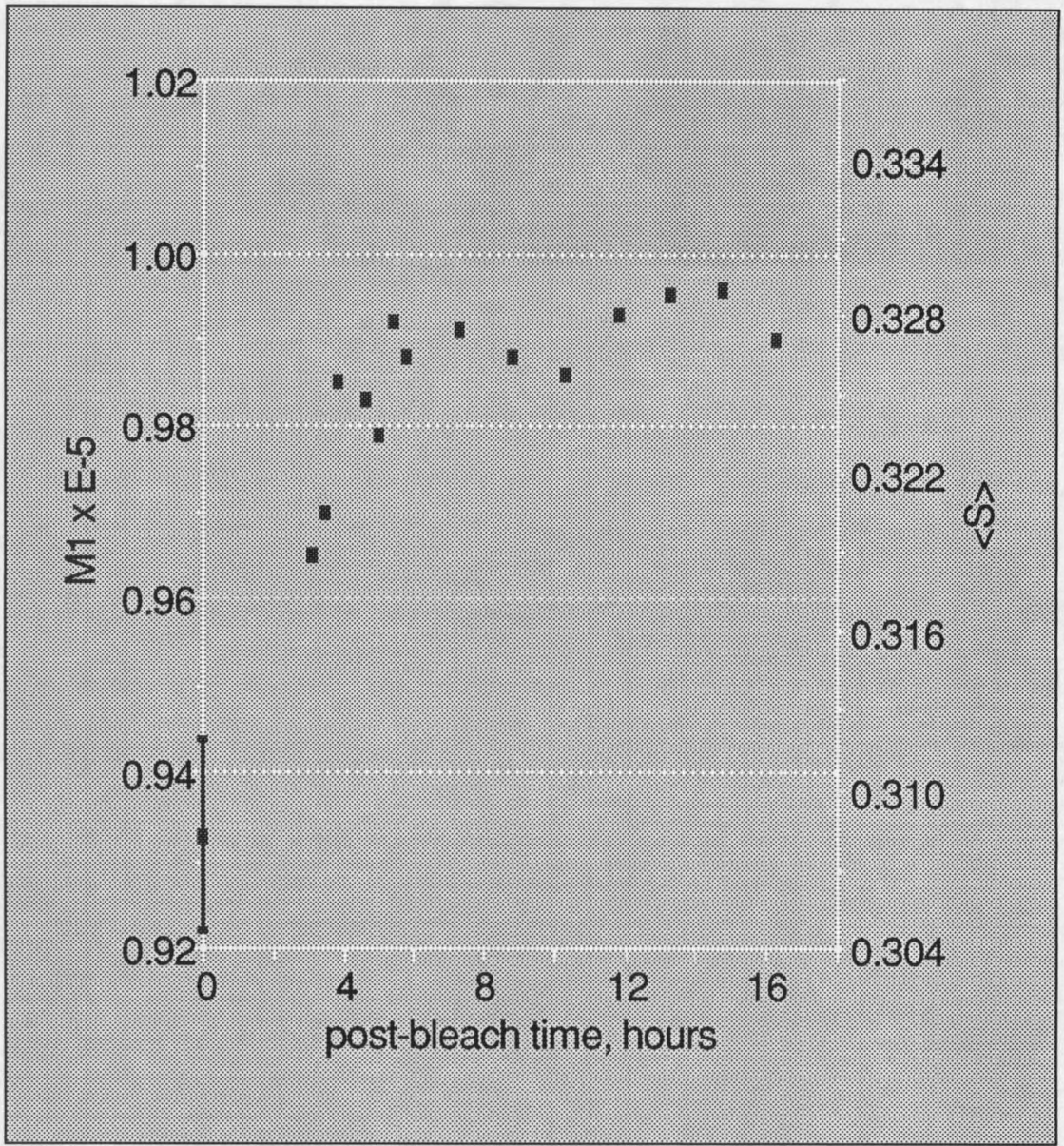


Figure 21. The first moment is plotted as a function of post-bleach time for prep A. A second Y-axis with corresponding <S> values is included on the right.

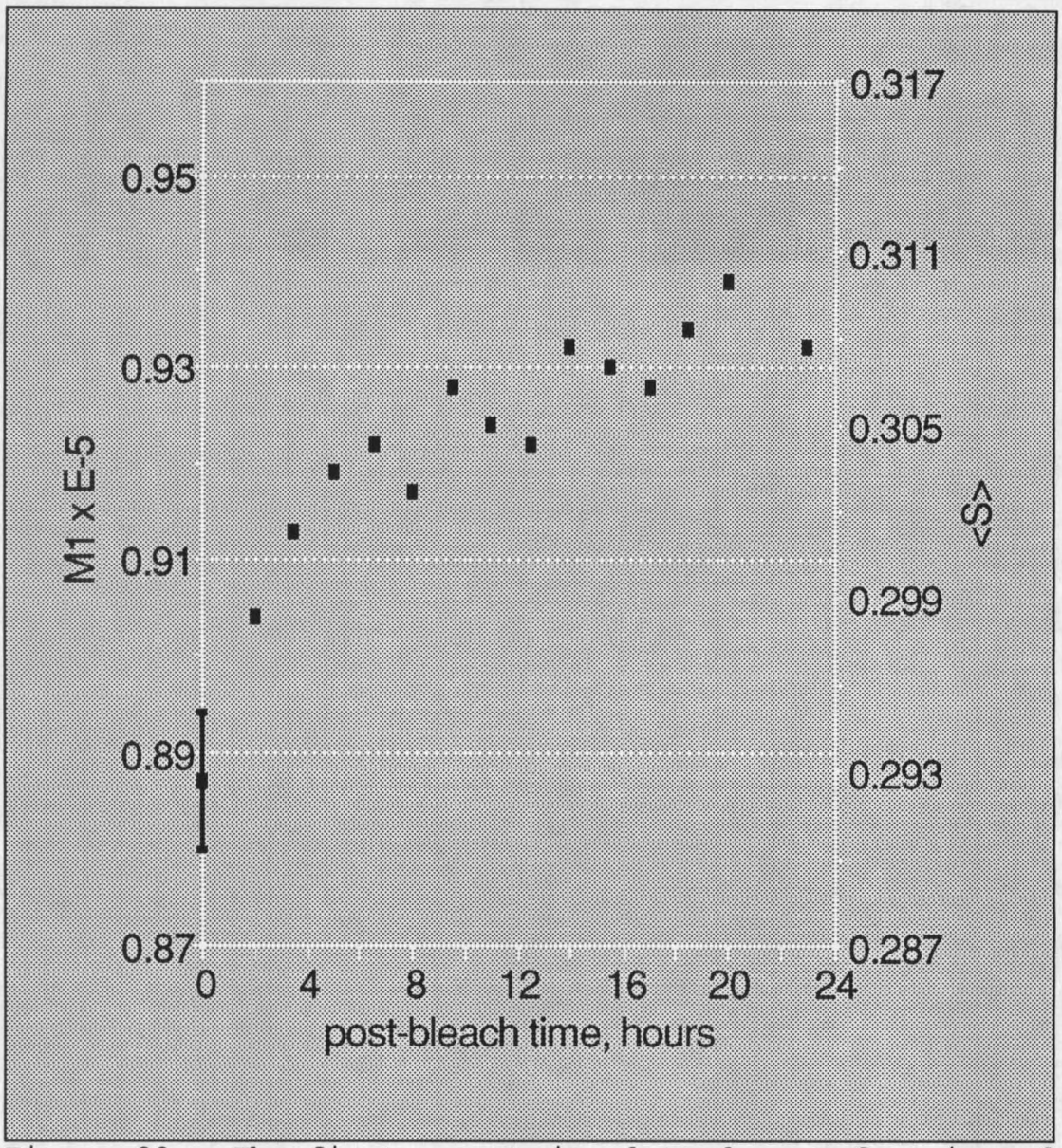


Figure 22. The first moment is plotted as a function of post-bleach time for prep B. A second Y-axis with the corresponding <S> values is included.

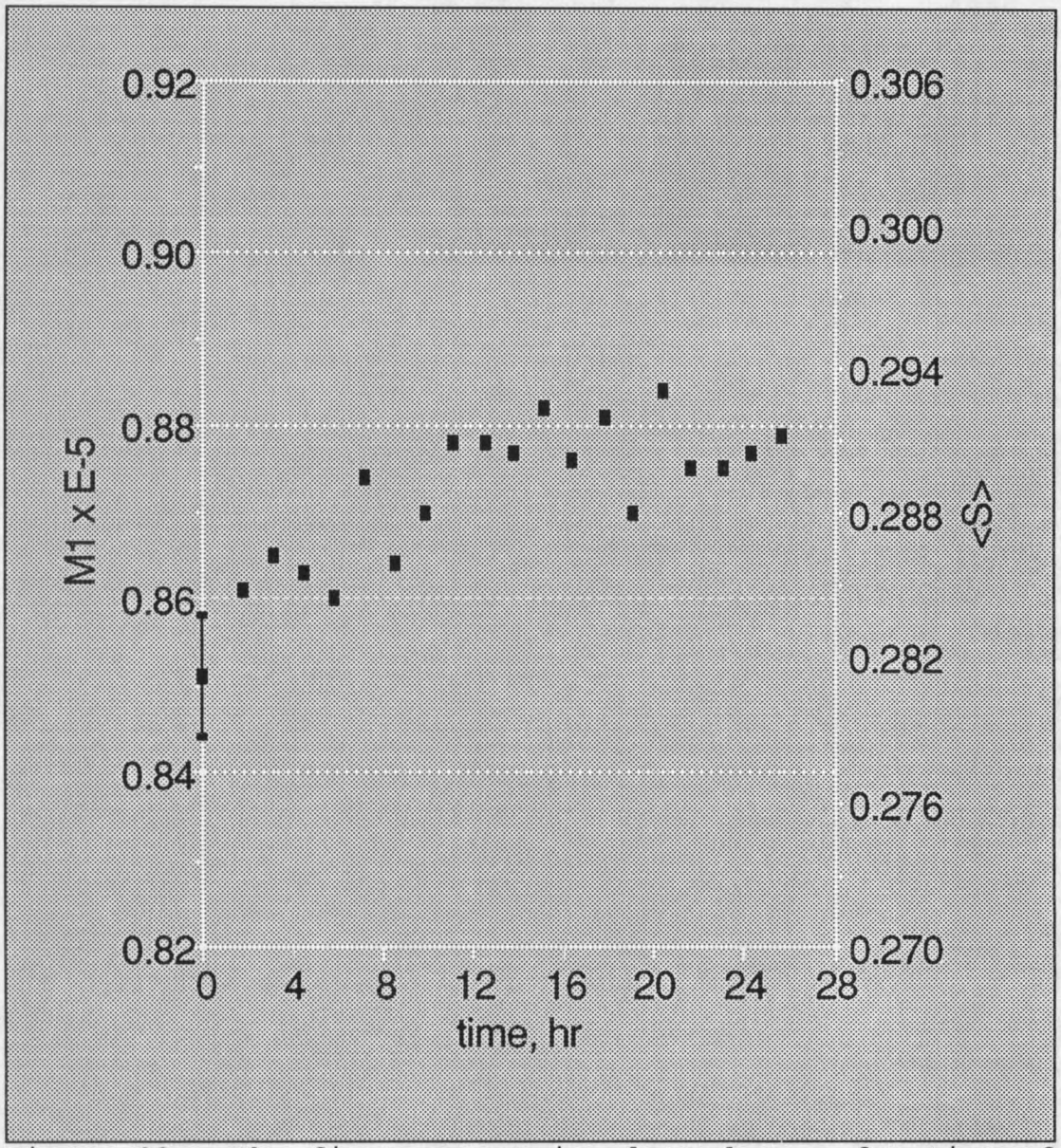


Figure 23. The first moment is plotted as a function of post-bleach time for prep C. A second Y-axis with the corresponding <S> values is included on the right.

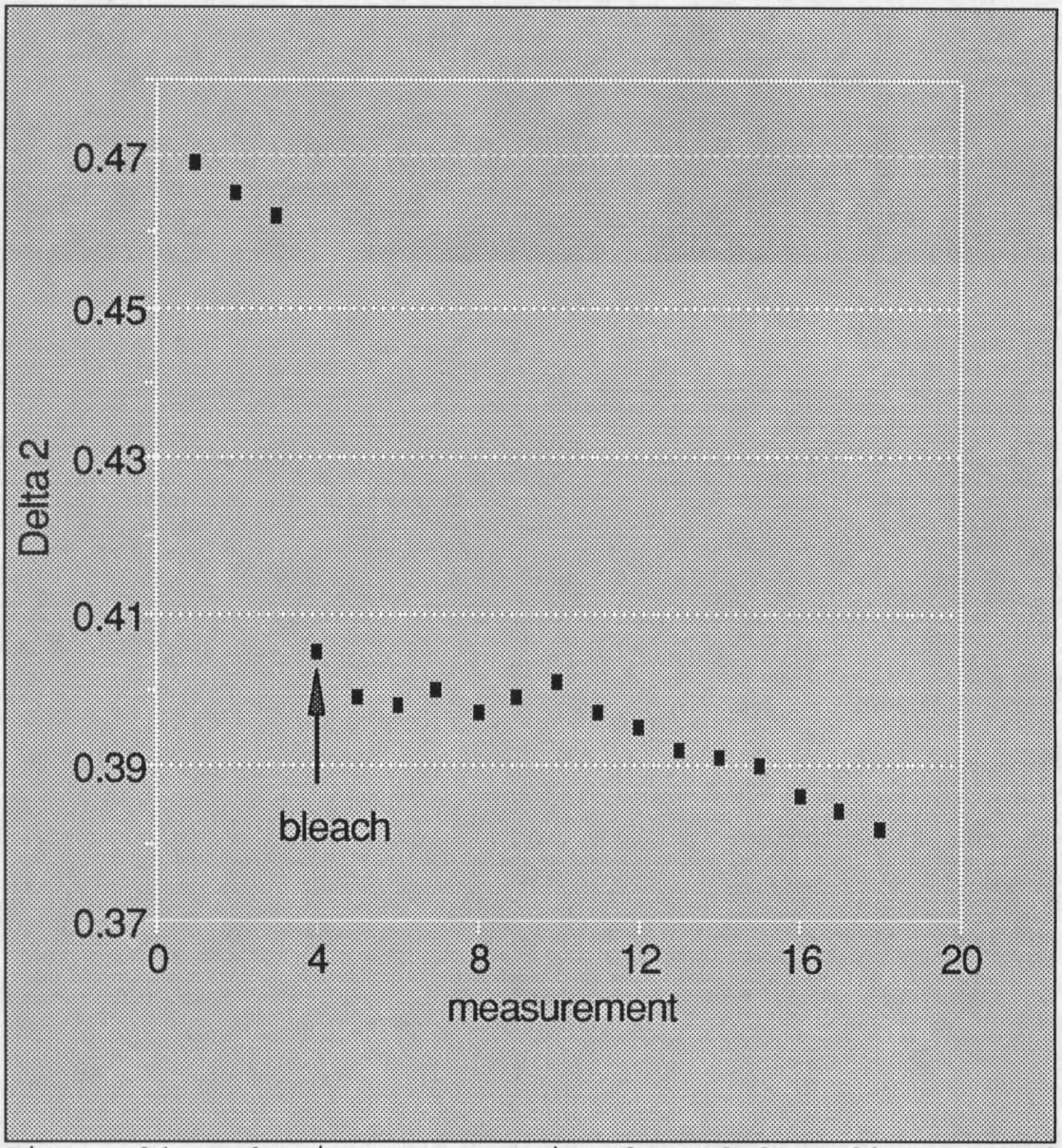


Figure 24. The Δ_2 parameter is plotted for all pre- and post-bleach ^2H NMR measurements taken for prep A. An arrow indicates the first post-bleach measurement.

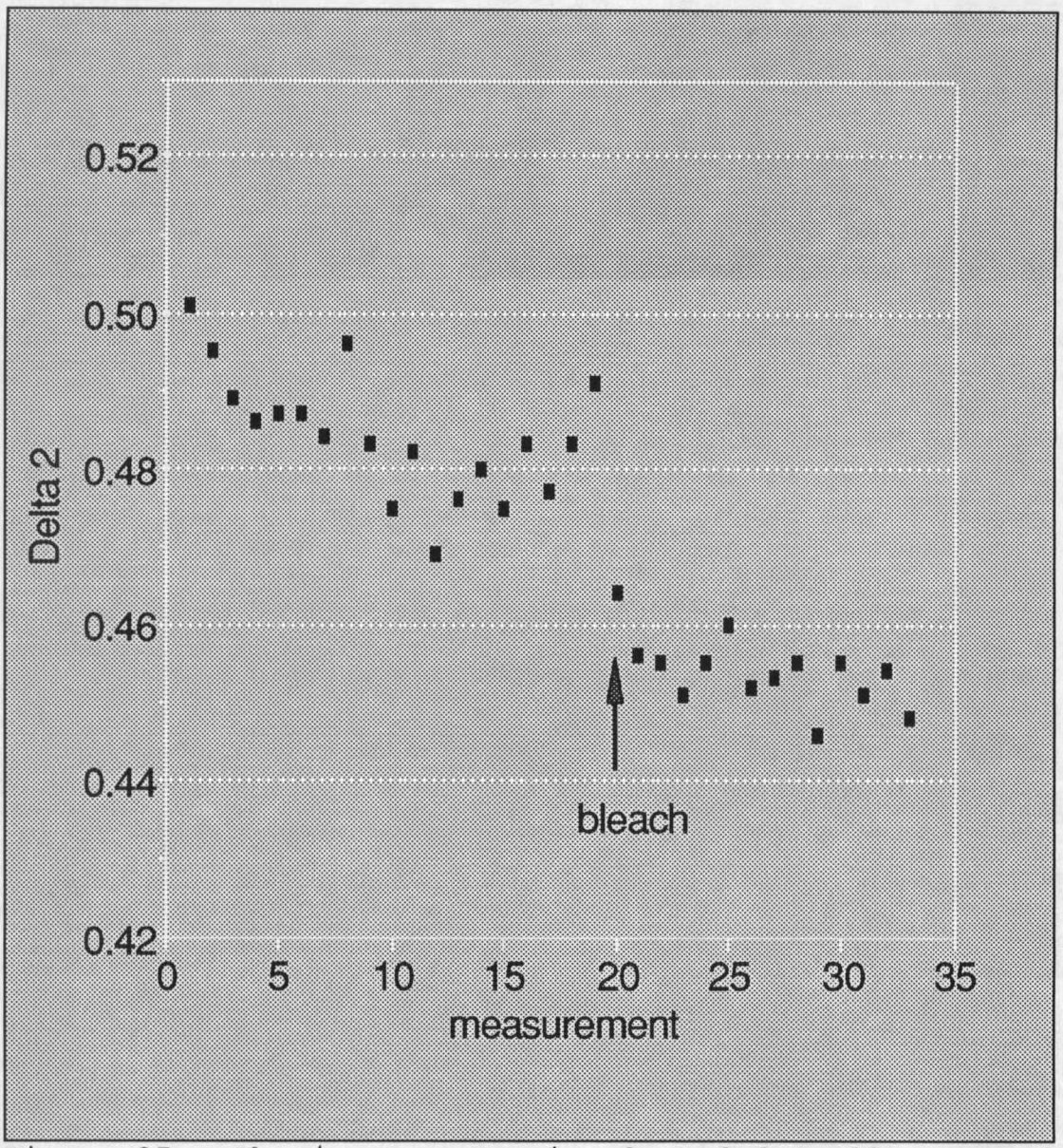


Figure 25. The Δ_2 parameter is plotted for all pre- and post-bleach ^2H NMR measurements for prep B. An arrow indicates the first measurement taken after bleaching.

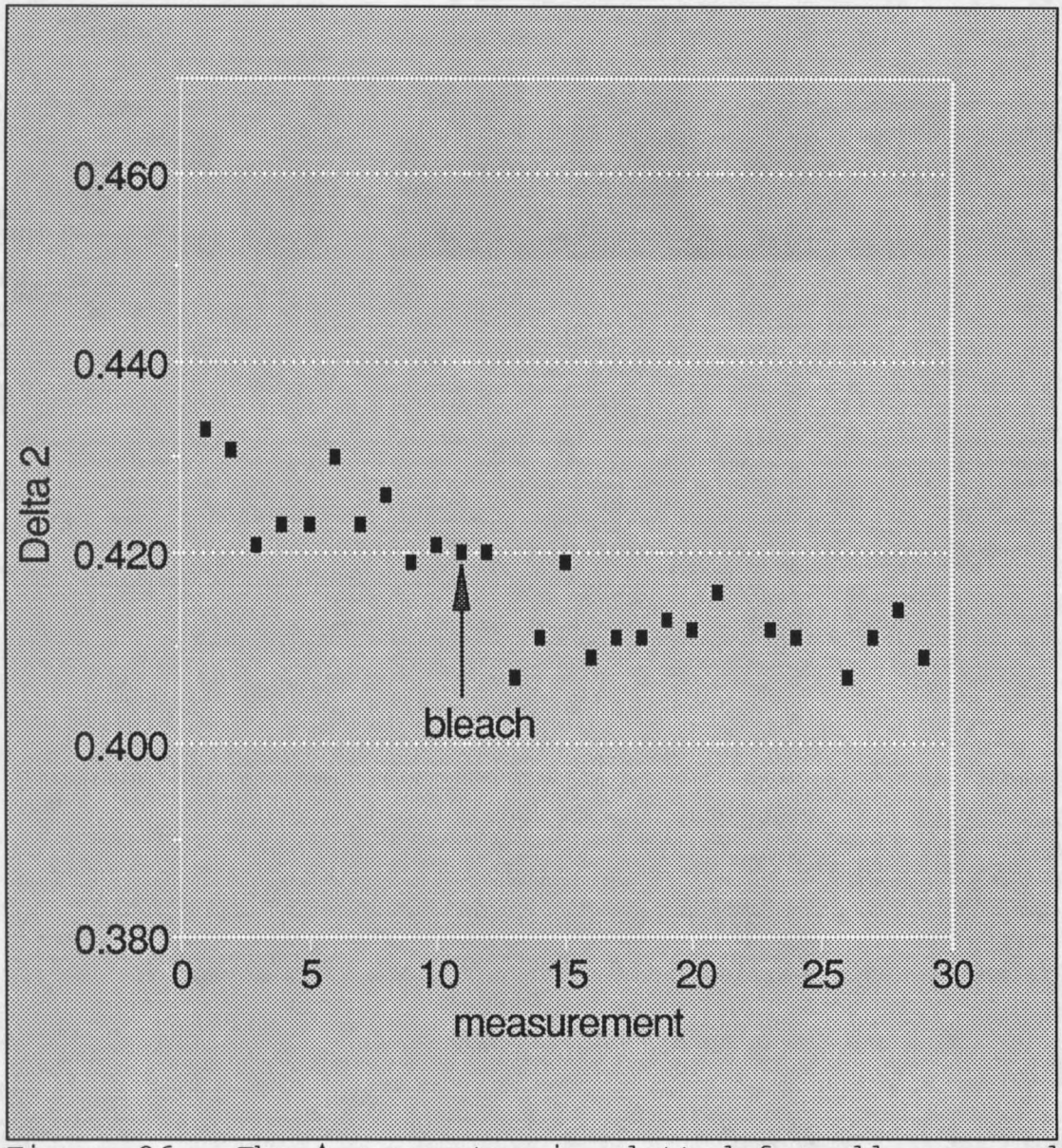


Figure 26. The Δ_2 parameter is plotted for all pre- and post-bleach ^2H NMR measurements for prep C. An arrow indicates the first measurement taken after bleaching.

after bleaching that decreases slightly with time after bleach.

This decrease indicates that the lipid bilayer conformational environment becomes more homogeneous when rhodopsin is in the MI $\leftrightarrow$ MII $\leftrightarrow$ MIII mixture. The relative change in the Δ_2 parameter is approximately proportional to the change observed in the first moment for each preparation.

The Zeroth Moment, M_0

A final piece of information from the moment analysis was derived from the zeroth moment, M_0. The zeroth moment is a calculation of the area under a curve. In this case, the curve is half the symmetric ^2H NMR spectrum. Since the quantity of sample has not been altered in any way during the course of this experiment, we would expect the spectral area, and thus M_0, to remain constant if there is no significant change in the amount of sample in the NMR coil before and after removing the sample from the NMR machine, bleaching it, and replacing it in the NMR receiver coil. Figures 27-29 show that the zeroth moment is constant before and after bleaching. Since all preparations included synthetic phospholipids containing the same number of ^2H labeled positions, it is also expected that M_0 would be the same for all preparations. This consistency in the zeroth moment is indicated by Figures 27-29.

The first moment of the ^2H NMR spectrum can be used as

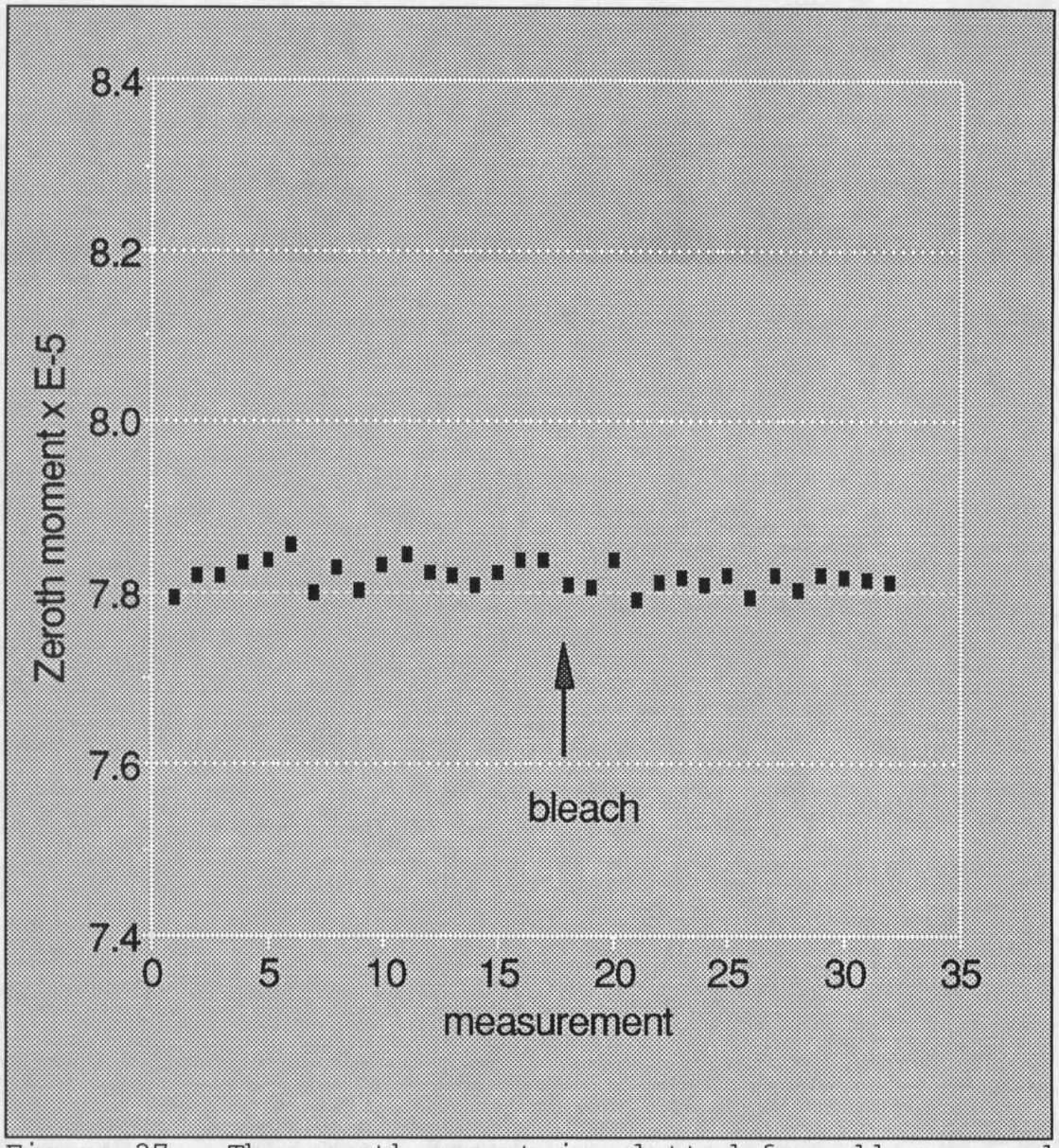


Figure 27. The zeroth moment is plotted for all pre- and post-bleach ^{2}H NMR measurements for prep A. An arrow indicates the first measurement taken after bleaching.

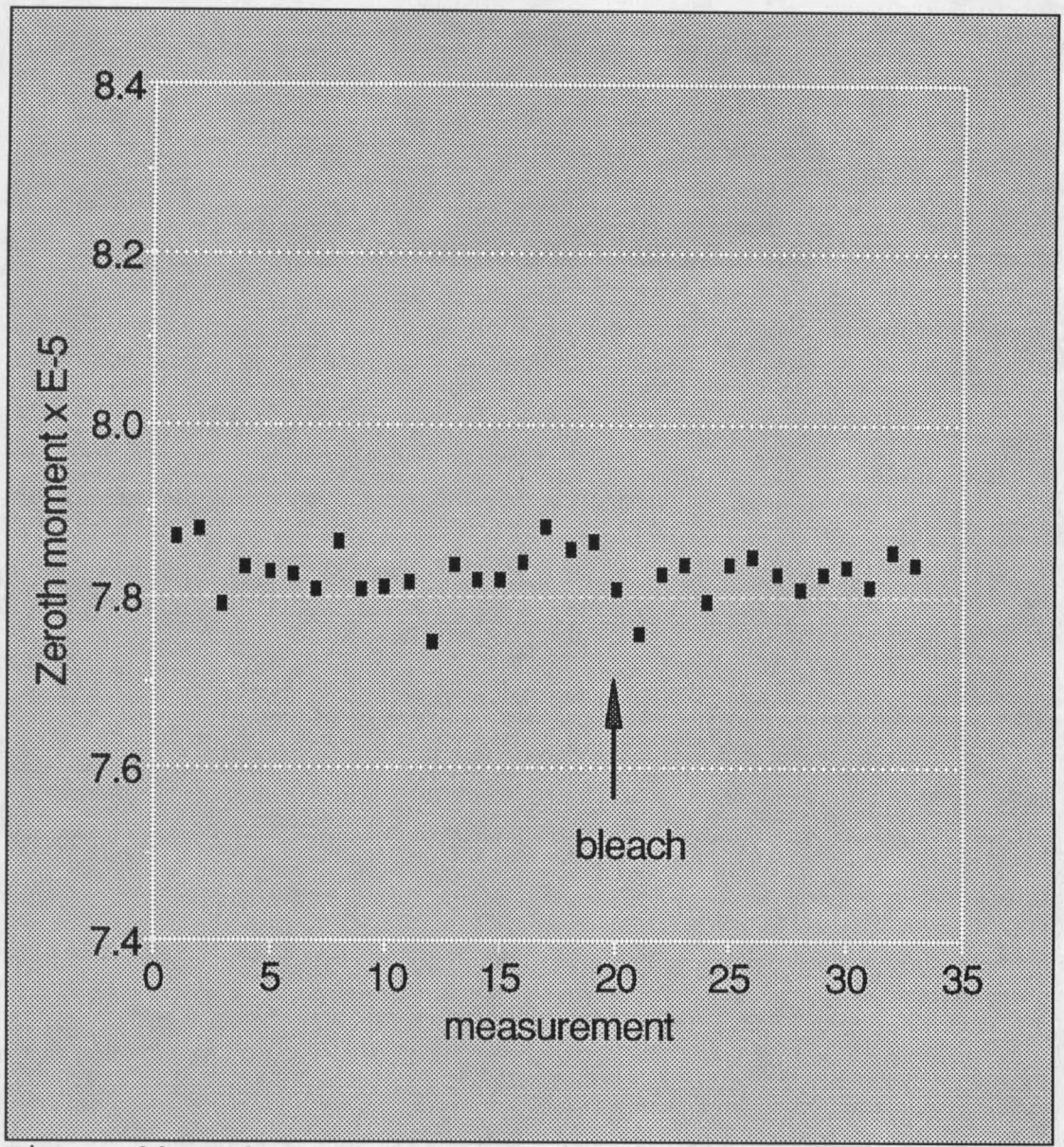


Figure 28. The zeroth moment is plotted for all pre- and post-bleach ^{2}H NMR measurements for prep B. An arrow indicates the first measurement taken after bleaching.

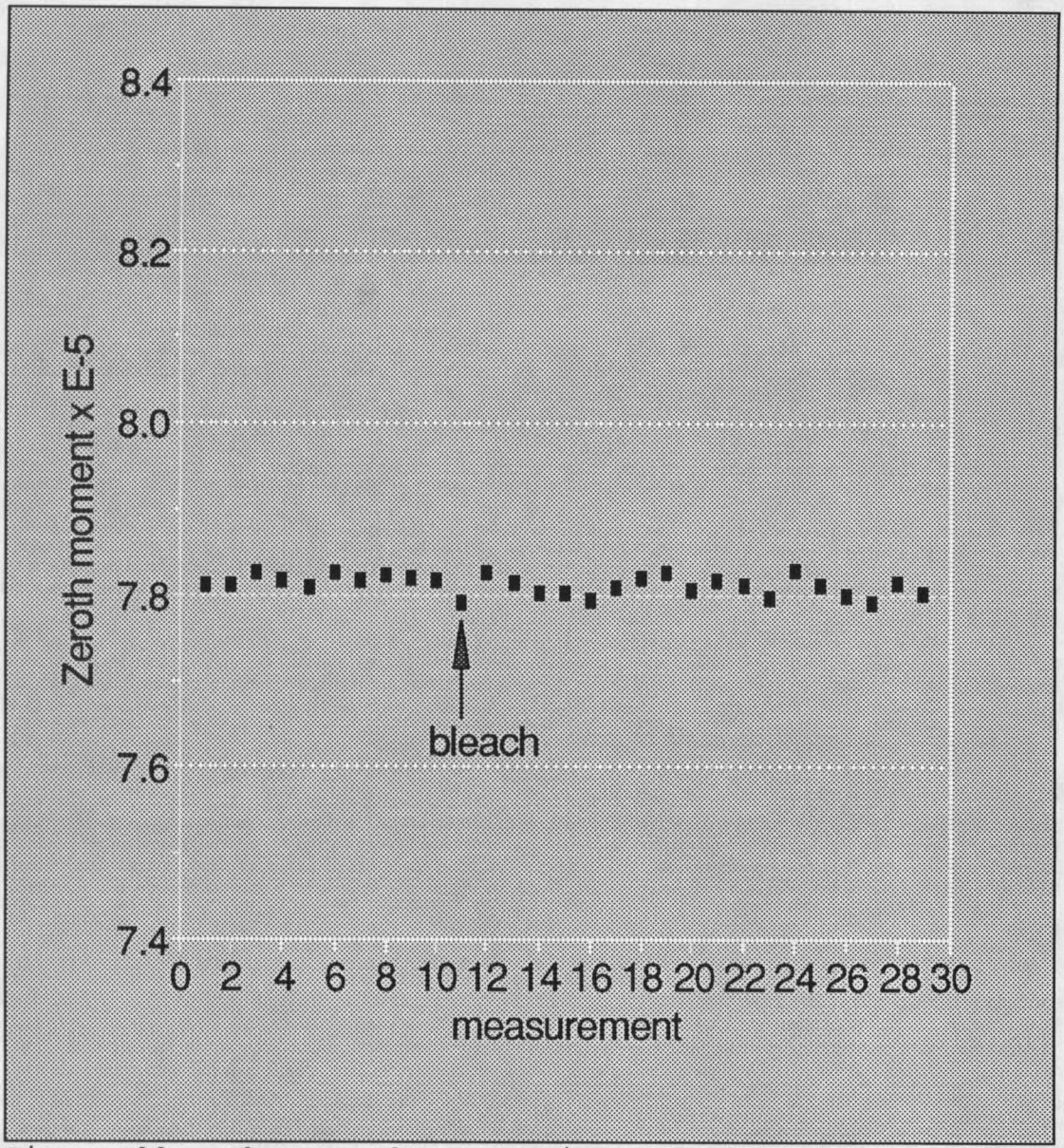


Figure 29. The zeroth moment is plotted for all pre- and post-bleach ^{2}H NMR measurements for prep C. An arrow indicates the first measurement taken after bleaching.

an indicator for the transition from the fluid liquid crystalline phase of pure phospholipid bilayers to the more ordered gel phase. We were interested in verifying the location of phase transitions since we were operating at -13.5°C which is close to the onset of the phase transition from fluid to gel for pure $16:0_{d31}22:6$PC bilayers (Deese et al.1981; Barry et al.1991). The production of intermediates beyond MI is greatly inhibited by temperatures below the fluid phase.

Multilamellar lipid vesicles, or liposomes, can be prepared with deuterated phospholipids by dispersing the dried lipid in excess buffer and collecting the vesicles by centrifugation. By monitoring the NMR spectrum of these vesicles as a function of temperature, phase transitions can be observed. With decreasing temperatures, phospholipids enter the gel phase and show an abrupt increase in M_1. Plots of the first moment of the ^{2}H NMR spectra as a function of both increasing and decreasing temperature for $16:0_{d31}22:6$PC are shown in Figure 30. The main phase transition occurs at a significantly different temperature when the sample is cooled versus when it is warmed. This difference is called hysteresis has been reported by others for 22:6 (Deese et al.1981; Barry et al.1991).

Mixed liposomes containing phosphatidylcholine, -ethanolamine, and -serine, 3:3:1 (molar ratios, respectively), containing $16:0_{d31}$ and 22:6 were subjected to

similar cooling and warming curves as for the pure phosphatidylcholine lipid. The results are shown in Figure 31. The hysteresis and sharpness seen in the phase transition region for pure $16:0_{d31}22:6$PC bilayers is not observed when three headgroups are present. Substantial broadening of the phase transition is also observed when rhodopsin is incorporated into reconstituted membranes containing $16:0_{d31}22:6$PC/PE/PS 3:3:1 as shown in Figure 32.

Discussion

The changes indicated by the moment analysis are consistent with an increased thickness of the lipid bilayer as rhodopsin is bleached and forms a mixture of intermediates between MI and MIII as predicted by the 'molecular spring' model. The M_1 calculated from ^2H NMR measurements gives the average of all lipid environments. A layer of approximately 24 phospholipids is believed to be necessary to coat the surface of rhodopsin (Marsh, et al, 1982). The remaining 40-60 lipids (This number is dependent on the lipid to protein ratio.) are farther away and have little or no direct contact with the protein. Considering this, it is quite likely that those lipids directly adjacent to the protein surface are perturbed to a greater extent by rhodopsin than those lipids in a "bulk" lipid environment but have their M_1 averaged (and thus decreased) by non-adjacent lipids that may be less affected. We have not been

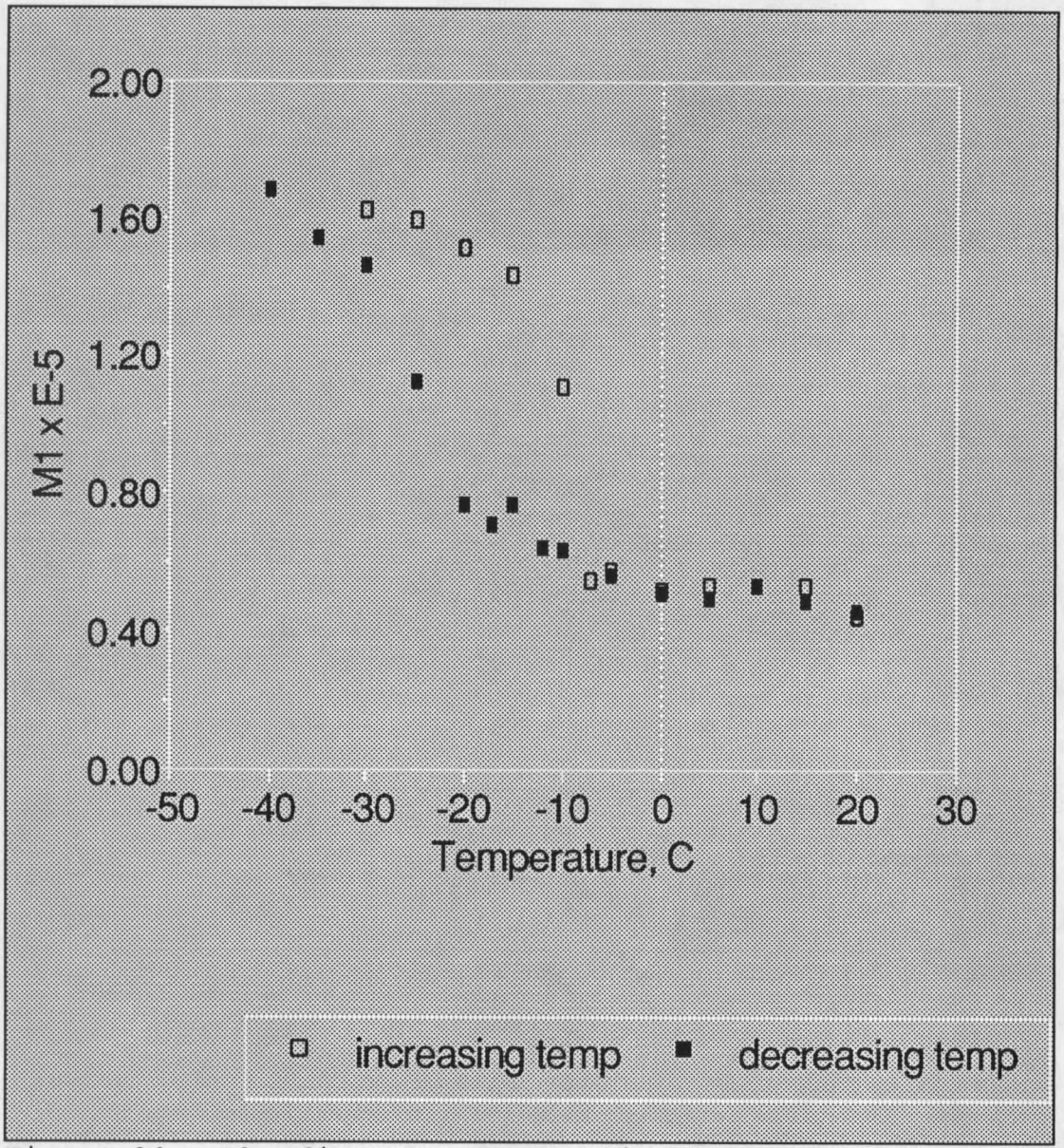


Figure 30. The first moment, M_1, is plotted as a function of temperature for $16:0_{d31}22:6$PC liposomes.

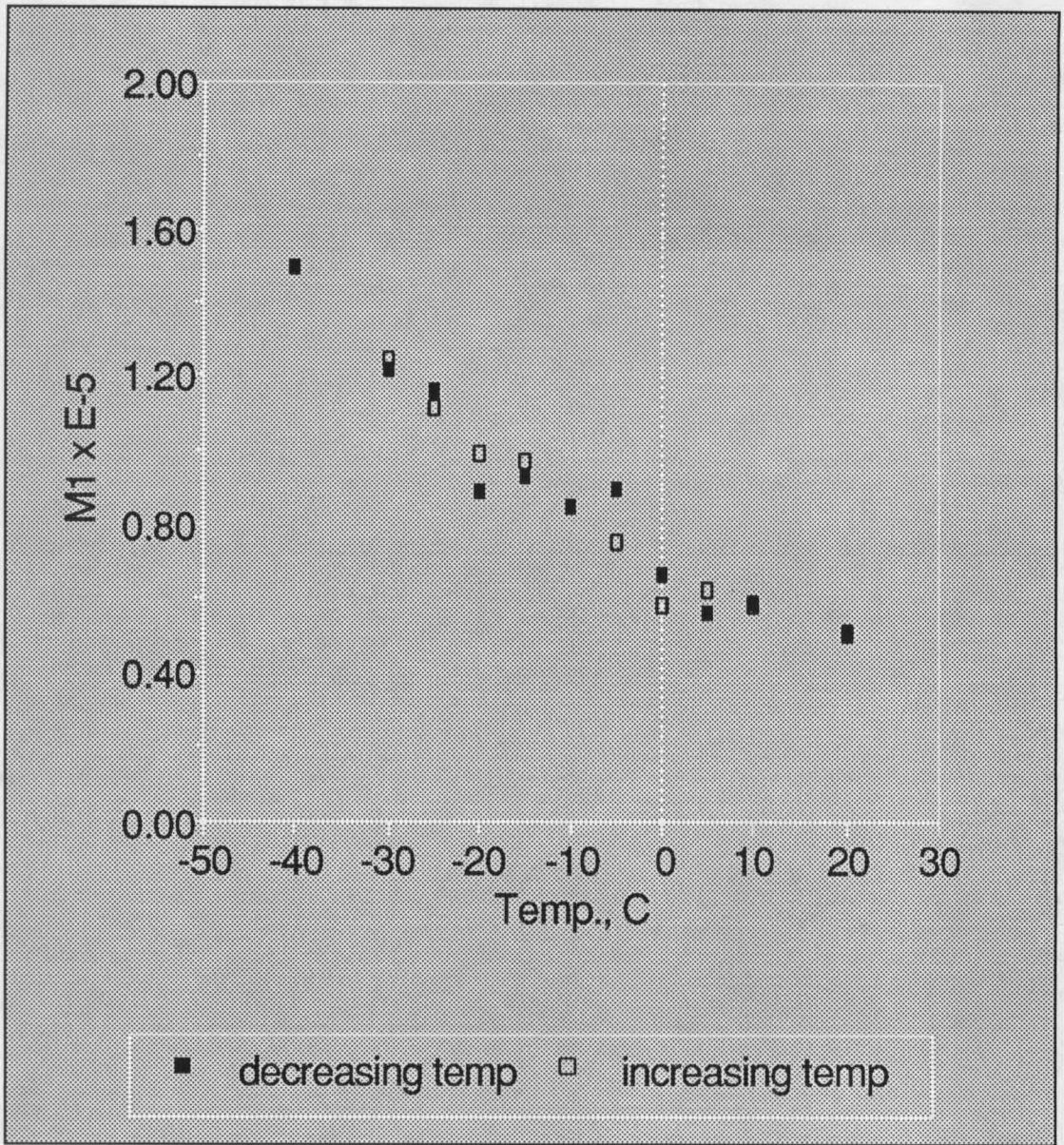


Figure 31. The first moment is plotted as a function of temperature for $16:0_{d31}22:6$PC/PE/PS (3:3:1) liposomes.

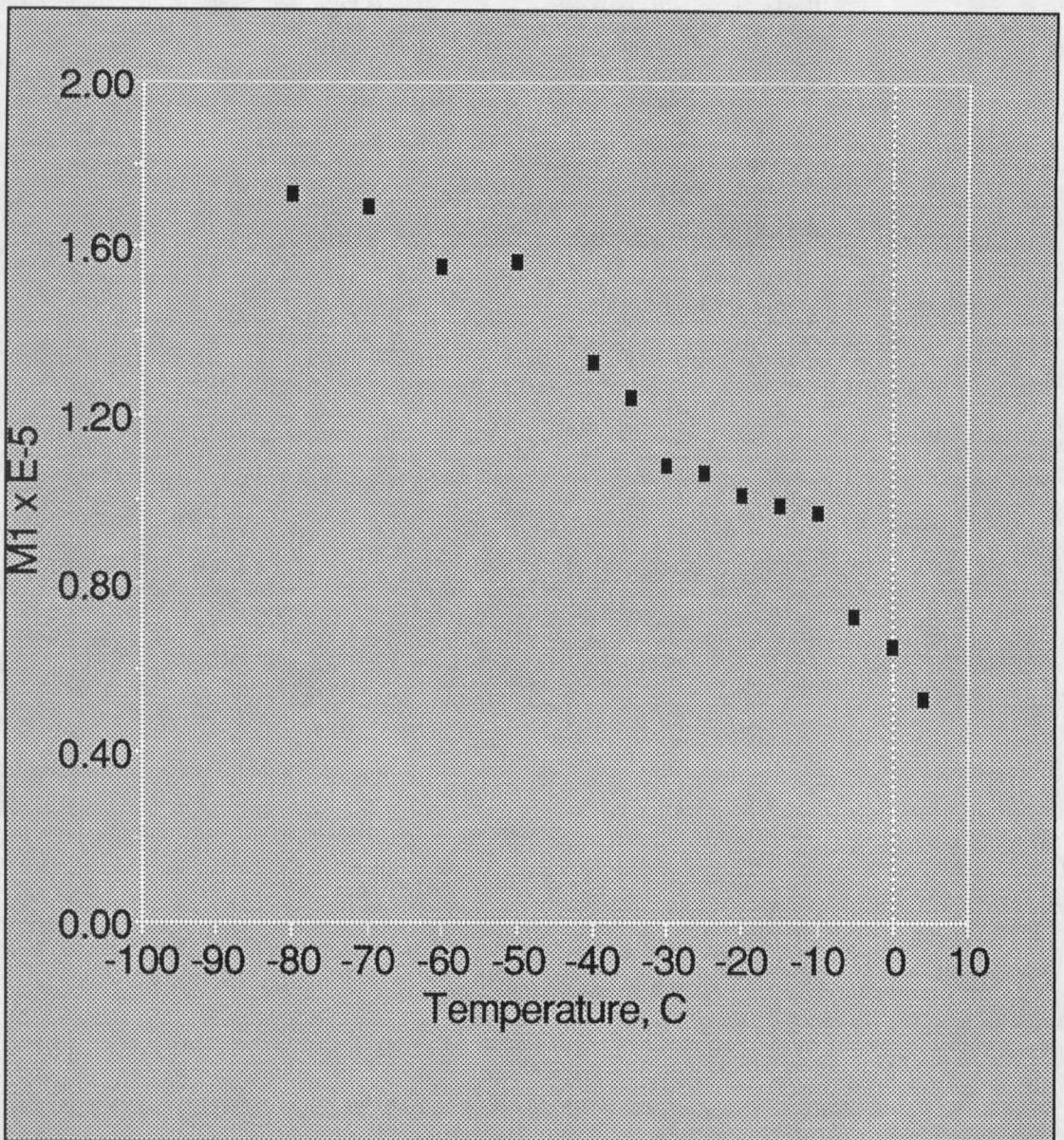


Figure 32. The first moment is plotted as a function of temperature for reconstituted membrane prep A.

able to stabilize pure MII and the thickness change we have detected may be considered to be a lower limit of the change in bilayer thickness caused by formation of MII.

The changes in the first moment for preps A, B, and C, were plotted together as a function of time and are shown in Figure 33. Comparing the three experiments, the largest changes in the first moment were observed with preps A and B with prep A being slightly larger. These preps were adjusted to pH 5.5 to favor the MI $\leftrightarrow$ MII in the direction of MII. In this environment, when equilibrium is established, it is likely that very little MI exists. Thus, most of the protein should be in an "open" conformation which is expected to have the greatest perturbation on the lipid bilayer. The slightly larger increase in M_1 observed for prep A may be due to the smaller lipid to protein ratio used in that preparation. With fewer lipids separating each protein, a larger percentage of the total lipids will be adjacent to the protein. The overall "bulk" lipid would be reduced and its averaging effect would not be as great.

The change in M_1 for prep C is approximately half that observed for the other preparations. The pH of this sample was adjusted to 8.0. Under this condition, the direction of the MI $\leftrightarrow$ MII equilibrium would favor MI. A curve fitting analysis of the absorption spectrum for this preparation showed that after 24 hours one third of the sample remained in MI. In MI, the protein is thought to have a "closed"

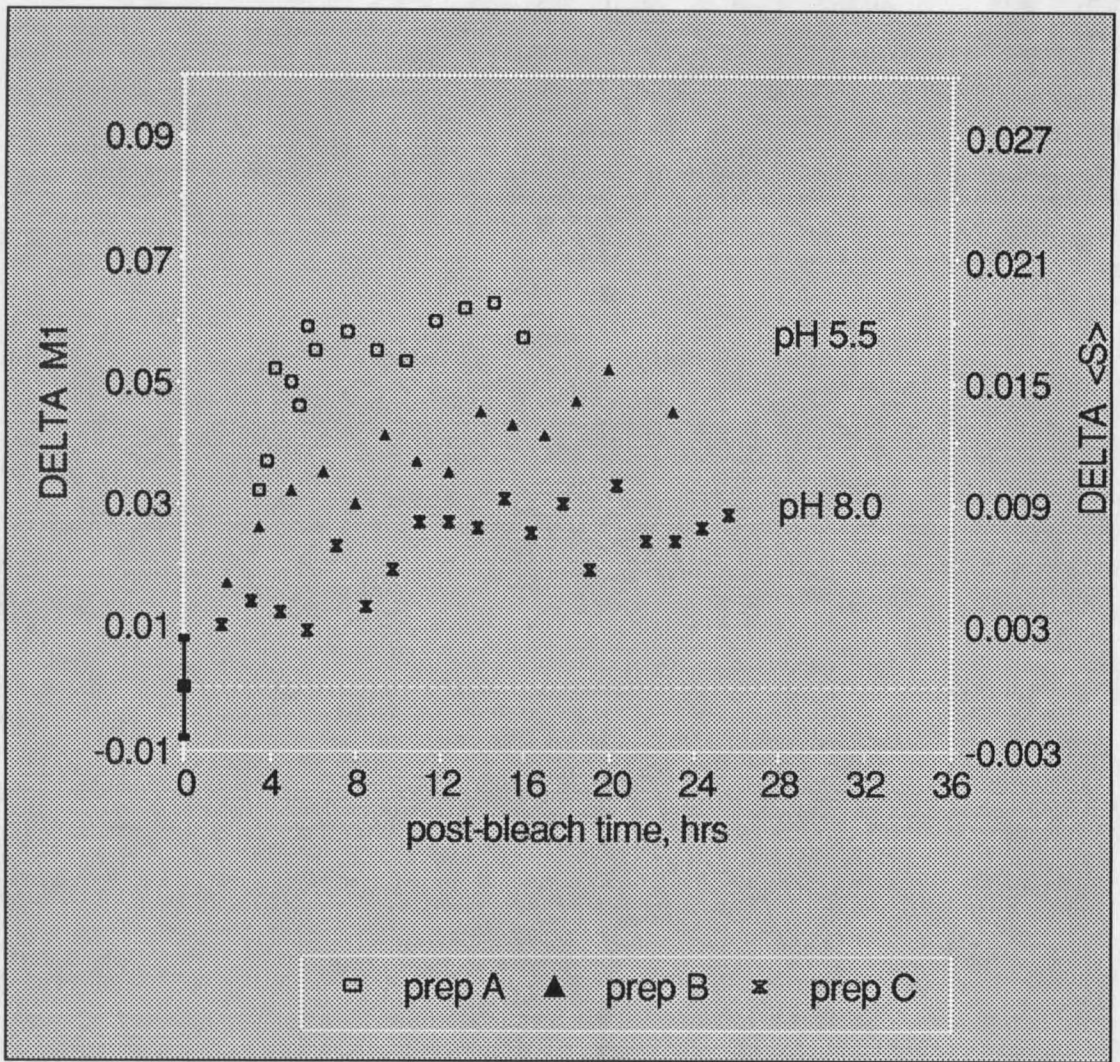


Figure 33. The change in the first moment for reconstituted membrane preps A, B, and C is plotted as a function of post-bleach time.

conformation as it does in rhodopsin and thus this intermediate would not be expected to perturb the lipid bilayer. With less of the protein in an "open" conformation, less change in the first moment would be expected, consistent with the first moment behavior shown by prep C in Figure 33.

The absorption experiments done with $16{:}0_{d31}22{:}6$PC (no PE or PS) showed that MII decayed rather quickly to a mixture of mostly MIII and retinal. ^{2}H NMR measurements taken on this sample before and after bleaching showed very little or no detectable change in membrane thickness. A possible interpretation of this result is that the protein has relaxed back to its closed conformation after the dissociation of retinal from the protein. No change in bilayer thickness would be expected in this case if the protein was in a closed conformation before and after bleaching. The inclusion of PE and PS headgroups to the reconstitution as well as the colder temperature have likely imparted additional stability to rhodopsin intermediates and slowed their decay to retinal + opsin.

There is evidence that amino phospholipids, phosphatidylserine and phosphatidylethanolamine, have a strong association with membranes proteins that is somewhat selective for phosphatidylserine (Sadler et al.1984). Negatively charged PS may be attracted by positively charged residues on the surface of the protein. This electrostatic

interaction may be strong enough to prevent or substantially decrease lateral diffusion of PS in the membrane. A boundary of PS lipid that did not laterally diffuse into the bulk on the NMR time scale would contribute to a larger change to the first moment than that observed in pure PC/rhodopsin bilayers. A potentially informative experiment involves incorporating the native PC/PE/PS mixture with rhodopsin where the perdeuterated $16:0_{d31}$ is in one of the lipids at a time. These experiments should be capable of providing high resolution information of the relative involvement of the different phospholipid head groups with rhodopsin during its functional transitions.

A 6% change in M_1 after the sample was bleached corresponds to a average of 1Å increase in fatty acid chain length. While this increase in chain length may not seem very large, this change provides evidence for a fairly substantial protein conformational change that may be fundamental for the mechanism of action of rhodopsin (and perhaps other G-protein coupled receptors as well).

When considering membrane thickness, it is useful to remember that the functionality of rhodopsin is very dependent on chain length of fatty acids in the phospholipid bilayer. Baldwin and Hubbel (Baldwin & Hubbell, 1985b; Baldwin & Hubbell, 1985a) showed that rhodopsin required a minimum phospholipid fatty acid chain length of 16 carbons for production of MII. Rhodopsin reconstituted in PC

vesicles containing 14 carbon fatty acids was not able to form MII at all. Later studies by Litman, et al. (Mitchell et al.1991) where these experiments were repeated showed that although rhodopsin reconstituted in DMPC (14:014:0PC) vesicles could form some MII, the production of MII was considerably less than that produced in native ROS. In any case, reducing phospholipid fatty acid chain length by 2 carbons either prevents or significantly reduces the ability of rhodopsin to produce MII, suggesting that there is an important role of bilayer thickness in mediating photochemical functionality of rhodopsin. It is thought that MII produces the largest conformational change in rhodopsin (Ostroy, 1977) and that it will have the largest impact on the lipid bilayer. Considering that only a portion of the bleached rhodopsin is in the MII conformation in our samples, the change in the lipid bilayer may be moderated by "non-MII" intermediates.

For bleached membranes, Δ_2 decreases indicating that the distribution of order parameters is getting narrower even though the average order parameter, <S>, increases. It seems reasonable that this occurs in a more ordered, thicker bilayer. One model for possible protein-induced perturbations of the lipid bilayer describes an initial compression of the bilayer near the protein due to mismatch in the length of the hydrophobic regions of the lipids and the protein (Mouritsen & Bloom, 1984). This may be

particularly descriptive of membranes studied at -13.5°C where bulk lipids are partially frozen and thus more extended than those adjacent to the protein, which remain "melted". The lipids adjacent to the protein become more extended when protein changes conformation and opens up. This would allow the lipids to help MII formation by relaxation to their desired thicker state. When the protein is in the open conformation of the bleached state, the lipid conformational environment becomes more uniform as protein adjacent lipids become more like bulk lipids. This description is consistent with the decrease in the Δ_2 parameter observed for bleached membranes.

Conclusions

We have assumed that the saturated chain is a faithful reporter of the membrane thickness when paired with a 22:6ω3 chain. The deuterium NMR measurements of hydrocarbon thickness agree rather well with x-ray and neutron diffraction measurements where calibrations have been possible (Seelig & Seelig, 1974; Bloom & Mouritsen, 1988; Ipsen et al.1990). There is strong experimental support for the accuracy of the hydrocarbon thicknesses measured by deuterium NMR in the present system.

Figure 34 shows some selected phospholipid chain conformations to clarify the following discussion. We have assumed that the glycerol unit is oriented perpendicular to

the membrane plane and that chain 1 (attached at glycerol C-1) is perpendicular to the bilayer while chain 2 (attached to glycerol C-2) is oriented initially parallel to the membrane surface and then bends down to the center as has been found in other membranes and in phospholipid crystals (Seelig & Seelig, 1977; Marsh, 1992). The generally accepted glycerol orientation means that the length of the sn-1 and the sn-2 chains are different for a given membrane thickness.

In order to pack the lipids into the membrane with the correct thickness the lipid on the right hand side of Figure 34 has a saturated sn-1 chain length of 12-12.5Å. The sn-2 chain has the same length after the bend at carbon 3. The membrane hydrocarbon thickness in the bilayer is calculated as the average of twice these values or 27.5-28.5Å. The best experimental value from x-ray and neutron diffraction is 27-28Å for the hydrocarbon thickness of the retinal rod disk membrane (Dratz & Hargrave, 1983).

The thickness of the hydrocarbon region of the retinal rod membrane can also be calculated from some very simple and reliable analytical chemistry and geometrical factors (Dratz & Hargrave, 1983). This geometrical argument will be recapitulated here since the hydrocarbon thickness turns out to be a strong criterion for eliminating lipid chain conformation models. The starting point for this calculation is the concentration of rhodopsin in the retinal

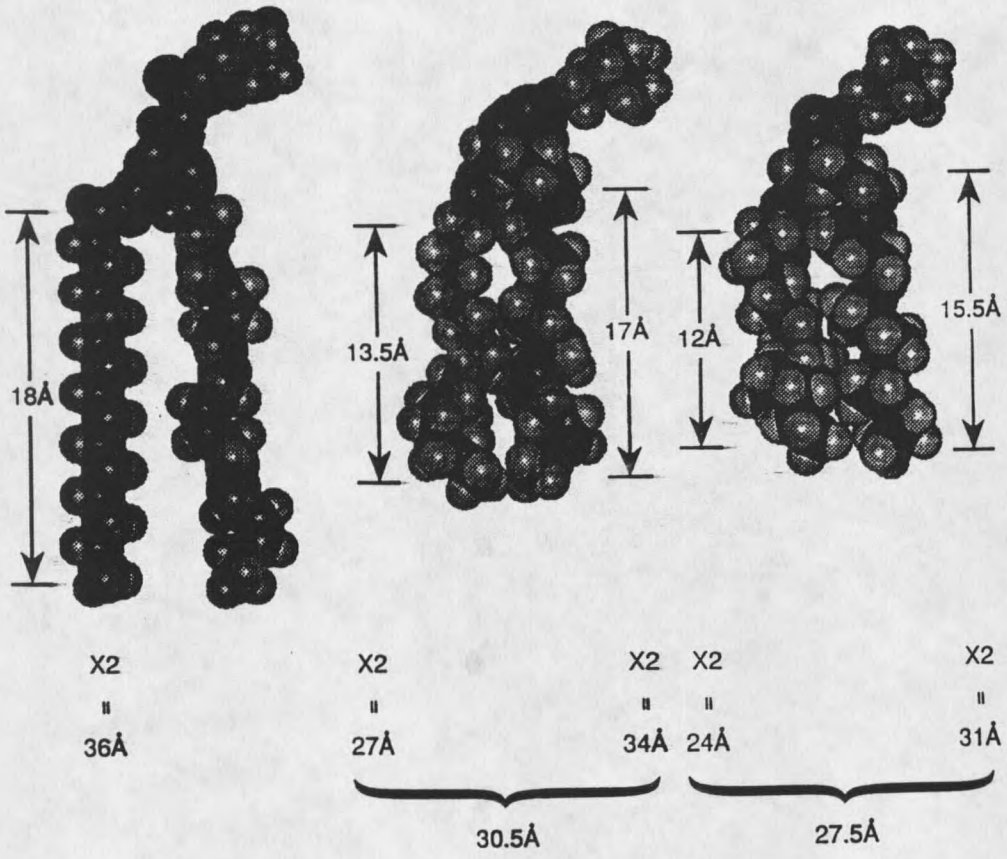


Figure 34. Representative fatty acid conformations of 16:022:6PC. The model on the left was derived from the most stable conformation proposed by Applegate and Glomset as discussed in the text. The model on the right agrees with the fatty acid chain conformation that best fits the deuterium NMR data obtained in the study for membranes containing rhodopsin. This model also agrees with X-ray diffraction and neutron diffraction data on the intact retinal rod membrane. The middle model shows twice the average change in fatty acid conformation that is proposed to occur when rhodopsin forms MII. The change shown is about twice the average change of all the lipids in the membrane and maximum effects that might be expected to occur near the excited protein. The numbers at the bottom refer to the membrane hydrocarbon thickness which is twice the average of the two fatty acid chains.

rod that has been established by microspectrophotometry to be 3.3-3.5mM (Dratz & Hargrave, 1983). The disk membrane pair repeat distance has been shown to be 295Å by x-ray diffraction in all species investigated. These numbers imply 3,300-3,500Å^2 of membrane area per rhodopsin molecule and its associated "unit cell" of 65 lipids. The membrane area covered by rhodopsin is in the range of 750-810Å^2 (Dratz & Hargrave, 1983; Dratz et al.1985) leaving 2,490-2,750Å^2 membrane area for the lipids. The number of different lipids per rhodopsin have been carefully determined (Miljanich et al.1979) and the volume of the lipid hydrocarbon can be calculated from its chemical composition and component density (Marsh, 1992). The lipid hydrocarbon volume calculated from the analytical chemistry and phospholipid physical properties is 74,000Å^3. Dividing this volume by the lipid membrane area from above gives a hydrocarbon thickness of 28±1Å. The NMR data for the membrane thickness of 27.5Å as shown in the right hand lipid conformation Figure 34 is in excellent agreement with the independent assessment of the membrane hydrocarbon thickness obtained above.

In the most extensive published theoretical study of 22:6ω3 conformation, Applegate and Glomset came to quite different conclusions (Applegate & Glomset, 1986). These authors calculated the minimum energy conformations of the polyunsaturated "subunit" 1,4-pentadiene and found the

minimum energy conformations at torsional angles of ±118° around the methylenes in each of the five pentadiene centers. Their conclusion for the lowest energy conformation of 16:022:6PC implies a highly extended chain with an approximately 18Å chain length after the chain turns from parallel to perpendicular to the membrane surface. This lipid conformation is shown on the left hand side of Figure 34. The hydrocarbon thickness of a membrane built of these lipids would be in the range of 36-40Å, at great variance with the experimental value of ca. 28Å. A problem with the calculational approach used by Applegate and Glomset is that their minimization of the chain energy corresponds to 0K with no consideration of thermal energy. We do find that 16:022:6PC/PE/PS (3:3:1) membranes thicken at lower temperatures to a thickness of about 39Å at -80°C. Therefore, Applegate and Glomset's approach may be appropriate for the low temperature, frozen form of the membrane, but clearly not for the melted bilayer found at temperatures between -15°C and physiological temperature.

Molecular dynamics has been used to introduce thermal energy into macromolecular structure and has recently been applied to melted, saturated chains in phospholipid bilayers with excellent results (DeLoof et al.1991; Pastor et al.1991). It may be possible to extend this more realistic calculational approach to polyunsaturated lipid systems as well. The general conclusion from molecular dynamics at

this point is that lipid chains can become entangled and that the representative models we show in Figure 34 give too "static" an impression. Once suitable calculational approaches are found that can account the experimental data it should be possible to greatly expand the predictive power to understand the behavior of 22:6ω3 and polyunsaturated fatty acids in membranes.

The average membrane thickening produced by the transition to the activated conformation of rhodopsin to metarhodopsin II, deduced from the increase in the average order parameter from prep A shown in Figure 33 corresponds to about 6%. The middle lipid in Figure 34 has a length extension of about twice that (12%) so that the difference is easier to visualize. However, the change measured is averaged over all the lipids in the membrane and it is expected that lipids close to the excited protein may be affected to a greater extent than the average. The change in helical twist would be equivalent to about ten degrees.

It is interesting to speculate on the possible consequences of such a change in conformation that may appear to be rather small. There is some evidence that 22:6ω3 favors the incorporation of water into the lipid bilayer hydrocarbon (Deese & Dratz, 1986) and the headgroups of all the lipids in bilayers are heavily hydrated (Wiener & White, 1992; Wiener et al.1991). Thickening of the lipid hydrocarbon layer will reduce the surface area per lipid and

might force a considerable fraction of this water out of the membrane, an event that might produce part of the favorable entropy change that supports the transition to the active MII protein conformation (Ostroy, 1977; Parkes & Liebman, 1984). The sketch of the molecular spring model in Figure 4 also suggests that there may be room for additional water inside the activated protein at MII.

A closer consideration of the thermodynamic parameters, $\Delta H°$ and $\Delta S°$, for the MI $\rightarrow$ MII transition for ROS membranes and detergent solubilized rhodopsin may offer insight to the involvement of phospholipids in this transition. In native ROS membranes, $\Delta H°$ and $\Delta S°$ were calculated from K_{eq} (at different temperatures) and are +19kcal/mol and +90eu, respectively (Parkes & Liebman, 1984). Similarly calculated for membranes solubilized in the detergent digitonin, $\Delta H°$ and $\Delta S°$ are +10kcal/mol and +35eu, respectively (Ostroy et al.1966).

The large positive $\Delta S°$ for the MI $\rightarrow$ MII transition in native membranes suggests a considerably more disordered system at MII. Uncoupling a large fraction of the lipids from the protein in the detergent solubilized system reduces the change in entropy by about 60% for the MI $\rightarrow$ MII transition. Our interpretation of this result is that when the lipids are coupled to the protein they introduce disorder to the solvent surrounding the protein (H_2O in this case) at MII. We explain the increase in entropy as

follows. In rhodopsin and MI, water molecules are attracted to and ordered by the negative charge on phospholipid headgroups, particularly phosphatidylserine, that surround the protein. As the protein opens up at MII, the lipid bilayer reduces surface area by extending, forcing water out of and away from the membrane surface. These water molecules that are forced out into the "bulk" solvent are much more disordered than when they were attracted to and ordered by the negative charge of a phospholipid head group which increases the entropy of the system at MII.

In the digitonin detergent solubilized system, the majority of lipids are no longer associated with the protein; thus, the phenomenon of bilayer expansion, forcing water out of the membrane at MII, would not be observed. This is consistent with the smaller change in entropy observed (40%) for detergent solubilized membranes.

We have also extended this rationale of water molecule polarization by phospholipid headgroups to describe the volume increase that is observed for the lipid protein complex as MI becomes MII. Volume changes for proteins undergoing structural changes, for example denaturation, have been attributed to changes in solvation of the new conformation as a dominant contribution over other sources to the total ΔV (Lamola et al.1974). Therefore, protein conformational changes in and of themselves are not expected to give much volume change.

Water molecules that are polarized by charge have a smaller molar volume than unpolarized molecules, a well-known phenomenon called electrostriction. The water molecules that are polarized by phospholipid headgroups at rhodopsin and MI may lead to a relatively compact overall volume for the lipid-protein-water complex at these intermediates. When the lipids become extended as rhodopsin forms MII, some "electrostricted" water may be expelled into the "bulk" water where it has a larger molar volume. This may result in a larger volume for the complex at MII. Some of the "expanded" water molecules may reside inside the now open protein.

To estimate the volume of an open rhodopsin molecule, the inside of the protein formed at MII was modeled as a cone (volume = $\frac{1}{3}\pi r^2 h$). The change in bilayer thickness (Δh) calculated from ^2H NMR measurements was used directly to calculate the increase in protein surface area (ΔA). Approximating this area as a circle yeilded a value for a radius. The height of the cone is taken as equal to the thickness of the lipid bilayer calculated from the moment analysis of ^2H NMR measurements. This approximate calculation of the volume inside an open rhodopsin molecule showed that perhaps 15 water molecules could occupy this space and gives a feeling for how many water molecules may rearrange during the MI $\rightarrow$ MII transition. The increased water inside the protein at MII could increase the solvation

of amino acid side chains but this may be a fairly neutral event from an entropy perspective. In summary, from the available thermodynamic data on rhodopsin and the ^{2}H NMR, x-ray and neutron diffraction data on lipid bilayers, we propose that it may be the water molecules and not the protein that are changing volume at MII.

Figure 35 shows a first attempt at a model for rhodopsin in a bilayer made of 16:022:6 phospholipids. The seven transmembrane helix protein backbone is taken from the high resolution, electron microscope structure of bacteriorhodopsin (Henderson et al.1990) that was energy minimized by Chris Lambert at MSU. The lipid conformations are taken from the best fit to the deuterium NMR, x-ray, and neutron diffraction data for membrane hydrocarbon thickness. As computers become more powerful and molecular dynamics simulations are able to cope with larger systems we may aspire to begin to study the detailed structure and motional dynamics of a system such as shown in Figure 35. At all times it is necessary to make sure that the theoretical simulations agree with all the available experimental data and that theory and experiment go hand in hand to solve the fascinating role of highly unsaturated fatty acids in membranes.

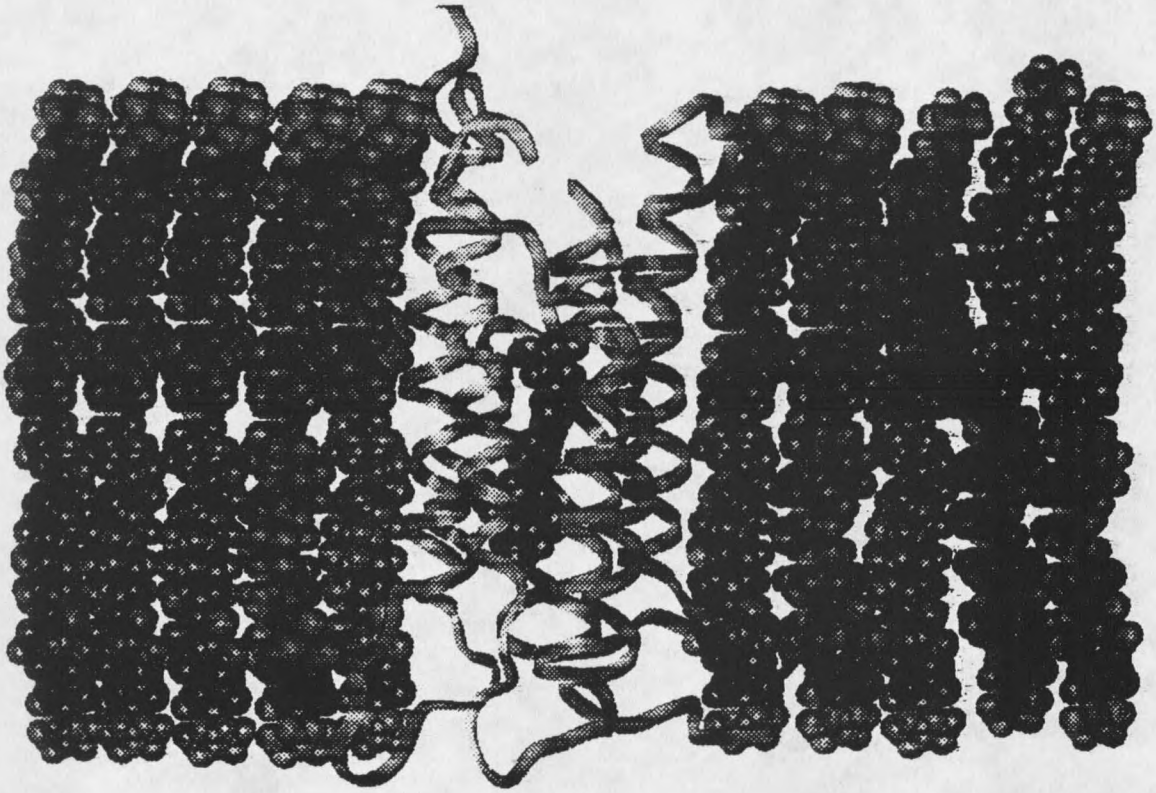


Figure 35. In this model rhodopsin is embedded in a bilayer made of 16:022:6 phospholipids. The protein backbone is taken from the structure of bacteriorhodopsin (Henderson et al.1990) and the lipid conformations are the best fit to the experimental data as described in the text.

LITERATURE CITED

Applebury, M.L. (1987) *Nat. 326*, 546-547.

Applegate, K.R. & Glomset, J.A. (1986) *J. Lipid Res. 27*, 658-680.

Armstrong, D., Sohal, R.S., Cutler, R.G. & Slater, T.F., eds. (1984) *Free Radicals in Molecular Biology, Aging and Disease*. Raven Press, New York.

Ashcroft, A., Chapman, J.R. & Cottrell, J.S. (1987) *J. Chrom. 394*, 15-20.

Baenziger, J.E., Jarrell, H.C., Hill, R.J. & Smith, I.C.P. (1991) *Biochem. 30*, 894-903.

Baenziger, J.E., Jarrell, H.C. & Smith, I.C.P. (1992) *Biochem. 31*, 3377-3385.

Baldwin, P.A. & Hubbell, W.L. (1985a) *Biochem. 24*, 2633-2639.

Baldwin, P.A. & Hubbell, W.L. (1985b) *Biochem. 24*, 2624-2632.

Barry, J.A., Trouard, T.P., Salmon, A. & Brown, M.F. (1991) *Biochem. 30*, 8386-8394.

Baumann, Ch. & Zeppenfeld, W. (1981) *J. Physiol. 317*, 347-364.

Bayerl, T.M. & Bloom, M. (1990) *Biophys. J. 58*, 357-362.

Bennett, N. (1980) *Biochem Biophys Res Comm 96*, 1695-1701.

Bennett, N., Michael-Villaz, M. & Kühn, H. (1982) *Eur. J. Biochem. 127*, 97-103.

Birch, E.E., Birch, D.G., Hoffman, D.R. & Uauy, R. (1992) *Investigative Ophthalmology and Visual Science 33*, 3242-3253.

Blazynski, C. & Ostroy, S.E. (1981) *Vision Res. 21*, 833-841.

Blazynski, C. & Ostroy, S.E. (1984) *Vision Res. 24*, 459-470.

Bloom, M., Davis, J.H. & Dahlquist, F.W. (1979) in *Magnetic Resonance and Related Phenomena, Proceedings of XXth Congress AMPERE* (Kundla, Lippman & Saluvere, Eds.) pp 551-551, Springer-Verlag, .

Bloom, M. & Evans, E. (1991) in *Biologically Inspired Physics* (Peliti, L., Ed.) pp 137-147, Plenum Press, New York.

Bloom, M. & Mouritsen, O.G. (1988) *Can. J. Chem. 66,* 706-712.

Bloom, M., Davis, J.H. & MacKay, A.L. (1992) *Chem. Phys. Letters 80,* 198-201.

Bownds, D. & Wald, G. (1965) *Nat. 205,* 243-257.

Bulkley, G.B. (1983) *Surgery 94,* 407-411.

Bush, R.A., Reme, C.E. & Malone, A. (1991) *Exp. Eye Res. 53,* 741-752.

Butler, W.L. & Hopkins, D.W. (1970) *Photochem. and Photobiol. 12,* 439-450.

Caprioli, R.M. (1988) *Biochem. 27,* 513-521.

Chabre, M. & Breton, J. (1979) *Vision Res. 19,* 1005-1018.

Chen, P.S.Jr., Toribara, T.Y. & Warner, H. (1956) *Anal. Chem. 28,* 1756-1758.

Corongiu, F.P., Banni, S. & Dessi, M.A. (1989) *Free Radicals in Biology and medicine 7,* 183-186.

Cosgrove, J.P., Church, D.F. & Pryor, W.A. (1987) *Lipids 22,* 299-304.

Dasgupta, A., Eser, A., Tomer, K.B. & Djerassi, C. (1987) *Chem. Phys. Lipids 43,* 101-111.

Davis, J.H., Jeffrey, K.R., Bloom, M. & Valic, M.I. (1976) *Chem. Phys. Letters 42,* 390-394.

Davis, J.H. (1979) *Biophys. J. 27,* 339-358.

Davis, J.H. (1983) *Biochim. et Biophys. Acta 737,* 117-171.

Deese, A.J., Dratz, E.A., Dahlquist, F.W. & Paddy, M.R (1981) *Biochem. 20,* 6420-6427.

Deese, A.J. & Dratz, E.A. (1986) in *Progress in protein -lipid interactions 2* (Watts, A. & DePont, J.J.H.H.M., Eds.) pp 45-82, Elsevier Science Publishers BV, Amsterdam.

DeGrip, W.J., Daemen, F.J.M. & Bonting, S.L. (1980) *Methods in Enzymology 67*, 301-320.

DeLoof, H., Harvey, S.C., Segrest, J.P. & Pastor, R.W. (1991) *Biochem. 30*, 2099-2113.

Devaux, P.F. (1983) in *Biological magnetic resonance* (Berliner, L.J. & Reuben, J., Eds.) pp 183-299, Plenum Press, New York and London.

Dratz, E.A., Farnsworth, C.C., Loew, E.C., Thomas, D.W., Stephens, R.J. & vanKuijk, F.J.G.M. (1989) in *Vitamin E: biochemistry and health implications* (Diplock, A.T., Machlin, L.J., Packer, L. & Pryor, W.A., Eds.) pp 46-60, New York Academy of Sciences (In press), New York.

Dratz, E.A. & Hargrave, P.A. (1983) *TIBS 8*, 128-131.

Dratz, E.A., VanBreemen, J.F.L., Kamps, K.M.P., Keegstra, W. & VanBruggen, E.F.J. (1985) *BBA 832*, 337-342.

Dratz, E.A. & Holte, L.L. (1992) *Proceedings of the 3rd International Congress on Essential Fatty Acids and Eicosanoids*. Journal of the American Oil Chemists Society, (in press).

Emeis, D., Kühn, H., Reichert, J. & Hofmann, K.P. (1982) *FEBS Letters 143*, 29-34.

Esterbauer, H. (1982) in *Free Radicals, Lipid Peroxidation and Cancer* (McBrien, D.C.H. & Slater, T.H., Eds.) pp 101-128, Academic Press, Inc., London.

Fager, R., Sejnowski, P. & Abrahamson, E.W. (1972) *Biochem Biophys Res Comm 47*, 1244-1247.

Fell, A.F. (1983) *Trends in Analytical Chemistry 2*, 63-66.

Frankel, E.N. (1980) *Prog. Lipid Res. 19*, 1-22.

Games, D.E. (1978) *Chem. Phys. Lipids 21*, 389-402.

Games, D.E., Pleasance, S., Ramsey, E.D. & McDowall, M.A. (1988) *Biomedical and Environmental Mass Spectrometry 15*, 179-182.

Hamm, H.E., Deretic, D., Arendt, A., Hargrave, P.A., Koenig, B. & Hofmann, K.P. (1988) *Science 241*, 832-835.

Henderson, R., Baldwin, J.M., Ceska, T.A., Zemlin, F., Beckmann, E. & Downing, K.H. (1990) *J. Mol. Biol. 213*, 899-929.

Hofmann, K.P. (1986) *Photobiochem. and Photobiophys. 13*, 309-327.

Holte, L.L., Deese, A.J., Ryba, N., Watts, A. & Dratz, E.A. (1990) *Biophys. J. 57*, 218a.(Abstract)

Ipsen, J.H., Mouritsen, O.G. & Bloom, M. (1990) *Biophys. J. 57*, 405-412.

Ito, Y., Takeuchi, T. & Ishii, D. (1985) *J. Chrom. 346*, 161-166.

Jensen, N.J. & Gross, M.L. (1988) in *Mass Spectrometry Reviews* (pp 41-69, John Wiley & Sons, Inc., .

Jensen, N.J., Tomer, K.B. & Gross, M.L. (1986) *Lipids 21*, 580-588.

Kibelbek, J., Mitchell, D.C., Beach, J.M. & Litman, B.J. (1991) *Biochem. 30*, 6761-6768.

Kimble, E.A. & Ostroy, S.E. (1973) *BBA 325*, 323-331.

Konig, B., Arendt, A., McDowell, J.H., Kahlert, M., Hargrave, P.A. & Hofmann, K.P. (1989) *PNAS 86*, 6878-6882.

Lamola, A.A., Yamane, T. & Zipp, A. (1974) *Biochem. 13*, 738-745.

Lewis, A., Fager, R.S. & Abrahamson, E.W. (1973) *J. Raman Spectrosc. 1*, 465-470.

Lewis, B.A. & Engelman, D.M. (1983) *J. Mol. Biol. 166*, 211-217.

Liebman, P.A., Parker, K.R. & Dratz, E.A. (1987) *Ann. Rev. Physiol. 49*, 765-791.

Marsh, D. (1992) *Handbook of lipid bilayers.* CRC Press, .

Marx, J.L. (1987) *Science 235*, 529-531.

Matthews, R.G., Hubbard, R., Brown, P.K. & Wald, G. (1963) *The Journal of General Physiology 47*, 215-240.

Miljanich, G.P., Sklar, L.A., White, D.L. & Dratz, E.A. (1979) *BBA 552*, 294-306.

Miljanich, G.P., Nemes, P.P., White, D.L. & Dratz, E.A. (1981) *J. Mem. Biol. 60*, 249-255.

Mitchell, D.C., Kibelbek, J. & Litman, B.J. (1991) *Biochem. 30*, 37-42.

Morrison, W.R. & Smith, L.M. (1964) *J. Lipid Res. 5*, 600-608.

Mouritsen, O.G. & Bloom, M. (1984) *Biophys. J. 46*, 141-153.

Munster, H., Stein, J. & Budqikiewicz, H. (1986) *Biomedical and Environmental Mass Spectrometry 13*, 423-427.

Neuringer, M., Connor, W.E., Lin, D.S., Barstad, L. & Luck, S. (1986) *Proc. Natl. Acad. Sci. USA 83*, 4021-4025.

O'Brian, P.J. (1987) in *Autoxidation of Unsaturated Lipids* (Chan, H.W.-S., Ed.) pp 233-280, Academic Press Inc., London.

Ostroy, S.E., Erhardt, F. & Abrahamson, E.W. (1966) *BBA 112*, 265-277.

Ostroy, S.E. (1977) *BBA 463*, 91-125.

Papermaster, D.S. & Dreyer, W.J. (1974) *Biochem. 13*, 2438-2444.

Parkes, J.H. & Liebman, P.A. (1984) *Biochem. 23*, 5054-5061.

Pastor, R.W., Venable, R.M. & Karplus, M. (1991) *PNAS 88*, 892-896.

Porter, N.A., Wolf, R.A., Yarbro, E.M. & Weenan, H. (1979) *Biochem Biophys Res Comm 89*, 1058-1064.

Prosser, R.S., Davis, J.H., Dahlquist, F.W. & Lindorfer, M.A. (1991) *Biochem. 30*, 4687-4696.

Radding, C.M. & Wald, G. (1956) *Journal of General Physiology 39*, 909-921.

Raubach, R.A., Franklin, L.K. & Dratz, E.A. (1974) *Vision Res. 14*, 335-337.

Rothschild, K.J., Gillespie, J. & DeGrip, W.J. (1987) *Biophys. J. 51*, 345-350.

Sadler, D.M., Rivas, E., Gulik-Krzywicki, T. & Reiss-Husson, F. (1984) *Biochem. 23*, 2704-2712.

Salem, N.Jr. & Karanian, J.W. (1992) in *Alcohol Research From Bench to Bedside. Physiology and Metabolism* (pp 183-197).

Salem, N.Jr., Kim, H.-Y. & Yergey, J.A. (1986) in *Health Effects of Polyunsaturated Fatty Acids in Seafoods* (Simopolous, A.P., Keifer, R.R. & Martin, R.R., Eds.) pp 263-317, Academic Press, New York.

Schoenlein, R.W., Peteanu, L.A., Mathies, R.A. & Shank, C.V. (1991) *Science 254*, 412-415.

Seelig, A. & Seelig, J. (1974) *Biochem. 13*, 4839-4845.

Seelig, A. & Seelig, J. (1977) *Biochem. 16*, 45-49.

Seelig, J. (1977) *Quar. Rev. Biophys. 10*, 353-418.

Seelig, J. & Seelig, A. (1980) *Quar. Rev. Biophys. 13*, 19-61.

Smith, I.C.P. (1983) in *NMR of Newly Accessible Nuclei* (pp 1-26), Academic Press, .

Smith, M. & Jungalwala, F.B. (1981) *J. Lipid Res. 22*, 697-704.

Sternin, E., Bloom, M. & MacKay, A.L. (1983) *J. Mag. Res. 55*, 274-282.

Stone, W.L., Farnsworth, C.C. & Dratz, E.A. (1979) *Exp. Eye Res. 28*, 387-397.

Thomas, D.D. & Stryer, L. (1982) *J. Mol. Biol. 154*, 145-157.

Tsui, F.C., Sundberg, S.A. & Hubbell, W.L. (1990) *Biophys. J. 57*, 85-97.

vanBreugel, P.J.G.M., Geurts, P.H.M., Daemen, F.J.M. & Bonting, S.L. (1978) *BBA 509*, 137-147.

vanKuijk, F.J.G.M., Thomas, D.W., Stephens, R.J. & Dratz, E.A. (1985a) *Journal of Free Radicals in Biology and Medicine 1*, 215-225.

vanKuijk, F.J.G.M., Thomas, D.W., Stephens, R.J. & Dratz, E.A. (1985b) *Journal of Free Radicals in Biology and Medicine 1*, 387-393.

vanKuijk, F.J.G.M., Sevanian, A., Handelman, G.J. & Dratz, E.A. (1987) *TIBS 12*, 31-34.

vanRollins, M. & Murphy, R.C. (1984) *J. Lipid Res. 25*, 507-517.

Weenen, H. (1982) in *Ph.D. Thesis* (pp 20-41), University of Nijmegen, The Netherlands, .

Wiedmann, T.S., Pates, R.D., Beach, J.M., Salmon, A. & Brown, M.F. (1988) *Biochem. 27*, 6469-6474.

Wiener, M.C., King, G.I. & White, S.H. (1991) *Biophys. J. 60*, 568-576.

Wiener, M.C. & White, S.H. (1992) *Biophys. J. 61*, 437-447.

Williams, D.H. & Fleming, I. (1980) *Spectrscopic Methods in Organic Chemistry*. McGraw-Hill Book Co., London.

MONTANA STATE UNIVERSITY LIBRARIES
3 1762 10062419 4